論文 / 著書情報
Article / Book Information

題目(和文)	極性ネマチック液晶ポリエステルに観察される特異な物質
Title(English)	Unusual physical properties observed in polar nematic liquid crystal polyester
著者(和文)	田口吉昭
Author(English)	yoshiaki taguchi
出典(和文)	学位:博士(工学), 学位授与機関:東京工業大学, 報告番号:甲第7930号, 授与年月日:2010年3月26日, 学位の種別:課程博士, 審査員:渡辺 順次,戸木田 雅利
Citation(English)	Degree:Doctor (Engineering), Conferring organization: Tokyo Institute of Technology, Report number:甲第7930号, Conferred date:2010/3/26, Degree Type:Course doctor, Examiner:,
学位種別(和文)	博士論文
Type(English)	Doctoral Thesis

Unusual Physical Properties Observed in Polar Nematic Liquid Crystal Polyester

A Dissertation Presented

By

Yoshiaki TAGUCHI

to

Department of Organic and Polymeric Materials

Faculty of Engineering

Tokyo Institute of Technology

Tokyo Japan

2010

Unusual Physical Properties Observed in Polar Nematic Liquid Crystal Polyester

Contents

Chapter 1

General Introduction

1-1 Introduction

1-1-1 Liquid Crystal Polymer VECTRA®

Main-chain type thermotropic liquid crystal polymers (LCPs) are typically composed of semi-rigid or wholly rigid rod-like molecules consisting of para-linked aromatic residues as a mesogenic group and flexible molecules which are incorporated to reduce deliberately molecular rigidity.

Especially, wholly aromatic polyesters are most important class of thermotropic LC polymers. They show outstanding physical properties and excellent chemical resistance suitable for commercial applications in electronics, automotive and aerospace industries as well as in medical fields.[1] Moreover we experientially know that **VECTRA® A950** can be easily processed to the fiber or film, but have had no idea of that reason. Typical thermotropic LC polyester is a copolymer composed of 4-hydroxybenzoic acid (HBA) and 6-hydroxy-2-naphtoic acid (HNA). Random incorporation of HNA units into poly(HBA) decreases the melting point to 250°C and makes the nematic LC phase thermally accessible.[2] It was first commercialized in 1985 as the **VECTRA®** series of moldable LCPs. Typical poly(HBA/HNA), called as **VECTRA® A950**, is composed of 73 mol % of HBA and 27 mol % of HNA. A tremendous number of research works have been devoted to elucidate the liquid crystalline and crystalline structures and physical properties of **VECTRA® A950**.

The weight-averaged molecular weight (M_w) and the polydispersity of the molecular weight of **VECTRA® A950** have been estimated to be 30000,[3] and 2.45,[4] respectively. And the polymer structure is composed of a random sequence distribution[5-10].

The most important feature of **VECTRA® A950** polyester which is completely different from others is that the component *p*-HBA and HNA units possess electron donating and electron withdrawing groups at the opposite ends. By this reason, the **VECTRA® A950** polyester has a polarization along its long axis as far as it sustains a rigid-like conformation.

In Table 1-1, the dipole moments are elucidated for the monomer, dimer, trimer and tetramer of HBA (the main comonomer unit of **VECTRA® A950;** Equation 1.1),[11,12]

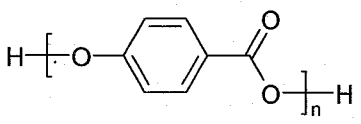

(1.1)

As expected, the largest component of molecular dipole moment is found to be parallel to the chain direction, and it increases in a proportion to the number of monomer units. The average increment per unit is about 2 Debyes so that the polymer with a DP of *n* has a dipole moment of approximately 2*n* Debyes.

It is noteworthy that the hyperpolarizability is relatively large as well.[11] Its value approximates to that of *p*-nitro aniline (refer to the last law of Table 1-1) and increases proportionally with the increase of **n**. It is thus reliable that the present polyester shows the strong SHG, which allows us to make a confident discussion on the polarity.

Table 1-1. Dipole moments (μ) and hyperpolarizabilities (β) calculated for *p*-HBA and *m*-HBA oligomers at B3LYP/6-31G*

	μ /D	β /10^{-30} esu
p-HBA (n = 1)	1.846	3.143
Dimer (n = 2)	4.157	9.096
Trimer (n = 3)	6.486	16.402
Tetramer (n = 4)	8.835	24.411
m-HBA[a]	0.638 – 3.197	0.024 - 1.719
Dimer (n = 2)[a]	1.440 – 2.311	0.501 – 3.506
Trimer (n = 3)[a]	1.564 – 3.501	3.113 – 5.116
p-nitro aniline[b]	7.121	6.798

[a] There are several conformations with similar minimum energies which give different values of μ and β.

[b] listed as a typical compound

1-1-2 Polar Liquid Crystals / Ferroelectric Liquid Crystals

Ferroelectric or polar ordering of molecules in liquid crystals is of considerable theoretical and technological interest.[13] It has been achieved in chiral and tilted smectic phases; the chirality of molecules and their tilted association into the smectic layer, which can reduce the overall symmetry of liquid crystal structure, are essential for their preparation.[14,15]

Recently, the great attention has been directed to the non-chiral ferroelectric system. Watanabe *et al.*[16,17] has proposed that the ferroelectric smectic phase with C_{2v} symmetry can be formed from main-chain liquid crystal polymers if two types of

odd-numbered aliphatic spacers are incorporated into the backbone in a regularly alternate fashion and are segregated into different microdomains. Although the preparation of ferroelectric liquid crystal in this case was failed because of the difficulty in polymer synthesis, the successful progress has been made by treating the banana-shaped molecules and bent dimer molecules.[18-24] In these exotic molecular systems, the ferroelectric and antiferroelectric responses were well identified in a relation to their characteristic packing structures. Bustamante *et al.*[25,26] have also reported the antiferroelectric smectic phase in certain mixtures of non-chiral side-chain polymers and their monomers as observed by pyroelectric and piezoelectric measurements.

The examples mentioned above are so-called improper ferroelectric liquid crystals, which emerge because of the introduction of chirality and the packing of polar bent-core molecules. Another approach to obtain the ferroelectric liquid crystals is based on the idea of proper ferroelectricity, which is realized by dipole-dipole interaction.[27,28] This idea has been suggested by the computer simulation and theoretical calculation. These demonstrate that ferroelectricity appears even in the nematic phase if the constituent rod-like molecules have a large dipole moment.[29-34] By considering the dipole-dipole interaction and hard-core repulsion using a simple mean field model within the Onsager formalism, Lee *et al.*[35,36] presented the phase diagram where the rod-like molecules exhibit conventional isotropic-nematic, nematic-ferroelectric nematic, and direct isotropic-ferroelectric nematic transitions as a function of temperature or pressure. Park *et al.*[34] discussed the same phase transition behavior in the context of the phenomenological theory. It is also worth noting that the isotropic-polar biaxial nematic phase transition in biaxial molecular systems has been

discussed at the phenomenological and molecular levels, suggesting interesting transition behaviors.[37]

These interesting predictions can be experimentally examined using the liquid crystalline aromatic polyesters which assume the rod-like conformation and simultaneously have the large dipole moment along the chain as a result of accumulation of dipole moment of repeating unit. At this aspect, interesting is the X-ray analysis by Coulter *et al.*[38] for the crystal of aromatic polyester based on *p*-HBA. It shows that the polar polymers are packed with a net chain directionality in the crystalline phase. And Watanabe *et al.*[39] confirmed the similar results using high-resolution solid state ^{13}C NMR. The polar crystal phases in a related polyester, **VECTRA® A950** comprising HBA and HNA, has also been suggested by second-harmonic generation (SHG) measurements by Stuetz[40] and Asada.[41] Although these experimental studies have been done for the solid state, it is strongly suggested that the polar ordering has been already formed in the nematic liquid crystals preceding to the crystalline phase. In fact, Watanabe *et al.* have observed strong SHG in the nematic liquid crystal formed on a process of polycondensation reaction of **VECTRA® A950**, furthermore, that polar structure have been formed the biaxilty.[42]

1-1-3 Flow Behavior of Liquid Crystal Polymer

For moldable thermotropic polymer, the share flow behavior is one of most important characterizations. But, the flow behavior of liquid crystalline polymers (LCPs) is certainly very complex to be reflected by their complex structures at both the level of rigid rod like molecules (molecular level) and the polydomain (mesoscopic domain level). Even in the simplest (and most studied) rheological experiment, i.e.,

steady simple share flow, such materials display a variety of peculiar features, many of which are still not completely understood.

LCPs usually show three regions in the shear flow curve[43]: an initial and a terminal shear thinning region at low and high shear rates and an intermediate plateau. The shear thinning at low shear rates is thought to result from the deformation and flow of the texture. The intermediate plateau is associated with tumbling of the molecules. The terminal shear thinning region is assumed to correspond to the development of orientation along the flow direction and the (eventual) degeneration of the texture and the development of a monodomain. These three regions are also shown by the thermotropic LC copolyesters of the **VECTRA®** type, even though they are less well difined[44-46].

Physical quantification for the textured structure of LCP was first introduced by Marucchi [47,48], who defined a characteristic texture length scale α corresponding to the average domain size and suggested a scaling law relating to shear flow strength:

$$\alpha \propto \sqrt{\frac{K}{\eta \cdot \gamma}} \tag{1.2}$$

where K denoted a typical Frank elasticity constant, η the viscosity, and γ the shear rate. The scaling law, Eq (1.2), was derived from the balance of Flank elastic energy density K/α^2 with viscous energy $\eta \cdot \gamma$ during shear flow. This provided only a lumped feature that domain size was decreased with the increase of shear rate. Larson and Doi[49] recently combined the two competing energy densities to produce the following defect density evolution equation:

$$\frac{dL}{dt} = a \cdot \gamma \cdot L - \frac{b \cdot K}{\eta \cdot L^2} \tag{1.3}$$

where the L was defined by $1/\alpha^2$, which meant a net disclination-length per unit volume

of texture, and a and b were dimensionless constants. Equation (1.3) was a tractable equation for the domain size evolution when the shear flow condition was changed. It could satisfy the phenomenological observation of texture evolution under flow such as domain shrinkage after imposition and texture coarsening after shear cessation.

Moreover, Chung *et al.* modified the defect density L, and Newtonian plateau region over very low shear rates, called "region 0" can be predicted[50]. And a "zero" region has also been reported for lyotropic LCPs at very low shear rates, where the viscosity again becomes constant[51].

1-1-4 Thermal Diffusivity

The study of thermal transport properties such as the thermal conductivity and thermal diffusivity of polymeric materials is important because of the crucial role played by these properties in both processing stages and product applications. Recently, electric and electronic apparatuses have been improved of heat from the internal conductor and have been designed to diffuse the heat efficiently. Especially, the conversion efficiencies of electric parts like the higher energy transduction element (for example, Light-Emitting Diode (LED), Photo Voltaic generation (PV), etc) decrease under the higher temperature. So, the materials, which are used in much electric and electronic apparatuses, are required higher thermal conductivity.

Typical thermal conductivity values in W / m K for some common materials are 0.2 – 0.3 for polymers, although crystalline polymers have higher conductivities and diffusivities than amorphous polymers, reflecting the increased order and high density, which provide more optimal pathways for thermal transport. Therefore most polymers are thermally insulating, because any electronic effects like the metallic bond are absent

in polymers and heat conduction occurs as a result of lattice vibrations. In polymers, heat is conducted by two mechanisums.[52] One mode is that molecular transmission or molecule-to-molecule transfer of energy occurs by the excitation of adjacent groups, i.e., by the translation, rotation or vibration of energized groups. Such a process is diffusional in nature and is relatively slow, contributing to the thermal conductivity of an amorphous solid. Another mode is due to the lattice vibration within a crystalline structure (intra molecular), in which thermal excitation creates waves of disturbance often referred to as phonons. This gives rise to a more efficient transfer of heat. In polymers both mechanisms of heat conduction may operate at the same time.

Thermal conductivity (κ) describes the ability of materials to transport heat. The thermal diffusivity (α) is the thermo physical parameter which characterizes the rate of temperature diffusion in the material due to heat flux in the unsteady state heat transfer process and in an important parameter influencing the rate of heating and cooling of solid bodies during the manufacturing process. It is closely related to the thermal conductivity κ according to the following formula (1.4) ,

$$k = \alpha \cdot C_p \cdot \rho \qquad (1.4)$$

where C_p denoted the specific heat capacity at constant pressure, and ρ the specific gravity. Although, C_p is mainly determined by the character of the polymer such as density, the α is determined by the crystallinity and orientation direction of the polymer, that is, the degree of phonon scattering.[53] By this reason, the thermal conductivity of ordered LCPs is 0.4 - 0.5 W / m K, which is higher thermal conductivity among the polymers.

For a further thermal conductivity improvement, one approach to improve the thermal conductivity of polymer is through the addition of a conductive filler material,

such as carbon and metal, [54,55] or polymer blends.[56] On the other hand, another approach to improve the thermal conductivity of polymer tried to control the high-order structure.[57]

1-2 Motivation

VECTRA® A950 is one of most famous thermotropic LCPs. But, there is little thing discussed about the relation between the polar structure and the physical property for **VECTRA® A950**. The SHG-active polar structure is sure to influence the textured structure, furthermore physical properties. If a unique physical property that originated in the polar structure existed, there will be potentials that a furthermore new physical property will be able to be created by controlling the polar structure. This is sure to become important information in the development of LCPs, and I should like to explore a further possibility of a polar nematic LCPs, which to the best of my knowledge has never been examined.

This thesis is intended as an investigation of more detailed polar structure in the nematic liquid crystals of **VECTRA® A950** and in the related polyesters through SHG observation. And the causal relation between the polar structure and the physical property of polar nematic LCPs is considered.

1-3 Objectives and Approach

The subject of this thesis is to elucidate that the head-tail nature influences the textured structure for LCPs. Here I deal with **VECTRA® A950** which is consisted of HBA and HNA (Equation 1.5). And as comparison sample, **VECTRA® A950** is modified using some kind of monomer.

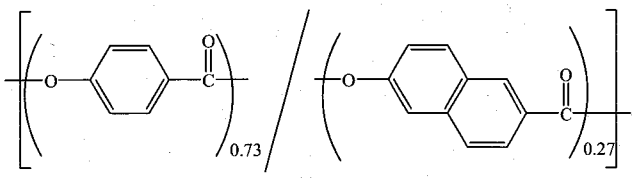

(1.5)

In my study, the degree of molecular orientation is the important factor. Therefore, I tried to straighten the degree of orientation of the sample by giving a constant shearing speed. This highly oriented sample was measured SHG signal and wide-angle X-ray scattering (WAXS). And **VECTRA®** is difficult to dissolve in conventional solvents such as chloroform and tetrahydrofuran, but in specific solvents like pentafluoro phenol(PFP) and 3, 5-bis(trifluoro methyl)phenol (BTFMP). I performed SHG measurement, small-angle laser light scattering (SALS) and polarized optical microscopy (POM) using the amorphous film casted from the dilute LCPs/PFP solution. The variations formed the polar structure during polycondensation and the mechanisms annihilated the disclination from amorphous state are discussed from these measurements. Moreover, it was examined that the melt-viscosity measurement due to suppose the textured structure of LCs, and measured thermal diffusivity of it.

1-4 Organization of the Thesis

This thesis consists of seven chapters. Chapter 1 is the general introduction. In the thesis, followed by the general introduction, through the detailed SHG observation, an unusual physical properties caused by the polar structure is discussed.

In Chapter 2, SHG and steady shear flow viscosities was measured for nematic liquid crystals in the aromatic copolyesters composed of 4-hydroxy benzoic acid (HBA), 6-hydroxy-2-naphthoic acid (HNA), terephthalic acid (TA) and biphenol (BP) whose molar contents are 0.73-**x**, 0.27-**x**, **x** and **x**, respectively. Moreover, the textured

structure in polar LCPs and non-polar ones were estimated by small-angle light scattering.

In Chapter 3, I prepared a modified **VECTRA® A950** including 3-hydroxybenzoic acid (*m*-HBA). SHG measurements are observed for their nematic liquid crystals, compared with LC phase diagram and SHG activity.

In Chapter 4, I performed SHG measurements, steady shear flow viscosity, and transparency measurements for different molecular weight of nematic LC formed by poly(HBA/HNA). Moreover I succeed in the in situ SHG intensity measurement during polymerization for a (HBA/HNA) oligomer, and observed the variation of SH response.

In Chapter 5, it was examined an annealing effect on the mechanically aligned monodomain state of polar nematic liquid crystals and of non-polar one using wide angle X-ray diffraction and polarized optical microscopy. And I expected a possible mechanism from the obtained results.

In Chapter 6, thermal diffusivity was measured for various nematic LCPs, and the relation between the polar structure and the thermal diffusivity was considered.

Chapter 7 will give the conclusions.

Reference

(1) Sawyer, L. C.; Linstid, H. C.; Romer, M. *Plast. Eng. (N.Y.)* **1998**, 54, 37.

(2) Blackwell, J.; Biswas, A. in *Developments in oriented polymers-2*; Ward I. M. Ed.; Elsevier: New York, **1987**, p. 153.

(3) Romo-Uribe, A.; Windle, A. H. *Macromolecules* **1996**, *29*, 6246.

(4) Kromer, H.; Khun, R.; Pielartzik H.; Siebke, W.; Eckhardt, V.; Schmidt, M. *Macromolecules* **1991**, *24*, 1950.

(5) Chivers, R. A,; Blackwell, J. Gutierrez, G. A. *Polymer* **1984**,25, 435.

(6) Blackwell. J.: Gutierrez. G. A.: Chivers. R. **A.** *Macromolecules* **1984**,17,i219.

(7) Blackwell, J.; Biswas, A.; Bonart, R. C. *Macromolecules* **1985**,18, 2126.

(8) Chivers, R. **A.;** Blackwell, J. *Polymer* **1985**,26, 997.

(9) Biswas, **A.;** Blackwell, J. *Macromolecules* **1987**,20, 2997.

(10) Mitchell, G. hell, G. R.; Windle, A. H. *Colloid Polym. Sci.* **1985**, 263,*230.*

(11) Imase, T.; Kawauchi, S.; Watanabe, J. *Mol. Cryst. Liq. Cryst.* **2000**, *346*, 107; *Nonlinear Optics* **2000**, *26*, 91.

(12) Imase, T.; Kawauchi, S.; Watanabe, J. *Macromol. Theory Simul.* **2001**, *10*, 434; *J. Mol. Struct.*, **2001**, *560*, 275.

(13) Goodby, J. W. In *Ferroelectric Liquid Crystals*; Gordon and Breach Press; Philadelphia, **1991**.

(14) Mayer, R. B.; Liebert, L.; Strzelecki, L.; Keller, P. *J. Phys.* **1975**, *36*, L69.

(15) Mayer, R. B. *Mol. Cryst. & Liq. Cryst.* **1977**, *40*, 33.

(16) Watanabe, J. ; Nakata Y. ; Simizu, K. *J. Phys. II, (France)* **1994**, *4*, 581.

(17) Watanabe, J.; Nakata, Y. *Polym. J.* **1997**, *29*, 193.

(18) Niori, T.; Sekine, T.; Watanabe, J.; Furukawa, T.; Takezoe, H. *J. Mater. Chem.* **1996**,

6, 1231.

(19) Niori, T. ; Sekine, T.; Furukawa, T.; Takezoe, H.; Watanabe, J. *Mol. Cryst. Liq. Cryst.* **1997**, *301*, 337.

(20) Sekine, T.; Watanabe, J.; Takanishi, Y.; Niori, T.; Takezoe, H. *Jpn. J. Appl. Phys.* **1997, *6***, L1201.

(21) Niori, T.; Watanabe, J; Choi, .S.W.; Takanishi, Y.; Takezoe, H. *Jpn. J. Appl. Phys.* **1998**, *37*, L401.

(22) Izumi, T.; Kang, S.; Niori, T.; Takanishi, Y.; Takezoe, H.; Watanabe, J. *Jpn. J. Appl. Phys.* **2006**, *45*, 1506.

(23) Izumi, T.; Naitoh, T.; Shimbo, Y.; Takanishi, Y.: Takezoe, H.; Watanabe, J. *J. Phys. Chem. B* **2006,** *110*, 23911.

(24) Takanishi, Y.; Toshimitsu, M.; Nakata, M.; Takada, N.; Izumi, T.; Ishikawa, K.; Takezoe, H.; Watanabe, J.; Takahashi, Y.; Iida, A. *Phys. Rev. E* **2006,** *74*, 051703.

(25)Bustamante, E. A. S.; Yablonskii, S. V.; Ostrovskii, B. I.; Beresnev, L. A.; Blinov, L. M.; Hasse, W. *Chem. Phys. Lett.* **1996**, *260*, 447.

(26)Bustamante, E. A. S.; Yablonskii, S. V.; Ostrovskii, B. I.; Beresnev, L. A.; Blinov, L. M.; Hasse, W. *Liq. Cryst.* **1996**, *21*, 829.

(27) Takezoe, H; Watanabe, J. *Mol. Cryst. Liq. Cryst.* **1999**, *328*, 325.

(28) Blinov, .L. M. *Liq. Cryst.* **1998**, *24*, 143.

(29) Palffy-Muhoray, P.; Lee, M. A.; Petschek, R. G. *Phys. Rev. Lett.* **1988**, *60*, 2303.

(30) Biscarini, F.; Zannoni, C.; Chiccoli, C.; Pasini, P. *Mol. Phys.* **1991**, *73*, 439.

(31) Lee, J.; Lee, S. -D. *Mol. Cryst. & Liq. Cryst.* **1994**, *254*, 395.

(32) Yu, C.-J.; Yu, M.; Lee, S.-D. *Jpn. J. Appl. Phys.* **2002**, *41*, L102-L104.

(33) Terentjev, E.M.; Osipov, M.A.; Sluckin, T.J. *J. Phys. A: Math. Gen.* **1994**, *27*, 7047.

(34) Park, B.; Wu, J. W.; Takezoe, H. *Phys. Rev. E* **2001**, *63*, 21707.

(35) Lee, J.; Lee, S. -D. *Mol. Cryst. & Liq. Cryst.* **1994**, *254*, 395.

(36) Yu, C.-J.; Yu, M.; Lee, S.-D. *Jpn. J. Appl. Phys.* **2002**, *41*, L102-L104.

(37) Mettout, B.; Toledano, P.; Takezoe, H.; Watanabe, J. *Phys. Rev. E* **2002**, 66, 031701-1

(38) Coulter, P. D.; Hanna, S.; Windle, A. H. *Liq. Cryst.* **1989**, *5*, 1603.

(39) Kurosu, H.; Ookubo, ; Tuchiya, H.; Ando, I.; Watanabe, J. *J. Mol. Struct.* **2001**, *574*, 153.

(40) Stuetz, D. E. *U. S. Patent* **1986**, 4 624 872.

(41) Asada, T. *Mol. Cryst. & Liq. Cryst.* **1994**, *254*, 125.

(42) Watanabe, T.; Miyata, S.; Furukawa, T.; Takezoe, H.; Nishi, T.; Migita, A.; Sone, M.; Watanabe, J. *Jpn. J. Appl. Phys.* **1996**, *35*, L505.

(43) Onogi, S. and T. Asada, "Rheology and reho-optics of polymer liquid crystals" in Rheology, Vol.1; Principles, edited by G. Astarita, G. Marrucci, and L. Nicolais (Plenum, New York, **1980**), pp. 127-147.

(44) Giles, D. W.; Denn, M. M. *J. Rheol.* **1994**, 38, 617.

(45) Langelaan, H. C.; Gotsis, A. D. *J. Rheol.* **1996**, 40, 107.

(46) Beekmans, F; Gotsis, A. D.; Norder, B. *J. Rheol.* **1996**, 40, 947.

(47) Marrucci, G. "Remarks on the viscosity of polymer liquid crystals," Proceedings of the Ninth International Congress on Rheology, Acapulco, Mexico, Oct. 8-13, **1984**, pp. 44-448.

(48) Marmcci, G. *Pure Appl. Chem.* **1985**, 57, 1545.

(49) Larson, R.G.; Doi, M. *J. Rheol.* **1991**, 35, 539.

(50) Kim, K. H.; Cho H.; Chung, I. J. *J. Rheol.* **1994**, 38, 1271.

(51) Sigillo, I.; Grizzuti, N. *J. Rheo.* **1994**, 38, 589.

(52) Bala, K.; Pradhan, P. R.; Saxena, N. S.; Saksena, M. P. *Applied Phys.* **1990**, 23, 748.

(53) Hansen, D.; Bernier, G. A. *Polym. Eng. Sci.* **1972**, 12,204.

(54) Rebecca A. H.; Jason M. K.; Julia A. King.;, Jennifer L. H. *J. Appl. Polym. Sci.* **2008**, 100, 2914

(55) Fabien, F.; Devaux, E.; Bourbigot, S; Rumeau, P.; Chapuis, P. -O.; Saha, S. K.; Volz, S. *Thermochim. Acta* **2008**, 477, 25.

(56) Jayasree, T.K.; Predeep, P.; Agarwall, R. Saxene, N. S. *Trends Applied Sci. Res.* **2006**, 3, 278.

(57) Akatsuka, M.; Takazawa, Y. *J. Appl. Polym. Sci.* **2003**, 89, 2464

Chapter 2

Difference in Steady Shear Flow Viscosity between Polar and Non-Polar Nematic Liquid Crystals in Aromatic Polyesters Derived from VECTRA®

Abstract

Steady shear flow viscosities was measured for nematic liquid crystals (LCs) composed of 4-hydroxy benzoic acid (HBA), 6-hydroxy-2-naphthoic acid (HNA), telephthalic acid (TA) and biphenol (BP) whose molar contents are 0.73-**x**, 0.27-**x**, **x** and **x**, respectively. Second harmonic generation (SHG) measurements showed that a SHG-active polar nematic LC formed by poly(HBA/HNA) with **x** = 0 is altered to a conventional non-polar nematic LC with an increase in **x** more than 0.07. The shear-rate dependence of melt viscosity measured for nematic LCs of all the copolymers showed four characteristic regions; a Newtonian plateau in lowest shear-rate region 0 in addition to the well-known three regions. The SHG-activity in nematic LCs reflected on the Newtonian plateau region 0. The viscosity of the SHG-active nematic LCs in this region 0 was 10 times higher than that of the non-SHG-active nematic ones. The higher viscosity of the SHG-active nematic LC was connected to the smaller domain size (or larger number of disclinations) estimated by small-angle light scattering. In the non-polar nematic LC, many disclinations initially formed were easily annihilated because of a coalescence of two disclinations with opposite signs, whereas in the polar nematic LC, such an annihilation hardly occurred because of the polar packing symmetry.

2-1. Introduction

VECTRA® A950 polyester is an extraordinary class of LC polymers, since a head-to-tail connection of HBA and HNA[3-5] results in a large dipole moment along the chain as a result of accumulation of the carbonyl dipole in ester linkage.[6] Because of such a polar rod-like conformation, poly(HBA/HNA) can form the polar nematic LC, which has been experimentally confirmed by second harmonic generation (SHG) measurements[7-10] and predicted by computer simulation and theoretical calculation considering the dipole-dipole interaction.[11-14] Mentioned in Chapter 1, SHG activity appears to only the polymer characterized the head-to-tail structure in a nematic liquid crystal polymer.

Another interesting aspect of nematic LC of poly(HBA/HNA) is observed on the shear-flow behavior. It shows very high shear-flow viscosity of around 10^3 Pa·s at shear rates lower than 10^{-2} s^{-1} while the conventional nematic LC in other commercialized polyesters show the viscosity of around 10^2 Pa·s.[15-17] These two characteristics, SHG-active polar nematic structure and high viscosity at low shear rates, seem to be significantly related to each other.

The head-to-tail character in poly(HBA/HNA), can be eliminated by introduction of symmetrical units of terephthalic acid (TA) and biphenol (BP) which cancels the dipole moments along the chain axis within a polymer chain. I have thus prepared an interesting series of poly(HBA/HNA/TA/BP) polyesters, in which the SHG active and non-active nematic LCs are formed depending on the content of TA and BP. By using this series of polyesters, in this chapter, I observed carefully the steady shear flow viscosity of the nematic LCs in a wide shear-rate range from 10^{-3} to 10^4 s^{-1} and obtained the well-defined viscosity curves which include a Newtonian plateau in lowest shear

rate region (region 0) in addition to the well-known three regions I, II, and III characteristic to the LC polymers.[18] The result indicates that the viscosity in region 0 strongly depends on whether the nematic LC is SHG-active or not whereas the viscosities in regions II and III do not. The viscosity of the SHG active nematic LC in region 0 is 10 times higher than that of the SHG non-active one. This difference in the viscosity of region 0 can be definitely connected to the difference in the domain size (or the number of defects) which is attributed to the difference in the annihilation modes of defects between polar and non-polar nematic LCs.

2-2 Experiment

2-2-1 Materials

VECTRA® A950 comprised of HBA and HNA units with a molar ratio of 73/27, which is commercially available, was supplied by Polyplastics Co. Ltd. In this Chapter, **VECTRA® A950** is treated as a standard polymer, and abbreviated here as **P-Std**.

The copolymers in which terephthalic acid (TA) and biphenol (BP) units were incorporated into **VECTRA® A950** were synthesized by the method according to the applied patent from Celanese.[21] The content of TA or BP that should be equimolar with each other in order to properly perform the polymerization was varied from 0 to 0.1. These copolymers with the following structure,

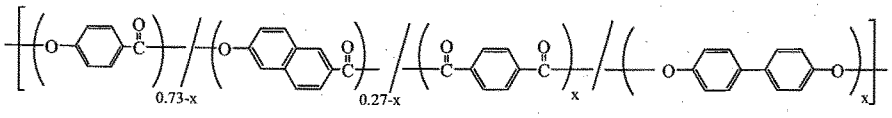

(2-1)

are designated as **P-x** where **x** is the molar content of TA or BP unit.

Inherent viscosities, η_{inh}, and crystal-nematic LC transition temperatures, T_m, of these polymers are listed in third and forth columns in Table 2-1, respectively. Here, η_{inh} of the polymers were measured for solutions of the equivolume mixture of pentafluoro phenol (PFP) and hexafluoro isopropanol (HFIP) at a concentration of 0.1 g dL^{-1} at 30 °C, and T_m was determined by differential scanning calorimetry (DSC) on heating at a rate of 20 °C min^{-1} (TA Instruments DSC Q-1000). At temperatures higher than T_m, all of the polymers were confirmed to form the nematic phase by polarized optical microscopy (Olympus BX 51 equipped with a Mettler FP82HT hotstage) and wide-angle X-ray diffraction (Cu Kα radiation, Rigaku UltraX18 generator equipped with the hotstage). No nematic to isotropic phase transition was observed in a temperature region up to 350 °C.

2-2-2 Methods

SHG measurement: SHG was used as a probe to monitor the spontaneous polarization in the medium.[22] Q-switched Nd:YAG laser light (λ = 1064 nm) was incident perpendicular to thin films with thickness of ~10 μm (illumination area; 0.1mm in diameter) after passing through a quarter-wave plate and a polarizer. SH light (λ = 532 nm) generated was detected by a Hamamatsu model-R955 photomultiplier tube in a transmitted direction after passing through an IR cut filter, an interference filter and an analyzer.

The oriented films with thickness of ~10μm were prepared by drawing out from a slit die (5 mm in wide, 1 mm in length and 10 mm in height) at a rate of 100 mm min^{-1} and pressed at 330 °C. SHG measurements were performed with both the polarizer and analyzer set parallel to the orientation (polymer chain) axis.[7] Relative SHG

intensities for all the **P-x** polymers were determined as a standard of **P-Std** by a contact method where the **P-x** film was contacted with the **P-Std** film and the SH signal intensity was detected by scanning the laser beam from the area of one polymer to that of the other.[7] The values thus determined are listed in fifth column of Table 2-1.

Viscosity measurement: Steady flow viscosity measurements were performed with a Rheometric SR200 equipped with parallel plate configuration with 12.5 mm in radius (R) and 1.5 mm in gap (H) under nitrogen atmosphere. Share rate $\dot{\gamma}$ is calculated by $\dot{\gamma} = (2\pi/60)\cdot(R/H)\cdot n$ where n is a rotational speed of the plate (min^{-1}). To avoid structural changes due to a squeezing flow on loading the sample,[23] powdered samples with the size of a few micrometers were first prepared from pellets and pressed into disc-like form without heating. The disc-like sample was then set between the parallel plates, heated up to 330 °C, and sheared at the lowest shear rate of 10^{-3} s^{-1}. Then, the viscosities were measured with increasing the shear rate up to 10^{2} s^{-1}. The temperature of 330 °C was selected to avoid the crystallization of the sample during measurements, which are completed within 30 min after the loading procedure of about 10 min.

Capillary flow measurements were performed at 330 °C with a Toyo Seiki CAPILLOGRAPH 1B with a capillary with 0.5 mm in diameter and 30 mm in length having a flat entrance angle. Shear rates were varied from 10^{2} to 10^{4} s^{-1}.

Light scattering measurement: Small-angle light scattering patterns were measured by using an Otsuka electric DYNA-3000. Here, the polymers were dissolved in 50/50 v/v mixture of PFP and chloroform, and cast on a slide glass. The film with a thickness of ~10 μm was then rinsed with chloroform and dried under vacuum at 80 °C. The scattering patterns were recorded after annealing the film in nematic LC at 330 °C for 30 min.

2-3 Results

2-3-1 Alteration of SHG-Active to Non SHG-Active Nematic LC by Introducing Symmetrical Comonomer Units into VECTRA® A950

P-x polymer chain loses the head-to-tail nature by an introduction of symmetric BP and TA units so that the resulting nematic LC loses the polarity as well. This trend is clearly observed in fifth column of Table 2-1, and in Figure 2-1 where the relative SHG of the nematic LCs in **P-x** is plotted against the content **x** of TA (or BP). SHG intensity sharply decreases with increasing **x** and becomes zero for **P-x** with **x** more than 0.07, indicating that the perfect alteration from the polar nematic LC to the non-polar (or conventional) one is accomplished on increasing **x** up to 0.07.

2-3-2 Steady Shear Flow Viscosity

Steady shear flow viscosities for nematic LCs of all the prepared polymers were measured at 330 °C by a parallel-plate type of rheometer in a wide shear-rate range from 10^{-3} to 10^{2} s^{-1}. Typical viscosity data (closed circles) are shown in Figures 2-2a - 2-2f. The viscosities were also measured by the capillary rheometer in high shear rate zone from 10^{2} to 10^{4} s^{-1} as shown by open circles. Both methods give the similar shear rate dependences of viscosity. Although the viscosity by the capillary rheometer is relatively larger than that of the rotation rheometer, both values do not need to be equal.

The flow-viscosity curve is well divided into four regions; a Newtonian plateau at the lowest shear-rate regime in addition to three regions which have been well elucidated in LC polymers.[18] Typical example is observed for **P-Std** in Figure 2-2a. On increasing the shear rate ($\dot{\gamma}$), the viscosity takes a constant value at $\dot{\gamma}$ up to 10^{-1} s^{-1} (region 0), and then decreases to one-tenth at $\dot{\gamma}$ from 10^{-1} to 10^{0} s^{-1} (region I). With

further increase of the shear rate, the viscosity becomes almost constant in a shear-rate region of 5×10^0 to 5×10^1 s^{-1} (region II), and then decreases again at $\dot{\gamma}$ larger than 10^2 s^{-1} (region III). Three of these four flow regions, namely regions I, II and III, are designated to keep a correspondence with those defined by Onogi and Asada,[18] and frequently observed in various polymeric LCs. In contrast, the region 0 is rarely observed. Only the observation of region 0 has been reported in a lyotropic LC of hydroxypropyl cellulose/water system.[24] As far as I know, this is the first clear observation of region 0 in thermotropic LC system. All the samples show the similar behavior although the region II becomes narrower or sometimes disappears as **x** increases more than 0.03 as found in Figures 2-2d - 2-2f.

In Figure 2-3, the viscosities in respective regions of 0, II and III are plotted as a function of η_{inh} of polymer. Here, the viscosity measured by the capillary rheometer at a shear rate of 4846 s^{-1} was adopted as the viscosity in region III. The viscosity in region II was determined for only four samples because region II becomes unclear on increasing TA or BP fraction as mentioned above. The viscosities in regions II and III show a simple positive correlation with η_{inh} of polymer, i.e. the molecular weight (see Figures 2-3b and 2-3c). The viscosity in region 0 as shown in Figure 2-3a, however, depends not only on η_{inh}, but also on whether the copolyester is SHG-active or not; the viscosities of the six SHG-active copolyesters are around 10^3 Pa·s, which is ten times larger than those of the four non-SHG-active copolyesters.

2-4 Discussion

First interesting result in this study is that the four characteristic regions were well established in the steady shear flow viscosities of polymeric nematic LCs. In

other words, there are four different shear flow mechanisms. Here, it should be emphasized that the shear has been applied for the polydomain nematic LC the domain size of which is dominated by the number of disclinations.

Previous works[18, 22-25] have shown that in such polydomain LCs the regions I, II and III, have been clearly observed and associated with deformation of LC structures. Two shear-thinning regions I and III separated by intermediate plateau region II are due to the presence of two largely different characteristic times in deformation modes. The shear thinning in the lower shear-rate region I is attributed to the long-range-order elastic deformation of disclinations in polydomain LC whereas the other in highest shear-rate region III is connected to molecular dynamics, the short-range-order elastic deformation of molecular order which produces a uniform molecular orientation.[26] From X-ray patterns taken in respective regions in Figure 2-4, in fact, some orientation of molecules along the shear direction is observed in region I, and then orientation in region III becomes more improved although no orientation can be detected in region 0. Newtonian region II may appear as an intermediate region where the characteristic distance between disclinations decreases on increasing shear rate on the one hand, and the molecules, on the other hand, surely flow. Thus, the three regions I, II and III, are associated with deformation or disturbance of polydomain structure whose length scale is larger with decreasing shear rate.

According to this tendency, the Newtonian plateau appearing in lowest shear-rate region 0 may be associated with flowing of the domains in such a way that an equilibrium defect density or domain size of the polydomain LC remains constant to a certain extent, which has been theoretically described by Chung *et al.*[26] by using the Larson-Doi defect density evolution equation[27] with the inclusion of the defect density

(number density of disclinations) in the initial polydomain LC. At this aspect, it is interesting to refer to the second interesting result that the difference in viscosity of region 0 between the SHG active and non SHG-active polymers can be really connected to the domain size difference. By the optical microscopic observations, all of the polymeric nematic LCs at 330 °C show very fine sanded texture where the disclinations and their related Schlierens tend to be very small and blurred, however the relatively large domain can be recognized in the non SHG-active nematic LCs (see Figure 2-5). The more quantitative analysis for the domain size can be done by small-angle light scattering (SALS) method.[28] The typical SALS patterns are shown in Figures 2-6a – 2-6c. All of the nematic LCs invariantly show four-leaves SALS pattern, but show the different sizes of the pattern which depend on whether the copolymer is SHG active or not. The SHG-active polymers show the scattering patterns expanding into the larger angle region than the non SHG-active polymers, indicating that in the initial polydomain state just before starting the shear flow viscosity measurement, the domain size (or the distances between disclinations) in the SHG active copolymers is smaller than that in non SHG-active ones. The domain sizes determined from the 2θ-intensity profile of Figures 2-6d – 2-6f, are listed in six column of Table 2-1. The domain sizes in the SHG active copolymers are commonly estimated to be about 5 μm, while those in non SHG-active ones are around 10 μm or larger than 10 μm. Such domain sizes can be qualitatively obtained as the distances between the disclinations in microscopic nematic texture in Figure 2-5. Thus, I conclude that the smaller size domains (i.e. the higher defect densities) in the SHG-active nematic LC are attributed to the larger shear-flow viscosity in region 0. This result is interestingly compared with the result obtained for highly concentrated emulsions of the water-in-oil type.[29] In the emulsion

system, flow viscosity curves clearly show a low shear-rate Newtonian region, and its viscosity increases with a decrease in droplet size of emulsions which may be equivalent to the domain size in the present system.

Here, I consider the reason why the SHG active nematic LC, i.e. the polar nematic LC,[10] possesses the high defect densitiy. Generally, the nematic LC may form many kinds of disclinations with various strengths of s = ±1/2, ±1 and so on, immediately after the powder samples are heated up to nematic temperature. The sum of the strengths for all disclinations should be zero. In an initial stage on the nematic LC formation, the number of disclinations would be almost same between the polar and non-polar phases. After a prolonged annealing, however, disclinations of equal and opposite strengths attract one another and are annihilated. One of the examples is shown in Figure 2-7 which illustrates the topological situation near the center of disclinations of |s| = 1/2 showing how the disclination lines of s = +1/2 and s = -1/2 are annihilated.[30] Thus, many of paired disclinations with opposite signs may disappear altogether or form a new one, leading to the development of the large domain texture with low defect density. Without surface anchoring nor external aligning fields, however, an appreciable number of disclinations are still remained in the pseudo-equilibrium state in which size and shape of domain no longer change with time.[30-33]

Such a simple development of domain texture promoted by the director orientation would be unlikely in the case of the polar nematic phase with a low packing symmetry. Figure 2-8 shows various types of disclinations in nematic LCs. When the dipole moment vectors indicated by the arrows are superimposed on the director curves, I know that the disclination lines or points with |s| = 1/2 are not compatible with the polar structure so that those have to escape into the disclinations with |s| = 1.

Further, neighboring disclinations cannot join each other as occasionally as in the non-polar phase, but conversely, the new disclinations have to be created with the simultaneous formation of polar structure following the uniaxial alignment of polymers. This may be a reason why the SHG active polar nematic phase possesses the smaller domains than the SHG non-active one. The detailed examination for the texture development in the polar nematic phase is now proceeding.

2-5 Summary

In this chapter, I prepared poly(HBA/HNA) and poly(HBA/HNA/TA/BP)s with various contents of TA (or BP) up to 0.10, and examined steady shear flow viscosity for their nematic LCs in wide shear-rate range from 10^{-3} to 10^{4} s^{-1}. The SHG-active nematic phase is formed from the standard poly(HBA/HNA), but the SHG activity is lost by an introduction of symmetrical TA (and BP) unit into poly(HBA/HNA) because the polymer chain loses the head-tail character. The shear-viscosity curves of nematic LCs in all these copolymers invariantly show a Newtonian plateau at lowest shear rate (region 0) in addition to three conventional regions, namely low-shear-rate and high-shear-rate shear-thinning regimes (region I and region III) and the intermediate Newtonian plateau (region II). In contrast to regions II and III where the apparent viscosity shows simply positive correlation with the molecular weight, region 0 shows the distinct dependence of the viscosities on the SHG-activity. The viscosity of the SHG active copolymer is 10 times larger than that of the SHG non-active copolymers. This difference in the viscosity is connected to the difference in the domain size measured by the small-angle light scattering method: the domain size in the SHG-active copolymer is smaller than that in the non SHG-active copolymer. The small size of

domains in the SHG-active nematic LC may be caused by its polar structure because the polar symmetry does not allow the simple annihilation for disclinations with respect to the director orientation which has been produced primarily in the powder sample.

References

(1) Sawyer, L. C.; Linstid, H. C.; Romer, M., *Plast. Eng. (N.Y.)* **1998**, 54, 37.

(2) Blackwell, J.; Biswas, A., in *Developments in oriented polymers-2*; Ward I. M. Ed.; Elsevier: New York, **1987**, p. 153

(3) Coulter, P.; Windle, A. H. *Macromolecules* **1989**, *22*, 1129.

(4) Jin, J. -I.; Antoun, S.; Ober, C.; Lenz, R. W. *Br. Polym. J.* **1980**, *12*, 132.

(5) Hummel, J. P.; Flory, P. J. *Macromolecules* **1980**, *13*, 479.

(6) Imase, T.; Kawauchi, S.;Watanabe, *J. Macromol. Theory Simul.*, **2001**,*10*, 434.

(7) Watanabe, T.; Miyata, S.; Furukawa, T.; Takezoe, H.; Nishi, T.; Migita, A.; Sone, M.; Watanabe, J. *Jpn. J. Appl. Phys.* **1996**, 35, L505.

(8) Park, B.; Kinoshita, Y.; Takezoe, H.; Watanabe, J. *Jpn. J. Appl. Phys.* **1998**, *37*, L136.

(9) Yen, C.-C.; Tokita, M.; Park, B.; Takezoe, H.; Watanabe, J. *Macromolecules* **2006**, 39, 1313.

(10) Yen, C.-C.; Taguchi, Y.; Tokita, M.; Watanabe, J. *Macromolecules* **2008**, 41, 2755.

(11) Yu, C.-J.; Yu, M.; Lee, S.-D. *Jpn. J. Appl. Phys.* **2002**, *41*, L102.

(12) Groh, B.; Dietrich, S. *Phys. Rev. E* **1997**, 55, 2892-2901.

(13) Terentjev, E. M.; Osipov, M. A.; Sluckin, T. J. *J. Phys. A* **1994**, 27, 7047-7059.

(14) Biscarini, F.; Zannoni, C.; Chiccoli, C.; Pasini, P. *Mol. Phys.* **1991**, 73, 439-461.

(15) Langelean, H.C.; Gotsis, A.D. *J. Rheol.* **1996**, 40, 107.

(16) Gotsis, A.D.; Baird, D.G. *J. Rheol.* **1985**, 29, 539.

(17) Taguchi, Y.; Tokita, M.; Watanabe, J. unpublished data.

(18) Onogi, S.; Asada, T., in *Proceedings of the VIIIth Inrenlarional Congress on Rheology*, Astarita, G., G. Marrucci, G., Nicolais, L. Eds.; Plenum: New York,

1980; pp. 127-147.

(19) Romo-Uribe, A.; Windle A. H. *Macromolecules* **1996**, *29*, 6246.

(20) Kromer, H.; Khun, R.; Pielartzik H.; Siebke, W.; Eckhardt, V.; Schmidt, M.; *Macromolecules* **1991**, *24*, 1950.

(21) Calundann, G. *U. S. Patent* **1979**, 4 161 470.

(22) Viney, C.; Donald, A. M.; Windle, A. H. *J. Mater. Sci.*, **1983**, *18*, 1136.

(23) Langellan, H. C.; Gotsis, A. D. *J. Rheol.*, **1996**, 40, 107

(24) Sigillo, I.; Grizzuti, N. *J. Rhol.* **1994**, *38*, 589.

(25) Wissbrum, K., *J. Rheol.* **1981**, *25*, 619.

(26) Kim K. M.; Cho, H.; Chung I. J. *J. Rheol.* **1994**, *38*, 1271.

(27) Larson, R.G.; Doi, M. *J. Rheol.* **1991**, *35*, 539.

(28) Hashimoto, T.; Nakai, A.; Shiwaku, T.; Hasegawa, H.; Rojstaczer, S.; Stein, R. S. *Macromolecules*, **1989**, *22*, 422.

(29) Malkin, A.Y.; Masalova, I.; Slatter, P.; Wilson, K. *Rheol Acta*, **2004**, *43*, 584.

(30) Shiwaku, T; Nakai, A; Wang, W; Hasegawa, H; Hashimoto, T; *LIQUID CRYSTALS* **1995**, 19, 679

(31) Saupe, A. Mol. Cryst. Liq. Cryst. **1973**, *21*, 211.

(32) Kleman, M. "*Points, lines and Walls, in Liquid Crystals, Magentic Systems, and Various Ordered Media*", Wiley, Chichester **1983**.

(33) Rey, A.D.; Tsuji, T. *Macromol. Theory Simul.* **1998**, *7*, 623.

Table 2-1. Characterization in a series of **P-x** copolyesters

Sample	Mole fraction of TA unit	η_{inh} /dL g^{-1}	T_m /°C [a]	Relative SHG Intensity	D/μm
P-Std	0	4.67	283	1.00	5.3
P-0.003	0.003	3.46	283	0.78	4.6
P-0.006	0.006	3.91	280	0.63	6.8
P-0.015	0.015	4.26	278	0.42	6.3
P-0.03	0.03	4.38	277	0.05	5.6
P-0.05	0.05	4.23	273	0.03	5.3
P-0.07	0.07	4.14	251	0.00	>10
P-0.08	0.08	3.36	248	0.00	>10
P-0.09	0.09	4.17	248	0.00	>10
P-0.10	0.10	4.31	219	0.00	>10

[a] based on heating DSC data.

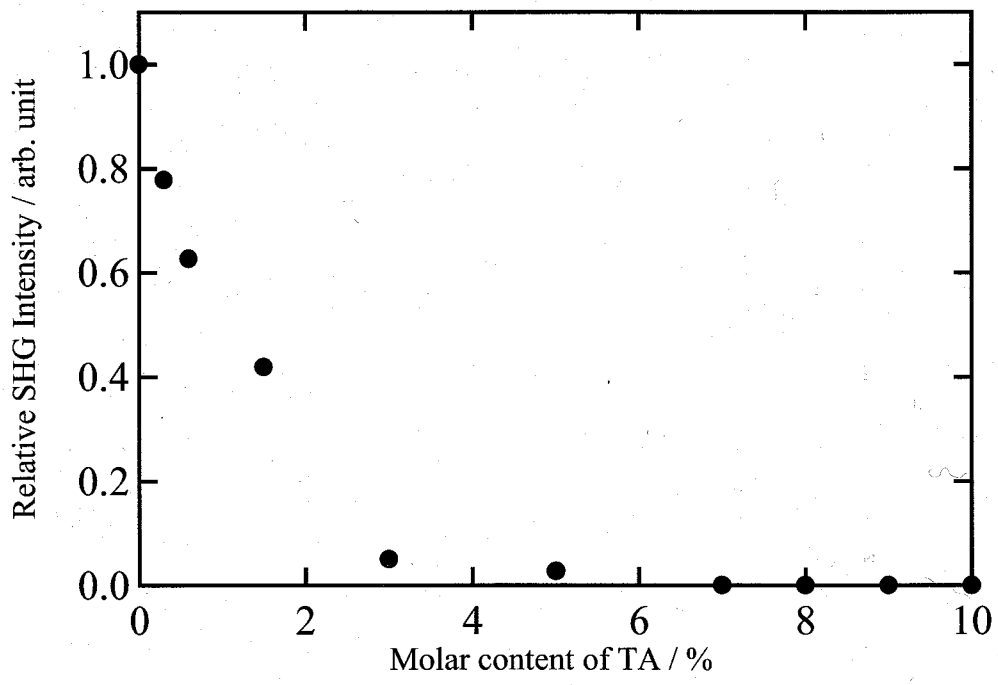

Figure 2-1. Variation of SHG intensity with the molar content of TA (or BP) unit in a series of **P-x** copolyesters. Here, the relative SHG intensity is evaluated as a standard of **P-Std**.

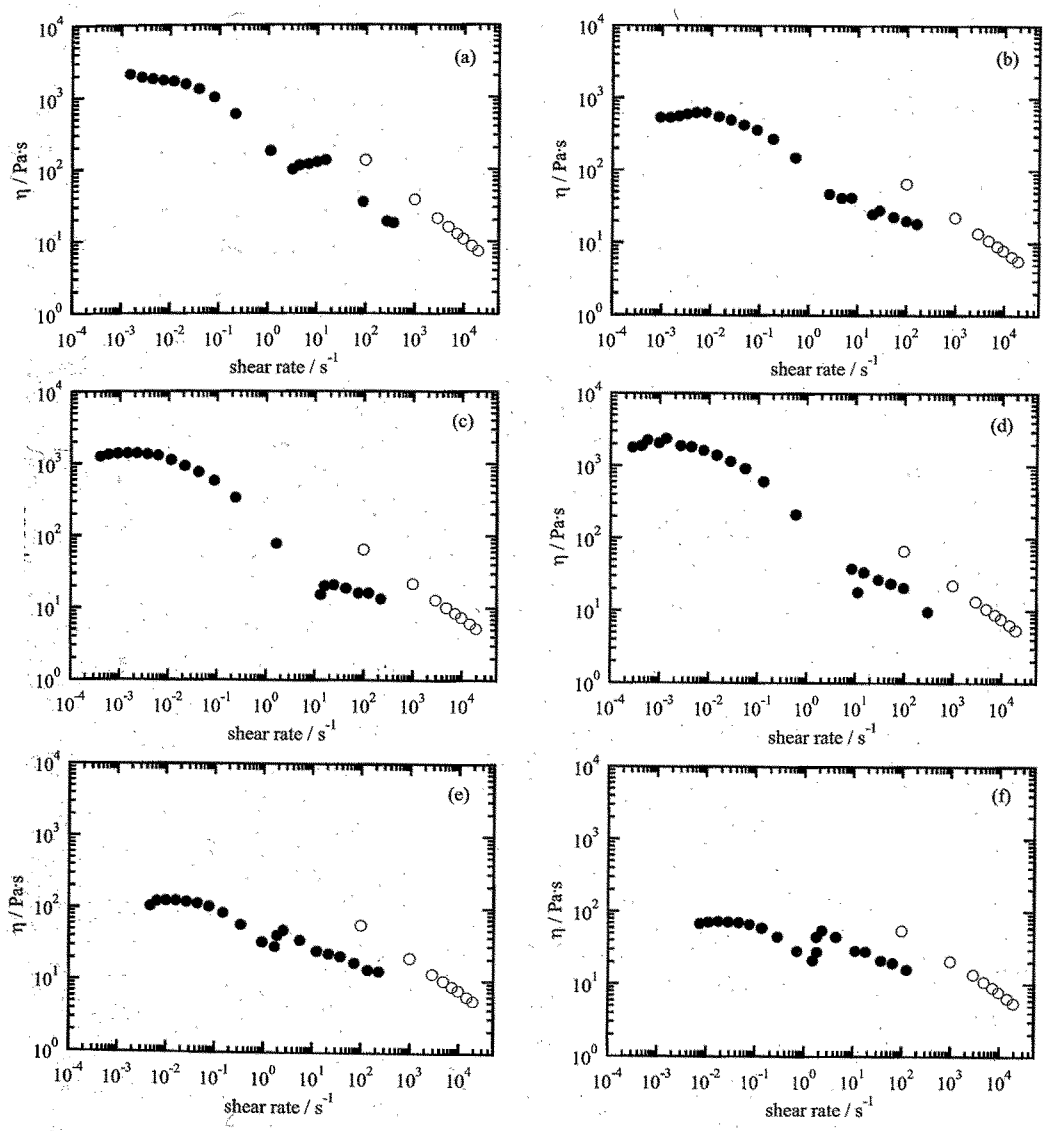

Figure 2-2. Steady-state viscosity for the nematic LCs of (a) **P-Std**, (b) **P-0.015**, (c) **P-0.03**, (d) **P-0.05**, (e) **P-0.08**, (f) **P-0.09** at 330°C. The data presented by closed and open circles are collected by the plate-and-plate rheometer and the capillary rheometer, respectively.

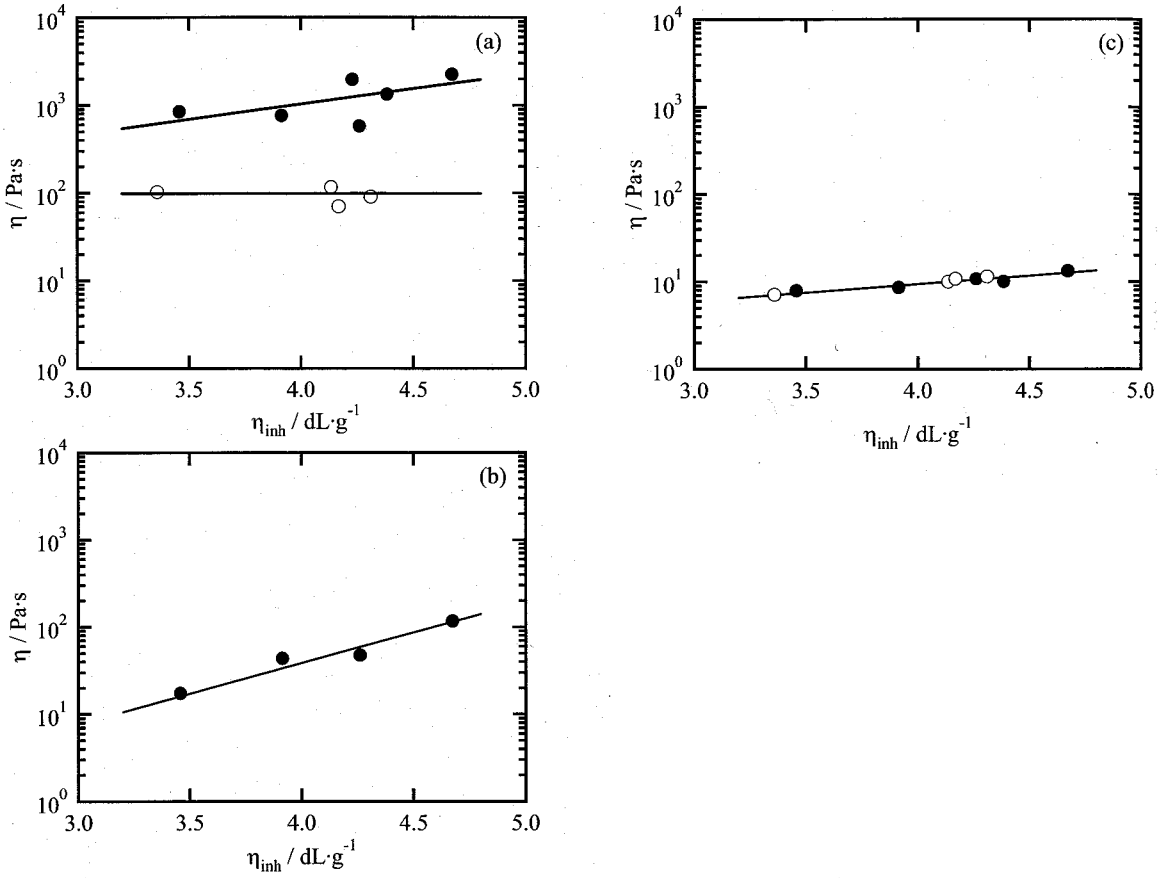

Figure 2-3. Variation of apparent viscosity (a) in the lowest-shear-rate Newtonian plateau (region 0), (b) in the high-shear-rate Newtonian plateau (region II), and (c) at a shear rate of 4864 s^{-1} in high-shear-rate shear-thinning region III with inherent viscosity of copolymers. The applied temperature is 330°C. The viscosities of the SHG-active and non-SHG-active polymers are plotted by closed and open symbols, respectively.

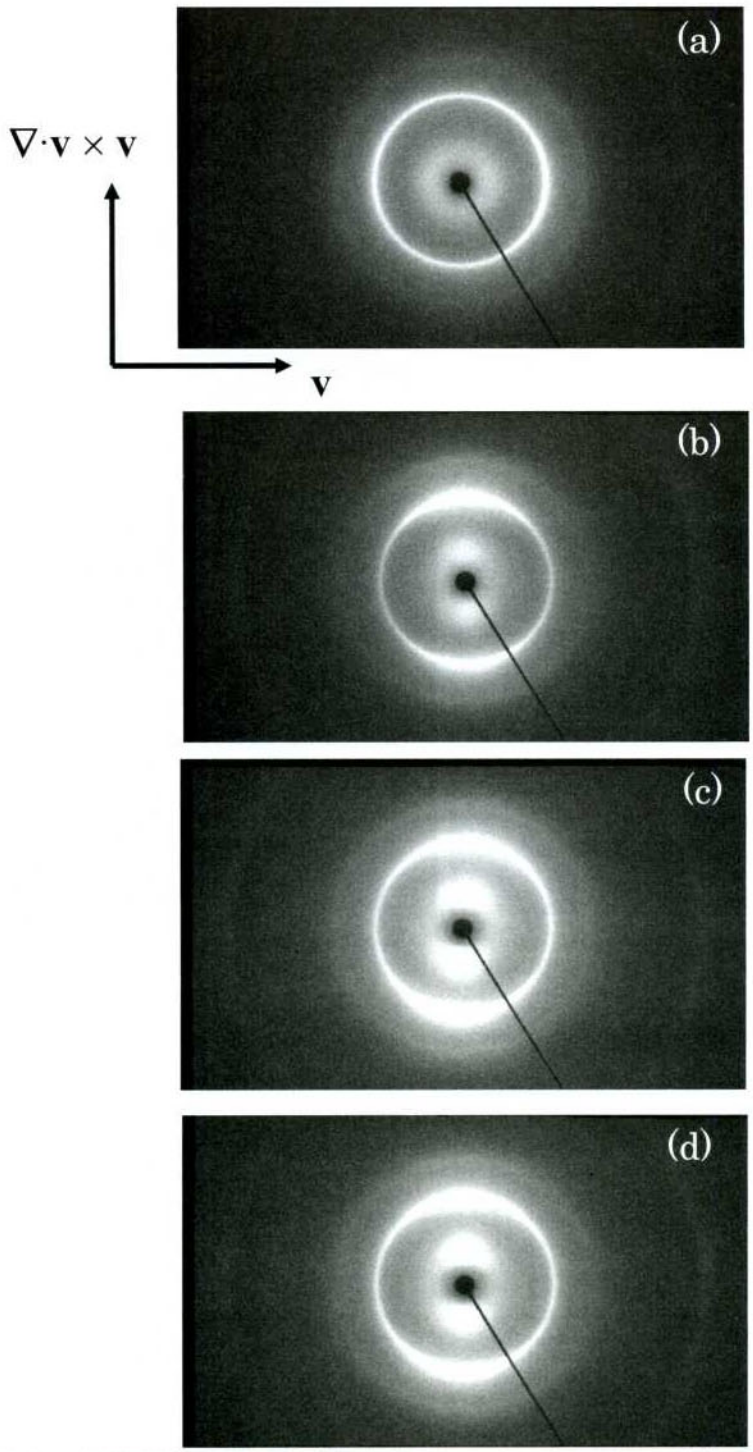

Figure 2-4. WAXD patterns of **P-Std** nematic film sheared by rotational rheometer in regions 0, I, II and III. X-ray beam was irradiated along the velocity gradient ($\nabla \mathbf{v}$) direction. The strong reflection in the central part has a spacing of 4.8 Å, which is attributed to the lateral packing of polymers.

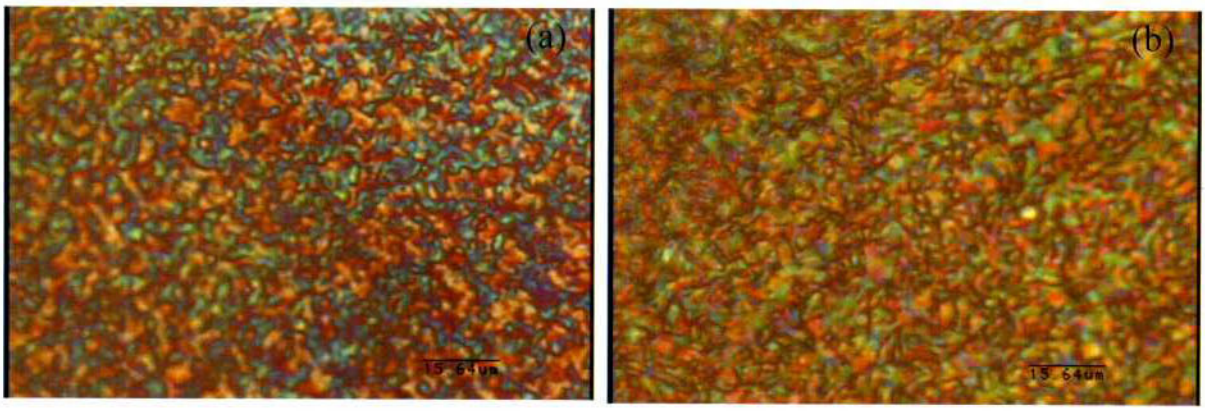

Figure 2-5. Optical microscopic nematic textures of (a) **P-Std** and (b) **P-0.07**. The sample thickness is around 10 μm.

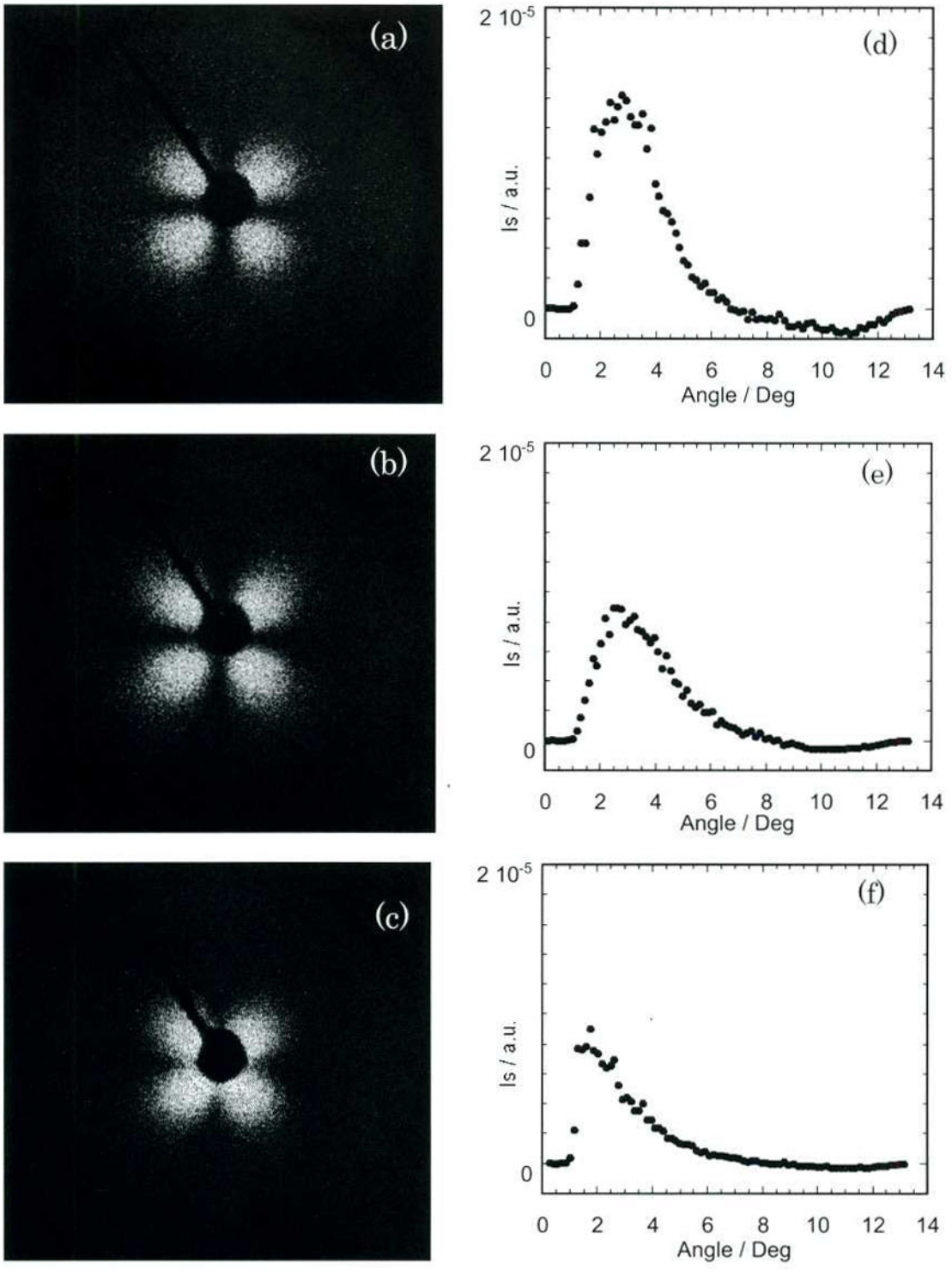

Figure 2-6. (a)~(c) Small-angle light scattering Hv pattern and (d)~(f) its 2-θ intensity profile observed for the nematic LC of (a), (d) **P-Std**, (b), (e) **P-0.05** and (c), (f) **P-0.08** at 330°C.

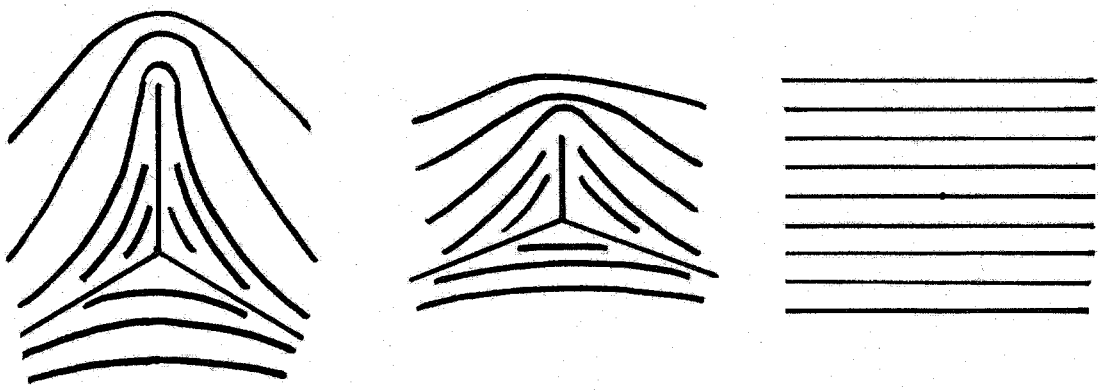

Figure 2-7. Schematic representation of the annihilation microprocess of a pair of s = ±1/2 disclinations and the corresponding variations of the schlieren texture with time in conventional nematic phase. Time is prolonged from left illustration to right

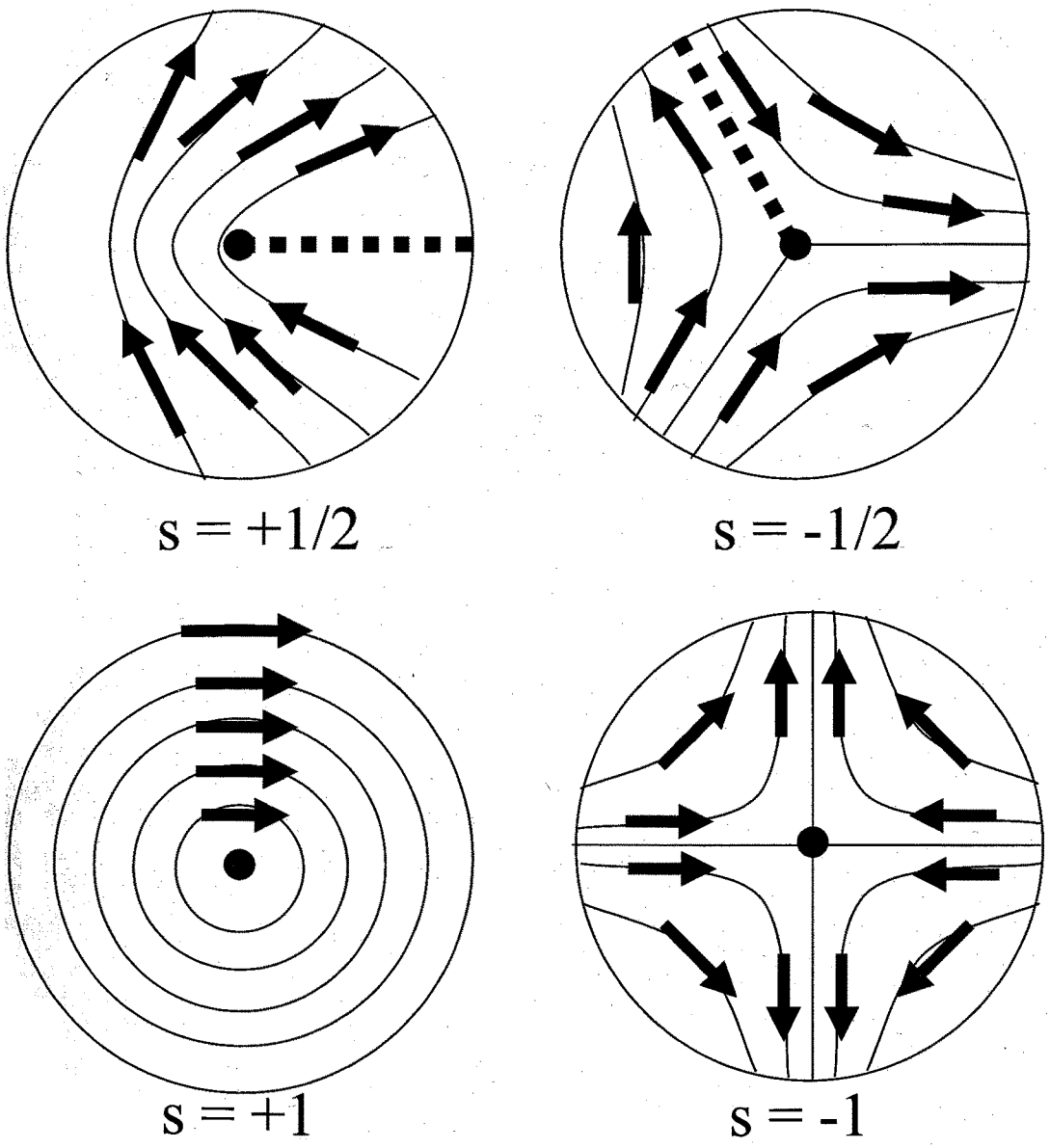

Figure 2-8. Illustration of polar molecules forming the disclinations with s = ±1/2 and ±1 in polar nematic LC. Arrows indicate the dipole moment vectors. It is found that there is an inconsistency (presented by the dashed line) in alignment of dipole moment vectors in disclinations of |s| = 1/2.

Chapter 3

Effect of Kink Conformation on Transition from Biaxial Polar to Uniaxial Polar Nematic Liquid Crystal Polymer

Abstract

I performed second harmonic generation (SHG) measurements in the nematic liquid crystal formed from polar aromatic polyester which comprises 4-hydroxybenzoic acid and 6-hydroxy-2-naphthoic acid in a molar ratio of 73/27. The polymer is commercially available and called **VECTRA® A950**. The shear-oriented nematic liquid crystal of **VECTRA® A950** shows strong SHG mostly along the n-director. From detailed analyses of the SHG intensity profiles measured with combinations of polarizer and analyzer directions to n-director, the nematic liquid crystal is found to possess the C_s packing symmetry, in other words, it is not uniaxial but biaxial and the polarization arises in the symmetry plane.

To search the origin of the spontaneous polarization, I prepared a modified **VECTRA® A950** including 3-hydroxybenzoic acid (*m*-HBA), the head-tail character is not lost, but their liquid crystallinity is destabilized because of kink conformation induced by *m*-HBA unit. In this system, the SHG is invariably observed for the nematic liquid crystals, but as one of the significant effects, polar biaxial nematic liquid crystal of **VECTRA® A950** is altered to the polar uniaxial one by the introduction of *m*-HBA above 5 mol%.

3-1. Introduction

Ferroelectric or polar ordering of molecules in liquid crystals is of considerable theoretical and technological interest.[1] It has been achieved in chiral and tilted smectic phases; the chirality of molecules and their tilted association into the smectic layer, which can reduce the overall symmetry of liquid crystal structure, are essential for their preparation.[2,3]

Recently, the great attention has been directed to the non-chiral ferroelectric system. Watanabe *et al.*[4,5] has proposed that the ferroelectric smectic phase with C_{2v} symmetry can be formed from main-chain liquid crystal polymers if two types of odd-numbered aliphatic spacers are incorporated into the backbone in a regularly alternate fashion and are segregated into different microdomains. Although the preparation of ferroelectric liquid crystal in this case was failed because of the difficulty in polymer synthesis, the successful progress has been made by treating the banana-shaped molecules and bent dimer molecules.[6-12] In these exotic molecular systems, the ferroelectric and antiferroelectric responses were well identified in a relation to their characteristic packing structures. Bustamante *et al.*[13,14] have also reported the antiferroelctric smectic phase in certain mixtures of non-chiral side-chain polymers and their monomers as observed by pyroelectric and piezoelectric measurements.

The examples mentioned above are so-called improper ferroelectric liquid crystals, which emerge because of the introduction of chirality and the packing of polar bent-core molecules. Another approach to obtain the ferroelectric liquid crystals is based on the idea of proper ferroelectricity, which is realized by dipole-dipole interaction.[15,16] This idea has been suggested by the computer simulation and

theoretical calculation. These demonstrate that ferroelectricity appears even in the nematic phase if the constituent rod-like molecules have a large dipole moment.[17-22] By considering the dipole-dipole interaction and hard-core repulsion using a simple mean field model within the Onsager formalism, Lee *et al.*[19,20] presented the phase diagram where the rod-like molecules exhibit conventional isotropic-nematic, nematic-ferroelectric nematic, and direct isotropic-ferroelectric nematic transitions as a function of temperature or pressure. Park *et al.*[22] discussed the same phase transition behavior in the context of the phenomenological theory. It is also worth noting that the isotropic-polar biaxial nematic phase transition in biaxial molecular systems has been discussed at the phenomenological and molecular levels, suggesting interesting transition behaviors.[23]

These interesting predictions can be experimentally examined using the liquid crystalline aromatic polyesters which assume the rod-like conformation and simultaneously have the large dipole moment along the chain as a result of accumulation of dipole moment of repeating unit. Typical monomer units are 4(*para*)-hydroxyl benzoic acid (*p*-HBA) and 6-hydroxyl 2-naphthoic acid (HNA). At this aspect, interesting is the X-ray analysis by Coulter *et al.*[24] for the crystal of aromatic polyester based on *p*-HBA. It shows that the polar polymers are packed with a net chain directionality in the crystalline phase. The polar crystal phases in a related polyester, **VECTRA® A950** comprising HBA and HNA, has also been suggested by second-harmonic generation (SHG) measurements by Stuetz[25] and Asada.[26] Although these experimental studies have been done for the solid state, it is strongly suggested that the polar ordering has been already formed in the nematic liquid crystals preceding to the crystalline phase. In fact, Watanabe *et al.* have observed strong SHG in the nematic

liquid crystal formed on a process of polycondensation reaction of **VECTRA® A950**.[27]

In this chapter, I examine more detailed polar structure in the nematic liquid crystals of **VECTRA® A950** and related polyesters through SHG observation. I examine how chemical modifications to **VECTRA® A950** affect the polar biaxial structure.

3-2. Experiment

3-2-1 Materials

The polymers used are aromatic copolyesters which basically comprise *p*-HBA and HNA units in a molar ratio of 73/27 shown below Equation 3.1.

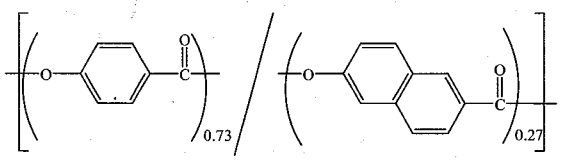

(3.1)

"VECTRA® A950"

This type of copolyester is called "**VECTRA® A950**" which is commercially available. The high molecular weight **VECTRA® A950** as a standard polymer (so named **P-Std**), was prepared by the method according to the applied patent from Celanese.[28] The resulting polymer is not soluble in conventional solvents such as chloroform and tetrahydrofuran, but in specific solvents like pentafluoro phenol (PFP) and hexafluoro isopropanol. The inherent viscosity was measured in a solution of PFP at a concentration of 0.1g/dL at 30 °C. The inherent viscosity of **P-Std** is 4.67 dL/g.

To prepare a homologous series of polymers, 3(*meta*)-hydroxy benzoic acid (*m*-HBA) which works as a kink unit was introduced to **VECTRA® A950**. The molar content of *m*-HBA was ranged from 0 to 100%. These copolymers with the following

structure

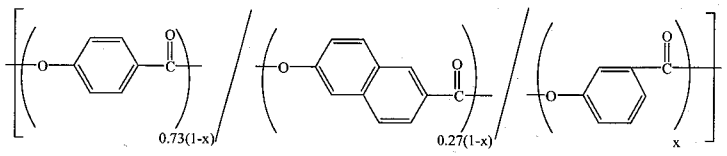

(3.2)

are designated as **M-x** where x is the molar content of *m*-HBA unit. The calorimetric characterization for **M-x** copolyesters are shown in Table 3-1. The inherent viscosities of the second and third series of polymer are around 4 dL/g which are comparable to that of **P-Std**.

3-2-2. Methods

SHG measurement: SHG was used as a probe to monitor the spontaneous polarization in the medium.[22] Q-switched Nd:YAG laser light (λ = 1064 nm) was incident perpendicular to thin films with thickness of ~10 μm (illumination area; 0.1mm in diameter) after passing through a quarter-wave plate and a polarizer. SH light (λ = 532 nm) generated was detected by a Hamamatsu model-R955 photomultiplier tube in a transmitted direction after passing through an IR cut filter, an interference filter and an analyzer.

The oriented films with thickness of ~10μm were prepared by drawing out from a slit die (5 mm in wide, 1 mm in length and 10 mm in height) at a rate of 100 mm min^{-1} and pressed at 330 °C. SHG measurements were performed with both the polarizer and analyzer set parallel to the orientation (polymer chain) axis.[7] Relative SHG intensities for all the **M-x** polymers were determined as a standard of **P-Std** by a contact method where the **M-x** film was contacted with the **P-Std** film and the SH signal intensity was detected by scanning the laser beam from the area of one polymer to that of the other.[7] And in detailed analysis, the SH light intensity was measured as a function of the

rotation angle of the polarizer or analyzer.

Differential scanning calorimetric (DSC) measurements were carried out with a Perkin-Elmer Pyris-1 at a scanning rate of 10°C/min. Wide-angle X-ray diffraction measurements were performed by using a Rigaku-Denki RU-200BH X-ray generator with Ni-filtered CuKα radiation. Polarized optical microscopic (POM) observations were carried out using Olympus BX50. Temperature of sample was controlled within 1°C by using Mettler FP82HT hot stage.

3-3. Results and Discussion

In the a series of **M-x** copolyesters, head-tail nature is retained, but the rod-like nature is lost because of the kink conformation of *m*-HBA when the rich amount of *m*-HBA are introduced. Figure 4.1 shows the phase behavior observed in **M-x** copolyesters. The nematic liquid crystals are uniformly formed in copolymers with the *m*-HBA contents lower than 30 mol%, while it is totally destabilized to transform to the isotropic liquid when the content of *m*-HBA becomes more than 60%. In the polymers with intermediate contents between 30% and 60%, the nematic and isotropic phases coexist. SHG intensities measured for the nematic liquid crystals are plotted against the mole fraction of *m*-HBA in Figure 4.2. One can see that the SHG intensity decreases with the molar content of *m*-HBA through four steps; the first step in a region of 0 to 3%, the second in a region of 4 to 5% , the third in a region of 5-30% and the fourth in a region of 30 to 60%. It is obvious that the decrease of SHG intensity at the fourth step is caused by the decrease in the relative volume of nematic phase to the isotropic one. Besides, it is reasonable that the SHG intensity in the nematic field steadily decreases with the increase of *m*-HBA content since the hyperpolarizability of

m-HBA is relatively smaller than that of *p*-HBA, as calculaed in Table 1.1.

A simple question arises. Why does the SH intensity decrease steeply in a limited region of 4 to 5%? To clarify this point, the packing symmetry was examined for oriented nematic liquid crystal by measuring the dependences of SH intensity on polarizer and analyzer angles. Figure 4.3 shows the content dependence of $I(\phi_p, 90°)$ profiles observed for the copolyesters with the *m*-HBA contents of 0 to 20%. One can find two-leaves pattern is altered to the four-leaves pattern when the mole fraction of *m*-HBA is increased from 3 to 5%. This means that the C_s symmetry is altered to the $C_{\infty v}$, in other words, the polar biaxial nematic liquid crystal is altered to the polar uniaxial one. The remarkable reduction of SHG at the second step is thus attributable to the loss of the polarization in one of the axes. Possibly, the conformational disordering enhanced by *m*-HBA kink unit may overcome the strongly correlated field which forces the *p*-HBA and HNA chains to assume the unusually confined conformation with the polarization perpendicular to the chain axis.

According to the conformational analysis by density functional theory (DFT) calculation,[29] Ph-C(=O)-O are confined on the same plane. With respect to O-Ph bond, there are two possible conformations with lowest energy. One conformation has 60° and another has 120° as an angle between the adjacent Ph-C(=O)-O planes. In Figure 3-4(a), the biaxial polar packing structure is illustrated by selecting one of the possible conformations, in which all the carbonyl groups are directed to the similar direction as an average, to produce the polarization along a perpendicular direction to the polymer chain as well as in the parallel direction. Here, ones would hardly believe that such a confined conformation is sustained in fluid nematic field since the potential energy barrier around O-Ph is fairly low (less than 1 kcal/mol) so that this bond can rotate

somewhat freely between two confomers.[29] Thus, I have to consider that the unusual conformational confinement would be caused by the strongly correlated dipole-dipole interaction field. It should be noted that the specific conformation of **VECTRA® A950** has also been suggested by NMR[30] and fluorescence data.[31] Similarly, the uniaxial polar packing structure (in Figure 3-4(b)) and the non-polar one (in Figure 3-4(c)) are illustrated by selecting one of the possible conformations. In the uniaxial polar packing, one polar axis is along the polymer chain axis only, but the carbonyl groups are undirected to the similar direction due to kink conformation for *m*-HBA, also even in the strongly correlated dipole-dipole interaction field. And in non-polar packing, the polar axis doesn't exist because the dipole moment is canceled by TA or BP.

3-4. Summary

In summary, SHG activity is lost by the chemical modification to destabilize the liquid crystallinity of **VECTRA® A950**. Further, introduction of kink conformation alters the C_s symmetry to $C_{\infty v}$ one. These effects obviously show that the polar C_s symmetry determined by SHG profiles is not of artificial.

The C_s symmetry is very significant since it requires the nematic liquid crystal of **VECTRA® A950** to possess the biaxiality. Generally, the biaxial nematic liquid crystal is expected for the board like shaped molecules.[48-53] In addition, the C_s symmetry requires another significant conformational constraint for each polymer chain; the polymer must take up a type of conformation which produces the polarization perpendicular to the chain axis. These two requirements are satisfied if the ester carbonyl groups are sticking out to similar direction as an average as illustrated in Figure

3-4(a) although at a general sense, such a peculiar conformation of aromatic polyesters is hardly accepted in a fluid field. This unusual conformational constraint suggests that the strongly correlated dipole-dipole interaction field may act not only in the parallel direction to the polymer chain, but also in the perpendicular one.[23] On the other hand, in case of uniaxiality, one polar axis is along the polymer chain axis only, but the carbonyl groups are undirected to the similar direction due to kink conformation for *m*-HBA, also even in the strongly correlated dipole-dipole interaction field, as illustrated in Figure 3-4(b). And as introducing TA and BP, the polar axis doesn't exist because the dipole moment is canceled by TA or BP, as illustrated in Figure 3-4(c).

Finally, it should be noted that I have never succeeded to obtain the macroscopically oriented polarization over the sample, which is the direct proof of the spontaneous polarization. The nematic liquid crystals can not respond to the applied electric field since the polymeric nematic liquid crystal is highly viscous. Especially, the viscosity of the nematic **VECTRA®** is extremely high probably due to the biaxiality.

References

1) Goodby, J. W. In *Ferroelectric Liquid Crystals*; Gordon and Breach Press; Philadelphia, 1991.

2) Mayer, R. B.; Liebert, L.; Strzelecki, L.; Keller, P. *J. Phys.* **1975**, *36*, L69.

3) Mayer, R. B. *Mol. Cryst. & Liq. Cryst.* **1977**, *40* , 33.

4) Watanabe, J. ; Nakata Y. ; Simizu, K. *J. Phys. II*, (*France*) **1994**, *4*, 581.

5) Watanabe, J.; Nakata, Y. *Polym. J.* **1997**, *29*, 193.

6) Niori, T.; Sekine, T.; Watanabe, J.; Furukawa, T.; Takezoe, H. *J. Mater. Chem.* **1996**, ***6***, 1231.

7) Niori, T. ; Sekine, T.; Furukawa, T.; Takezoe, H.; Watanabe, J. *Mol. Cryst. Liq. Cryst.* **1997**, *301*, 337

8) Sekine, T.; Watanabe, J.; Takanishi, Y.; Niori, T.; Takezoe, H. *Jpn. J. Appl. Phys.* 1997, ***6***, L1201.

9) Niori, T.; Watanabe, J; Choi, .S.W.; Takanishi, Y.; Takezoe, H. *Jpn. J. Appl. Phys.* **1998**, *37*, L401.

10) Izumi, T.; Kang, S.; Niori, T.; Takanishi, Y.; Takezoe, H.; Watanabe, J. *Jpn. J. Appl. Phys*. **2006**, *45*, 1506.

11) Izumi, T.; Naitoh, T.; Shimbo, Y.; Takanishi, Y.: Takezoe, H.; Watanabe, J. *J. Phys. Chem. B* **2006,** *110*, 23911.

12) Takanishi, Y.; Toshimitsu, M.; Nakata, M.; Takada, N.; Izumi, T.; Ishikawa, K.; Takezoe, H.; Watanabe, J.; Takahashi, Y.; Iida, A. *Phys. Rev. E* **2006,** *74*, 051703.

13) Bustamante, E. A. S.; Yablonskii, S. V.; Ostrovskii, B. I.; Beresnev, L. A.; Blinov, L. M.; Hasse, W. *Chem. Phys. Lett.* **1996**, *260*, 447.

14) Bustamante, E. A. S.; Yablonskii, S. V.; Ostrovskii, B. I.; Beresnev, L. A.; Blinov, L.

M.; Hasse, W. *Liq. Cryst.* **1996**, *21*, 829.

15) Takezoe, H; Watanabe, J. *Mol. Cryst. Liq. Cryst.* **1999**, *328*, 325.

16) Blinov, .L. M. *Liq. Cryst.* **1998**, *24*, 143.

17) Palffy-Muhoray, P.; Lee, M. A.; Petschek, R. G. *Phys. Rev. Lett.* **1988**, *60*, 2303.

18) Biscarini, F.; Zannoni, C.; Chiccoli, C.; Pasini, P. *Mol. Phys.* **1991**, *73*, 439.

19) Lee, J.; Lee, S. -D. *Mol. Cryst. & Liq. Cryst.* **1994**, *254*, 395.

20) Yu, C.-J.; Yu, M.; Lee, S.-D. *Jpn. J. Appl. Phys.* **2002**, *41*, L102-L104.

21) Terentjev, E.M.; Osipov, M.A.; Sluckin, T.J. *J. Phys. A: Math. Gen.* **1994**, *27*, 7047.

22) Park, B.; Wu, J. W.; Takezoe, H. *Phys. Rev. E* **2001**, *63*, 21707.

23) Mettout, B.; Toledano, P.; Takezoe, H.; Watanabe, J., *Phys. Rev. E*, **2002**, 66, 031701-1.

24) Coulter, P. D.; Hanna, S.; Windle, A. H. *Liq. Cryst.* **1989**, *5*, 1603.

25) Stuetz, D. E. *U. S. Patent* **1986**, 4 624 872.

26) Asada, T. *Mol. Cryst. & Liq. Cryst.* **1994**, *254*, 125.

27) Watanabe, T.; Miyata, S.; Furukawa, T.; Takezoe, H.; Nishi, T.; Migita, A.; Sone, M.; Watanabe, J. *Jpn. J. Appl. Phys.* **1996**, *35*, L505.

28) Calundann, G. *U. S. Patent* **1979**, 4 161 470.

29) Imase, T.; Kawauchi, S.; Watanabe, J. *Macromol. Theory Simul.* **2001**, *10*, 434; *J. Mol. Struct.*, **2001**, *560*, 275.

30) Kurosu, H.; Ookubo, ; Tuchiya, H.; Ando, I.; Watanabe, J. *J. Mol. Struct.*, **2001**, *574*, 153.

31) Uchida, Y.; Huang, H. W.; Horie, K.; Qing, L.Y.; Tuchiya, H.; Watanabe, J. *J. Polym. Sci.: Part B: Polym Phys.*, **2000**, *38*, 2922.

32) Luckhurst, G. R. *Thin Solid Films*, **2001**, *393*, 40.

33) Chandrasekhar, S.; Nair, Greetha G.; Rao, Shankar D.S., Prasad, S.; Krishna, Praefcke, K.; Blunk, D. *Liq. Cryst.*, **1998**, *24*, 67.

34) Pratibha, R.; Madhusudana, N.V.; Sadashiva, B.K. *Science*, **2002**, *288*, 2184.

35) Acharya, B.R.; Primak, A.; Dingemans, T.J.; Samulski, E.T.; Kumar, S. *Pramana*, **2003**, *61*, 231.

36) Acharya, B.R.; Primak, A.; Kumar, S. *Phys. Rev. Lett.* **2004**, *92*, 145506.

37) Fu, K.; Sone, M.; Tokita, M.; Watanabe, J. *Polymer J.*, **2006**, *38*, 1.

Table 3-1. Characterization in a series of **M-x** copolyestrs

Calorimetric Data[a]				
	Transition temperatures			Enthalpy of fusion[b]
	heating process		cooling process	
	T_g/°C	T_m/°C	T_i/°C	ΔH_i/KJ·mol^{-1}
Poly(HBA/HNA)		283	238	1.9
Poly(HBA/HNA/*m*-HBA)				
Molar content of *m*-HBA				
0.01	-	271	223	1.7
0.02	102	270	218	1.4
0.03	100	266	213	0.5
0.04	95	252[c]	202	1.2
0.05	99	259[c]	197	0.97
0.1	98	240[c]	183	0.97
0.2	101	236	-	-
0.3	100	-	-	-
0.4	105/121	-	-	-
0.5	112/137	-	-	-
0.6	134	-	-	-
0.7	140	-	-	-
0.8	133	-	-	-
0.9	131	-	-	-
1	125	-	-	-

[a] Based on DSC data measured at a rate of 10°C/min .

[b] Based on cooling DSC data

[c] Based on lower transition temperature in heating process

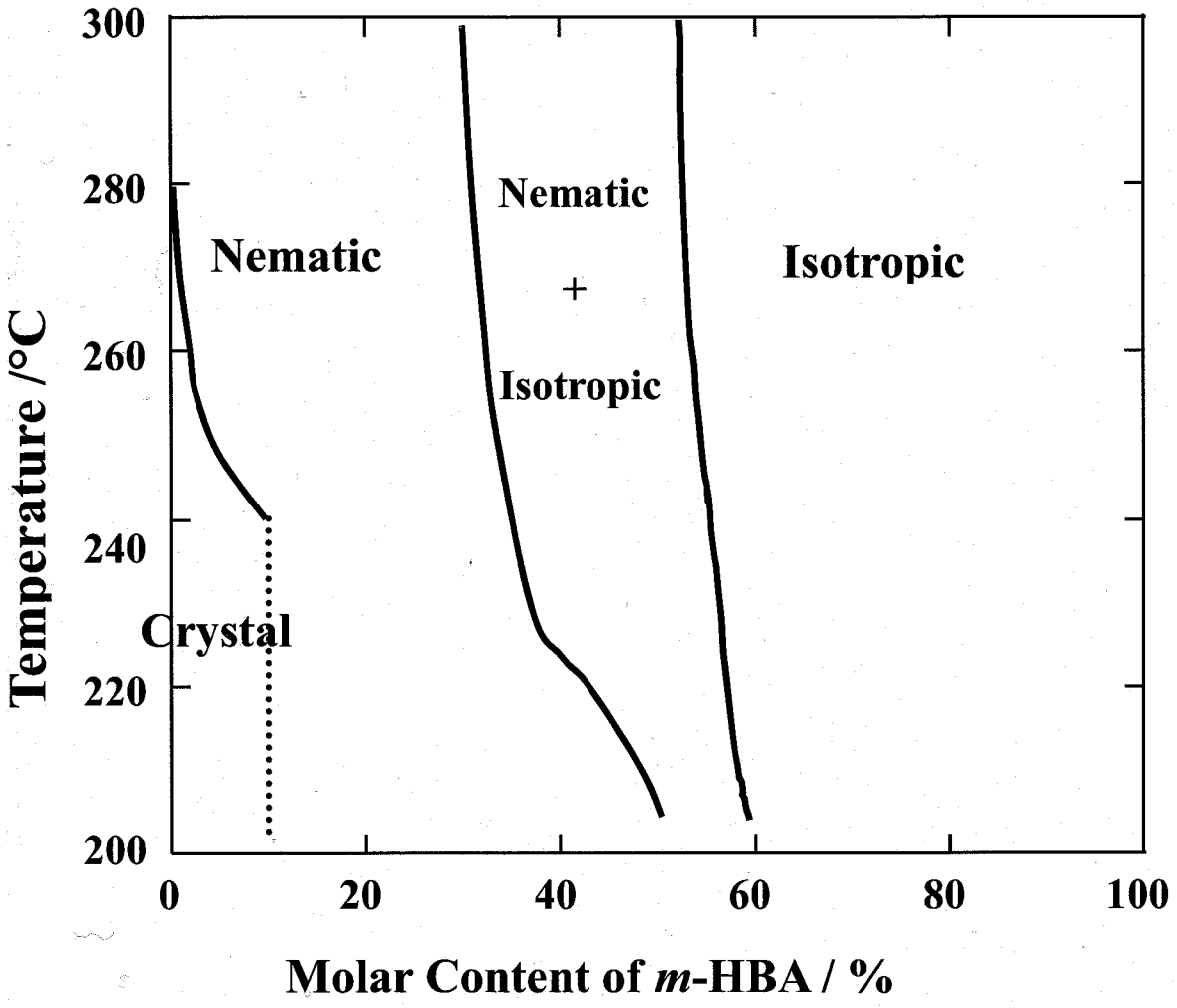

Figure 3-1. Phase behavior observed as a function of the molar content of *m*-HBA unit in a series of **M-x** copolyesters.

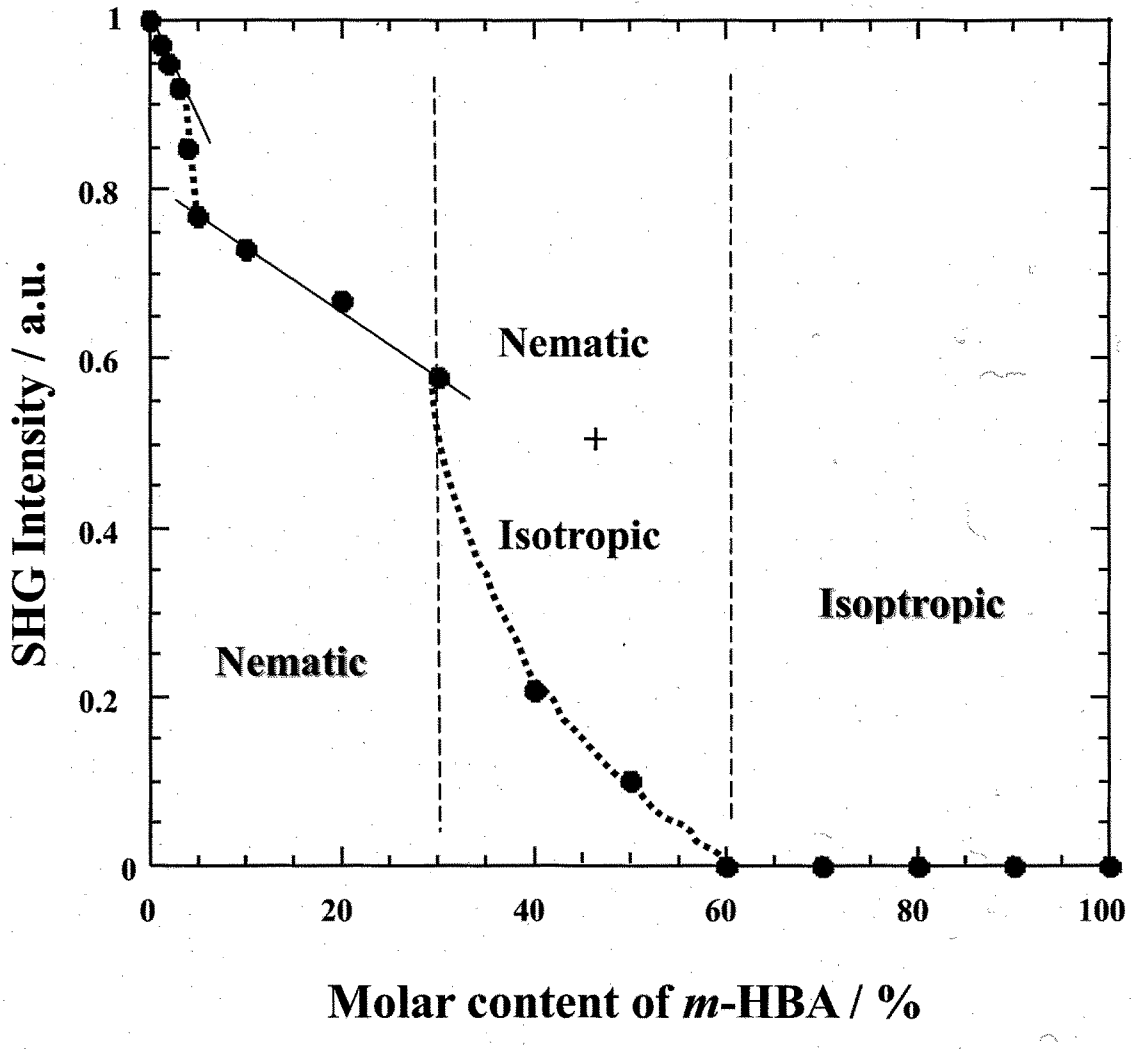

Figure 3-2. Variation of SH intensity with the molar content of *m*-HBA unit in a series of **M-x** copolyesters.

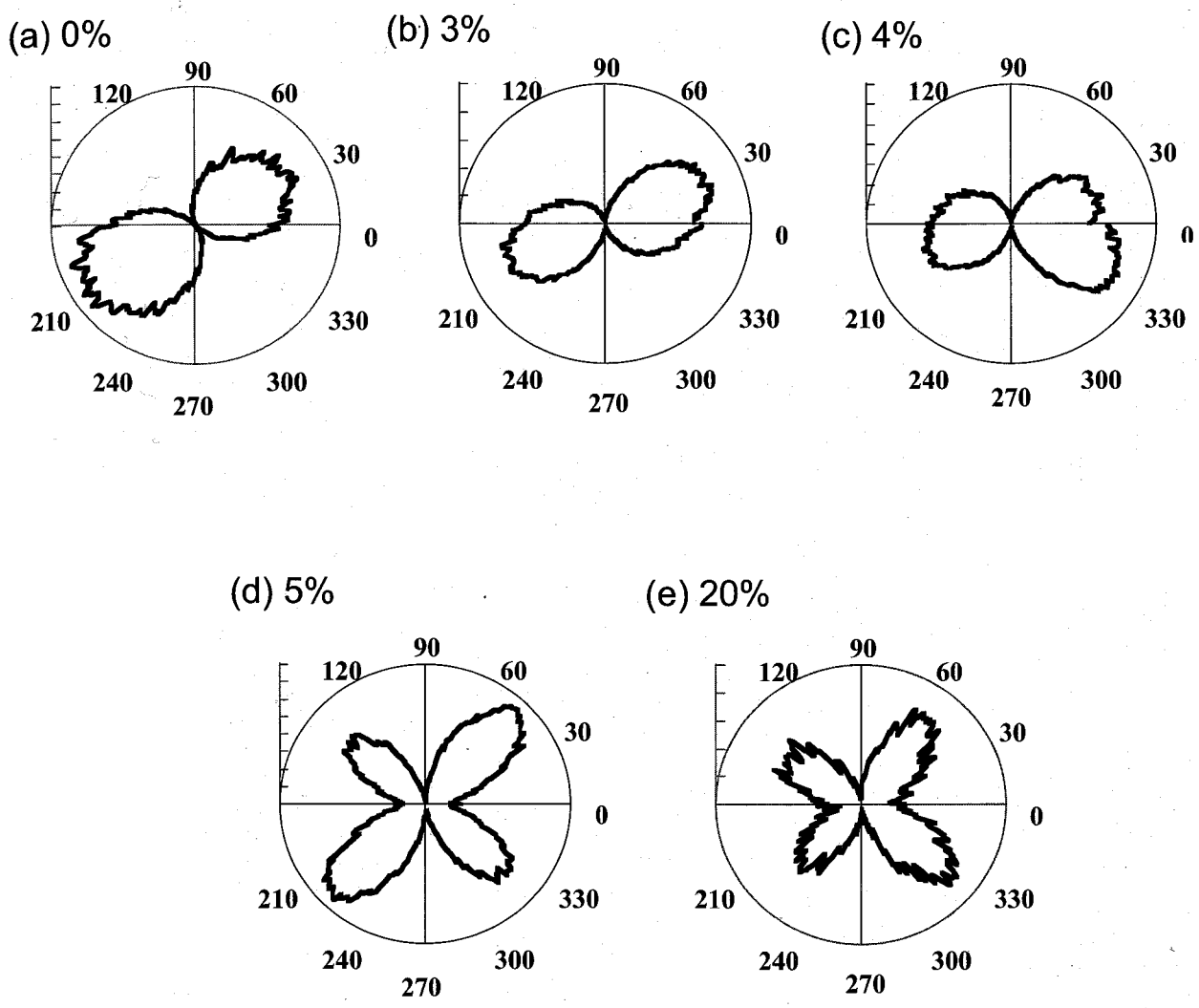

Figure 3-3. SHG profiles, $I(\phi_p, 90°)$, varied with mole fraction of *m*-HBA in a series of **M-x** copolyesters.

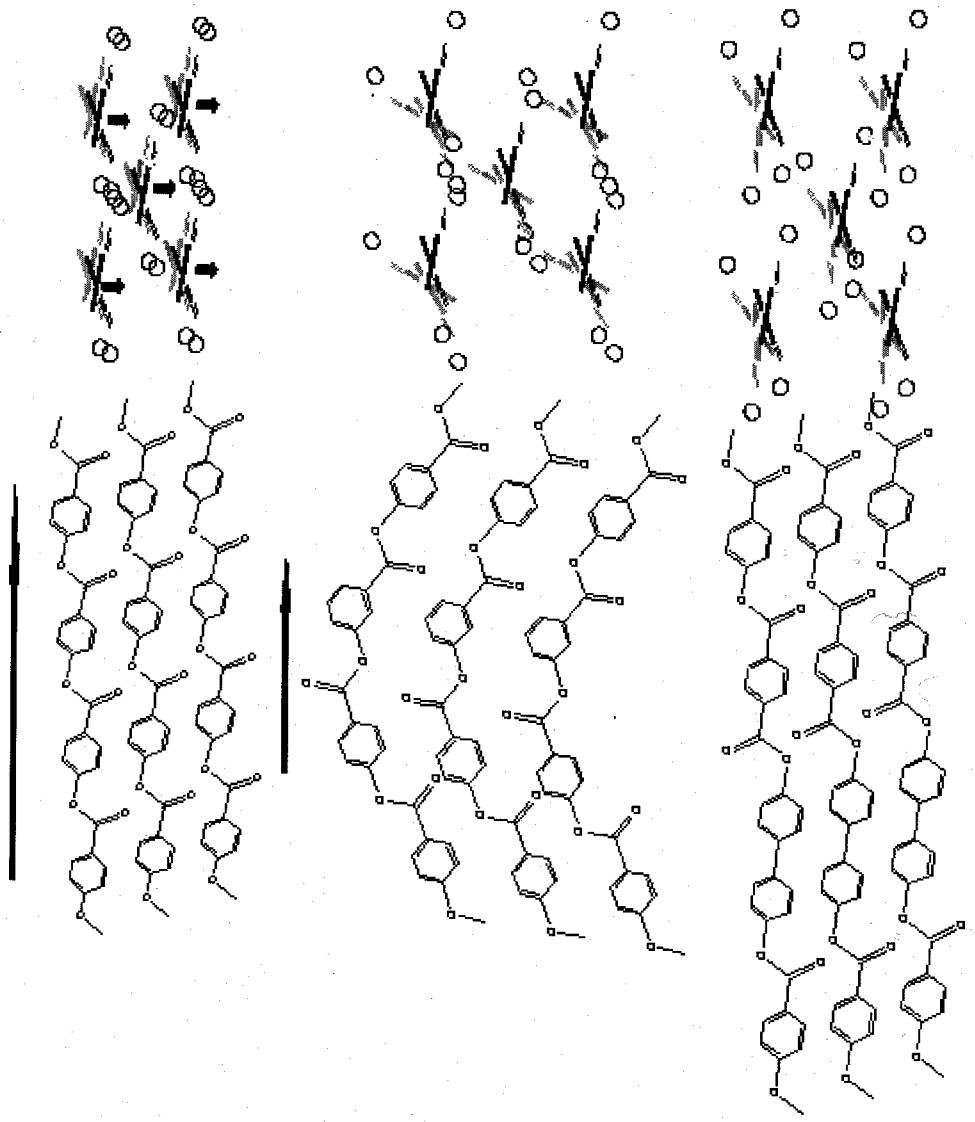

Figure 3-4. (a) Illustration of polar nematic liquid crystal with Cs symmetry which satisfies the SHG data for **P-Sdt**. The nematic liquid crystal should be biaxial and both axes should be polar as schematically illustrated in (a). (b) Illustration of polar nematic liquid crystal with $C_{\infty v}$ symmetry which satisfies the SHG data for **M-x** above **x** 0.05. The nematic liquid crystal should be uniaxial and molecular axes should be polar as schematically illustrated in (b). (c) Illustration of non-polar nematic liquid crystal for **P-x** above **x** 0.07. The nematic liquid crystal shouldn't be polar axis as schematically illustrated in (c).

Chapter 4

Effect of Molecular Weight on Transition from Non-Polar to Biaxial Polar Nematic Liquid Crystal Polymer

Abstract

I performed second harmonic generation (SHG) measurements, steady shear flow viscosity, and transparency measurements for different molecular weight of nematic LC formed by poly(HBA/HNA). With increasing molecular weight, SHG intensity increased steeply, but at around 2.2dL/g, it changed a sudden dip. This time, polar structures transfered from uniaxiality to biaxiality. At the same time the transparency also changed at this η_{inh} region. Moreover I succeed in the in situ SHG intensity measurement during polymerization from a (HBA/HNA) oligomer, and the alternation in SHG intensity became a similar tendency to it in the polymer of different molecular weight. The melt viscosity measured for these nematic LCPs showed the Newtonian plateau region 0, which is affect with domain size (or larger number of disclinations). The melt viscosity on region 0 of biaxial polar nematic LCPs was 5 times higher than that of uniaxial polar nematic LCPs. These results mean that the number of disclinations decreased, accordingly the polar structure changes from biaxial polar nematic LCPs to uniaxial polar ones.

4-1 Introduction

Aromatic polyesters are most important class of thermotropic liquid crystal polymers (LCPs). They show outstanding physical properties and excellent chemical resistance suitable for commercial applications in electronics, automotive and aerospace industries as well as in medical fields.[1] Typical thermotropic LC polyester is a copolymer composed of 4-hydroxybenzoic acid (HBA) and 6-hydroxy-2-naphtoic acid (HNA). Random incorporation of HNA units into poly(HBA) decreases the melting point to 250°C and makes the nematic liquid crystal (LC) phase thermally accessible.[2] It was first commercialized in 1985 as the **VECTRA®** series of moldable LC polymers. Typical poly(HBA/HNA), called as **VECTRA® A950**, is composed of 73 mol % of HBA and 27 mol % of HNA.

VECTRA® polyester is an extraordinary class of LCPs, since a head-to-tail connection of HBA and HNA [3-5] results in a large dipole moment along the chain as a result of accumulation of the dipole moment of the carbonyl group. Because of such a polar rod-like conformation, poly(HBA/HNA) can form the polar nematic LCP, which has been experimentally confirmed by second harmonic generation (SHG) measurements[6-10] and predicted by computer simulation and theoretical calculation considering the dipole-dipole interaction.[11-14] Another interesting aspect of nematic LC of poly(HBA/HNA) is observed on the shear-flow behavior.[15] I have already reported these two characteristics, a SHG-active polar nematic structure and high viscosity at low shear rates, seem to be significantly related to each other in poly(HBA/HNA/TA/BP) system in Chapter 2 and previous paper.[15]

In this chapter, I examined the SHG measurement for different molecular weight of poly(HBA/HNA). The most interesting result is that, with increasing molecular weight, the polar structures of these LCPs transferred from uniaxiality to biaxiality. By this alternation of polar structure, the transparency was lower, and the steady shear flow viscosity of region 0 of biaxial polar nematic LCPs was 5 times higher than that of uniaxial polar ones. Moreover this transition was appeared in the in situ observation of SHG intensity during polymerization from the (HBA/HNA) oligomer. I found that this difference in the viscosity of region 0 can be connected to the difference in the domain size, mentioned in Chapter 2. The possible explanation is given in a relation to the SHG-activity, i.e. polarity, of nematic LC, and was adapted for the transition from biaxial polar nematic LCPs to uniaxial polar ones.

4-2 Experiment

4-2-1 Materials

VECTRA® A950 comprised by HBA and HNA units with a molar ratio of 73/27, which is commercially available, was supplied by Polyplastics Co. Ltd. The weight-averaged molecular weight (M_w) and the polydispersity of the molecular weight of **VECTRA® A950** have been estimated to be 30000,[16] and 2.45,[17] respectively. In this chapter, **VECTRA® A950** is treated as a standard polymer, so it is designated as **P-Std**.

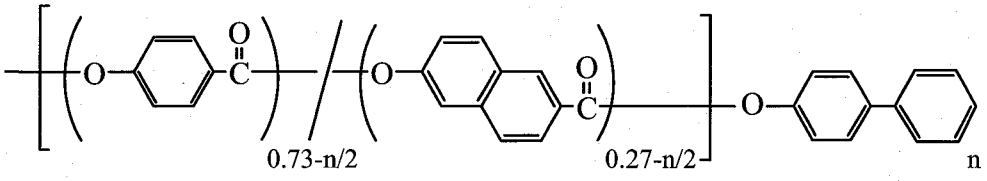

(4.1)

To prepare a homologous series of polymer with various molecular weights, I performed the polymerization by adding mono-functional hydroxy biphenyl (HBP) as an end capping compound. The copolymers in which HBP units were incorporated into **VECTRA® A950** were synthesized by the method according to the applied patent from Celanese.[18] The molar percents of HBP to the (HBA/HNA) mixture were changed from 1 to 5 %. And the higher molecular weight copolymer than **VECTRA® A950** is prepared with the longer polymerization time. Moreover as in situ observation sample during polymerization, the (HBA/HNA) oligomer with a molar ratio of 73/27 was prepared above synthesizing method with shorter polymerization time.

The inherent viscosities, η_{inh} and the crystal-nematic LC transition temperatures, T_m of these polymers are listed in the third, fourth and fifth columns in Table 4-1, respectively. The η_{inh} of the polymers were measured for the solutions of the equivolume mixture of pentafluoro phenol (PFP) and hexafluoro isopropanol at a concentration of 0.1g dL^{-1} at 30°C. T_m was determined by differential scanning calorimetry (DSC) on heating at a rate of 20°C min^{-1}(TA Instruments DSC Q-1000). At temperatures higher than T_m, all of the polymers were confirmed to form the nematic phase by polarized optical microscopy (Olympus BX 51 equipped with a Mettler FP82HT hotstage) and wide-angle X-ray diffraction (Cu Kα radiation, Rigaku UltraX18 generator equipped with the hotstage). All of the polymers treated here show no transition from nematic to isotropic in a temperature region up to 350°C. Here, the samples are abbreviated as **P-n** where **n** indicates molar content of HBP, and the (HBA/HNA) oligomer is abbreviated **P-o**.

4-2-2 Methods

SHG measurement: SHG was used as a probe to monitor the spontaneous polarization in the medium.[19] Q-switched Nd:YAG laser light (λ = 1064 nm) was incident perpendicular to the thin films with about 10 μm thickness (illumination area; 0.1mm in diameter) after passing through a quarter-wave plate and a polarizer. SH light (λ = 532 nm) generated from the sample was detected by a Hamamatsu model-R955 photomultiplier tube after passing through an IR cut filter, an interference filter and an analyzer. As reflection method geometry, incident laser light was set a 45 ° with the sample surface, and SH light was detected in the specular reflected direction.

The oriented 10μm-films were prepared by drawing out from a slit die (5 mm in wide, 1 mm in length and 10 mm in height) at a rate of 100mm min^{-1} and pressed at 310 °C. The SHG measurements were performed with the polymer chain axis set parallel to both the polarizer and the analyzer.[6] The relative SHG intensities for all the **P-n** polymers were determined as a standard of **P-Std** by a contact method where the sample film was contacted with the **P-Std** film and the SH signal intensity was detected by scanning the laser beam from the area of one polymer to that of the other.[6,7] The values thus determined are listed in the sixth column in Table 4-1.

Transmittance and Reflectance measurement: Transmittance and reflectance measurements were performed with a JASCO V-570. Incident wave length was fixed in 1064nm. The sample films thickness were 100μm, which were pressed at 310°C.

Viscosity measurement: Steady flow viscosity measurements were performed with a Rheometric SR200 equipped with parallel plate configuration with 12.5 mm in radius

(R) and 1.5 mm in gap (H) under nitrogen atmosphere. Share rate $\dot{\gamma}$ is calculated by $\dot{\gamma} = (2\pi/60)\cdot(R/H)\cdot n$ where n is the rotational speed of the plate (min^{-1}). To avoid structural changes due to the squeezing flow on loading the sample,[20] the powdered samples with the size of a few micrometers were once prepared from the pellets and shaped into disc form by pressure without heating. The disc-like sample was set between the parallel plates at 330 °C, held for 10 minutes. After that it was cooled down to 310 °C. Then, the viscosities were measured with increasing the shear rate up to 10^3 s^{-1}. This complicated temperature profile is to avoid the crystallization of the sample.[21] The measurements were completed within 30 min after the loading procedure of about 15 min.

4-3 Results and Discussion

4-3-1 Thermal Transition of P-n Polymer and of (HBA/HNA) Oligomer

VECTRA® (**P-Std**) is known to form the nematic phase as has been identified by optical microscopy and X-ray diffraction.[2,3,6] Similarly, all **P-n** polymers was conformed to form the nematic phase by optical microscopy and X-ray diffraction. The crystallization takes place only partially from the nematic liquid crystal. The melting temperature of crystal to the nematic liquid crystal is 283°C for **P-Std** (see the third column in Table 4-1). With introducing HBP unit, the melting temperature of **P-n** polymer was decreasing, and **n** > 0.010, another higher melting temperature was appeared. This higher melting temperature may be the transition from the pseudo-hexagonal crystal to the orthorhombic crystal.[22] And the melting temperature

of crystal to the nematic liquid crystal is 117°C for **P-o**, although that is increasing during DSC measuring. But no nematic-to-isotropic transition for all **P-n** polymers and **P-o** oligomer was observed up to the decomposition temperature of around 350°C.

4-3-2 Alteration of SH Response in Nematic LC by Decreasing Molecular Weight

I examined the dependence of SHG intensity on the molecular weight of **P-n** polymer. Here, the relative intensities of SHG for all the **P-n** polymers were determined as a standard of **P-Std** by a contact method.[6] The polymer with a thickness of 10μm was contacted with same thickness of **P-Std**. Then, the SH signal intensity was detected by scanning the laser beam from the area of one polymer to that of the other. The relative SHG intensities of **P-0** to **P-0.050** are listed in the sixth of Table 4-1 and plotted against η_{inh} in Figure 4-1. It is found that SHG intensity increase remarkably up to 2.2dL/g, after that, it decrease in a time of crisis, and it increases steeply again. If it is considered on the basis of Lee's suggestion,[11] this result will be strange.

This result might be effect on the transparency. Figure 4-2 shows the alternation of transmittance and reflectance for a 100mm-film by decreasing molecular weight of **P-n** polymers. When η_{inh} were between 1dL/g and 2.2dL/g, transmittance and reflectance were almost constant. But η_{inh} > 2.2dL/g, transmittance was decreasing, and reflectance was increasing. The sum of transmittance and reflectance in each sample is almost 100%. This means, the **P-n** polymers don't have a special

absorbent in this wavelength region. This is, the strong SH signal intensity between 1 and 2.2 on η_{inh} by transmission method is affected higher transmittance. Shown in Figure 4-3, SH signal intensity between 1 and 2.2 on η_{inh} is very weak by reflection method.

Moreover, the alternation of morphology with an increase on η_{inh} was observed by a polarized optical microscope with crossed polarizer. Figure 4-4 shows the morphology for **P-0.017** (a) and **P-0.029** (b). With increasing on η_{inh}, the number of disclinations was increasing.

4-3-3 In Situ Measurements of SH Response during Polymerization from (HBA/HNA) Oligomer

I tried to measure the SH signal intensity during polymerization from **P-o** oligomer. Sample was prepared as a 10mm-cast film. To carry out the observation, **P-o** was prepared as a 10mm-cast film on a glass slide from the 0.1g dL^{-1} **P-o**/PFP solution. After evaporation of the solvent, the film sandwiched between two glass slides with a ring spacer. The ring spacer was made of stainless steel with a thickness of 0.5 mm. The ring spacer provided space for easy removal or release of acetic acid during polymerization.[23] Without the spacer, it was found that the reproducibility was quite low and the film quality was poor because the evaporation (or release) of acetic acid at elevated temperatures was vigorous. The whole package was placed on a heating stage of a microscope or of SHG measurement and held at 330 °C during the whole reaction process, and the reaction time began to be recorded. Here, the SH

signal intensities during polymerization were absolute unit, which is different from the relative SH signal intensities. Figure 4-5 shows an alternation with the progress of SHG intensity. There is no SH response until 4 minutes from the beginning of polymerization. But over 4 minutes, SHG intensity was observed, and it was increasing rapidly by 8 minutes. After that, SHG intensity was decreasing once, and it was increasing again from 11 minutes. This alternation of SH response is analogous to the result of different molecular weight of **P-n** polymer.

Moreover, the reaction process was observed in situ by a polarized optical microscope with crossed polarizer. The alternation of morphology with polymerization time was observed. Figure 4-6 shows the morphology at 3.5minutes from the beginning of polymerization (when is the period with no SH response), at 6 minutes (when is the period with the increasing SHG intensity rapidly), and at 28.5 minutes (when is the period with the increasing SHG intensity gradually). With prolonging the polymerization time, the number of disclinations was increasing step by step.

4-3-4 Alteration of Biaxial Polar Nematic LC to Uniaxial Polar Nematic LC by Decreasing Molecular Weight

Here, a question arises on why SHG intensity for **P-n** polymers change a sudden dip with an increase on molecular weight and the transparency became lower, or SH signal intensity during polymerization from **P-o** oligomer decreases at once.

I examined the intensities of SH light from the oriented nematic films of **P-n**

polymer at room temperature under various polarization conditions. Here, the laser beam was irradiated normal to the film (along the y-axis), and SHG intensities were plotted against the rotation angles of the polarization (ϕ_p) for the fundamental beam or the polarization (ϕ_a) for the SHG light. The rotation angle was defined as an angle from polymer chain axis (z direction). With respect to the z-direction, the clockwise rotation was defined as positive when viewed along the y-direction and the polar plots were made under four configurations of ϕ_p-ϕ_a (ϕ_p-0°, ϕ_p-90°, 0°-ϕ_a, and 90°-ϕ_a). Figure 4-7 displays SHG profiles, (a) I(ϕ_p, 0°), (b) I (ϕ_p, 90°) and (c) I(0°, ϕ_a), observed for **P-Std** at room temperature. I(90°, ϕ_a) was too weak to detect reasonable signal. All three profiles show the two-leaves pattern due to C_s symmetry.[7] The solid line in this figure indicates the fitting results dealt with C_s symmetry. The obtained parameters were χ_{xxx}=0.12, χ_{xyy}=0.14, χ_{xzz}=0.29, χ_{zxx}=0.05, χ_{zyy}=0.53, χ_{zzz}=1.67, and the agreement is very good.

Figure 4-8 displays SHG profiles, (a) I(ϕ_p, 0°), (b) I (ϕ_p, 90°) and (c) I(0°, ϕ_a), observed for **P-0.025** at room temperature. To the above mentioned similar, I(90°, ϕ_a) was too weak to detect reasonable signal. SHG profiles of (a) I(ϕ_p, 0°) and (c) I(0°, ϕ_a) for **P-0.025** were similar to it for **P-Sdt**. On the other hand, SHG profile of (b) I (ϕ_p, 90°) for **P-0.025** is four–leaves pattern. This means that the symmetry of polar structure for **P-0.025** is different from it for **P-Sdt**. Here, when it is assumed $C_{\infty v}$ symmetry,[7] the fitting results were indicated by solid lines in Figure 4-7. The obtained parameters were χ_{zxx}=1.00, χ_{zzz}=0.91. I can conclude that the polar structure change from C_s symmetry to $C_{\infty v}$ symmetry by a decrease on molecular weight, that is, the

transition from biaxial polar nematic to uniaxial one is observed.

4-3-5 Steady Shear Flow Viscosity

The steady shear flow viscosities for the nematic melts at 310 °C were measured by a parallel-plate type of rheometer in a wide shear-rate range from 10^{-3} to 10^{3} s^{-1}. Sample was melted at 330 °C, and held for 10 minutes. After that it was cooled down to 310 °C. This complicated temperature profile is to avoid the crystallization of the sample.[21] Figure 4-9(a) shows flow curve of **P-Sdt**, **P-0.01**, and **P-0.025**. For all **P-n** polymers, with the exception of **P-0.025**, the flow curve is well divided into the four regions (in case of **P-0.025**, the fourth region wasn't able to be measured because of exceeding the measuring limit). Three of these four flow regions, namely regions I, II and III, are designated to keep correspondence with the flow regions defined by Onogi and Asada.[24] Region 0 has been found experimentally for a lyotropic LC of hydroxypropyl cellulose/water system[25] and the previous paper.[15]

The flow behavior in region II and III was influenced by molecular weight.[25] As found in Figure 4-9(a), first, region II shifted to high shear rate as **n** increases. Similar phenomenon is measured by Sigillo.[25] But, the decades of region II were almost same for each sample.

In Figure 4-9(b) and (c), the viscosities in characteristic regions II and 0 are plotted as a function of η_{inh}. The viscosities in regions II show a positive correlation with the inherent viscosity of polymer, i.e. the molecular weight. The viscosity on region 0, however, does not depend on η_{inh} in the present range of 1 to 5.5dL/g. It may

depend on whether the copolyester is biaxial polar structure or uniaxial polar structure. The viscosities of the four of six biaxial polar structure copolyesters are around 3000Pa·s, which is 5 times larger than those of the three uniaxial polar ones. I have already reported the viscosity in R0 is affected by the domain size in nematic LCPs; the viscosity of biaxial polar LCPs was 10 times larger than it of non-polar LCPs.[15] Therefore, the difference of the viscosity on region 0 is suggested the change of domain size as the polar structure transfer from biaxial to uniaxial, supported by alternation of optical microscopic images in Figure 4-3 and 4-5.

4-4 Summary

In this chapter, I prepared different molecular weight of poly(HBA/HNA) by adding HBP as an end capping compound, and examined SHG, and transmittance and reflectance, and steady shear flow viscosity in wide shear-rate range from 10^{-3} to 10^{3} s^{-1} for their nematic LCPs. The biaxial polar nematic phase is formed from the basic poly(HBA/HNA), but the it is transferred to the uniaxial polar nematic below η_{inh} 2.2dL/g, and the transparency increases. The viscosity of region 0 also changes around the transition point, which is from biaxial polar nematic to uniaxial one. The viscosity of the biaxial polar nematic is 5 times higher than that of the uniaxial one, although the viscosity of region II depends on positive correlations with the molecular weight. Mentioned previous paper,[15] this difference in the viscosity might be connected to the difference in the domain size: the domain size in the biaxial polar nematic copolymers is smaller than that in the uniaxial ones. The small size of

domains in the biaxial nematic LCPs; in other words, a lot of disclinations is occurred low transparency, because the disclinations scatter the light strogly.[26]

Moreover, the alternation of in situ observation of SHG during polymerization from **P-o** oligomer changes analogous to that of different molecular weight of **P-n** polymer, and with prolonging polymerization time, the domain size is smaller.

References

(1) Sawyer, L. C.; Linstid, H. C.; Romer, M. *Plast. Eng. (N.Y.)* **1998**, 54, 37.

(2) Blackwell, J.; Biswas, A. in *Developments in oriented polymers-2*; Ward I. M. Ed.; Elsevier: New York, **1987**, p. 153

(3) Coulter, P.; Windle, A. H. *Macromolecules* **1989**, *22*, 1129.

(4) Jin, J. -I.; Antoun, S.; Ober, C.; Lenz, R. W. *Br. Polym. J.* **1980**, *12*, 132.

(5) Hummel, J. P.; Flory, P. J. *Macromolecules* **1980**, *13*, 479.

(6) Watanabe, T.; Miyata, S.; Furukawa, T.; Takezoe, H.; Nishi, T.; Migita, A.; Sone, M.; Watanabe, J. *Jpn. J. Appl. Phys.* **1996**, 35, L505.

(7) Koike, M.; Yen C. C.; Yuqing, L.; Tsuchiya, H.; Tokita, M.; Kawauchi, S.; Takezoe, H.; Watanabe, J. *Macromolecules* **2007**, 40, 2524.

(8) Park, B., Kinoshita, Y., Takezoe, H. & Watanabe, J. *Jpn. J. Appl. Phys.* **1998**, *37*, L136.

(9) Yen, C.-C.; Tokita, M.; Park, B.; Takezoe, H.; Watanabe, J. *Macromolecules* **2006**, 39, 1313.

(10) Yen, C.-C.; Taguchi, Y.; Tokita, M.; Watanabe, J. *Macromolecules* **2008**, 41, 2755.

(11) Yu, C.-J.; Yu, M.; Lee, S.-D. *Jpn. J. Appl. Phys.* **2002**, *41*, L102.

(12) Groh, B.; Dietrich, S. *Phys. Rev. E* **1997**, 55, 2892-2901.

(13) Terentjev, E. M.; Osipov, M. A.; Sluckin, T. J. *J. Phys. A* **1994**, 27, 7047-7059.

(14) Biscarini, F.; Zannoni, C.; Chiccoli, C.; Pasini, P. *Mol. Phys.* **1991**, 73, 439-461.

(15) Taguchi, Y.; Yen, C.-C.; Kang, S.; Tokita, M.; Watanabe, J. *Macromolecules* **2009**, 42, 8, 3179.

(16) Romo-Uribe, A.; Windle A. H. *Macromolecules* **1996**, *29*, 6246.

(17) Kromer, H.; Khun, R.; Pielartzik H.; Siebke, W.; Eckhardt, V.; Schmidt, M.; *Macromolecules* **1991**, *24*, 1950.

(18) Calundann, G. *U. S. Patent* **1979**, 4 161 470.

(19) Viney, C.; Donald, A. M.; Windle, A. H. *J. Mater. Sci.* **1983**, *18*, 1136.

(20) Langelean, H.C.; Gotsis, A.D. *J. Rheol.* **1996**, *40*, 107.

(21) Lin, Y. G.; Winter, H. H. *Macromolecules* **1988**, *21*, 2439.

(22) Viney, C.; Windle, A. H. *J. Mater. Sci.* **1982**, *17*, 261.

(23) Wang, Y.; Chung, T. S.; Cheng, S. X.; Xu, J.; *J. Phys. Chem. B* **2004,** *108,* 1596.

(24) Onogi, S.; Asada, T., in *Proceedings of the VIIIth Inrenlarional Congress on Rheology*, Astarita, G., G. Marrucci, G., Nicolais, L. Eds.; Plenum: New York, **1980**; pp. 127-147.

(25) Sigillo, I.; Grizzuti, N. *J. Rhol.* **1994**, 38,589.

(26) Shiwaku, T; Nakai, A; Wang, W; Hasegawa, H; Hashimoto, T *LIQUID CRYSTALS* **1995**, 19, 679.

Table 4-1. Characterization in a series of **P-n** copolyesters

Sample	Molar fraction of HBP unit	η_{inh}/dL g^{-1}	T_m / °C[a]		Relative SHG Intensity
P-Std	0	4.67	283	-	1
P-0	0	5.53	281	-	1.33
P-0.010	0.01	3.92	278	-	0.81
P-0.013	0.013	3.83	279	293	0.72
P-0.017	0.017	2.95	275	294	0.55
P-0.020	0.02	2.49	272	293	0.46
P-0.025	0.025	2.15	267	289	2.03
P-0.029	0.029	2.07	265	289	1.99
P-0.033	0.022	1.45	262	287	0.60
P-0.050	0.05	1.15	-	281	0.16
P-o	-	0.16	117	-	-

[a] based on heating DSC data.

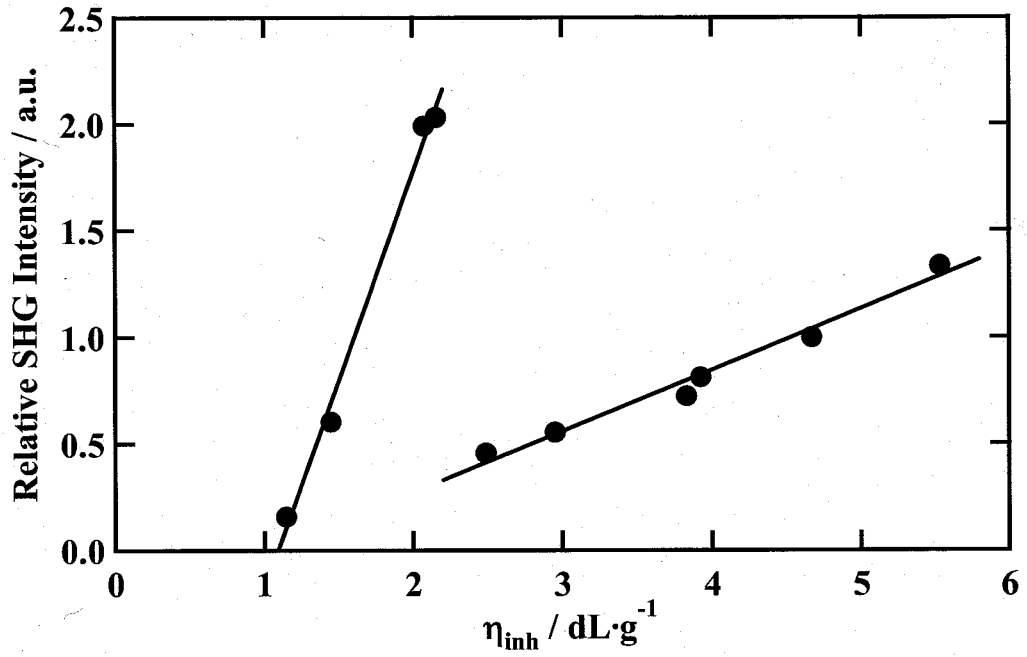

Figure 4-1. Variation of SHG intensity with η_{int} in a series of **P-n** copolyesters.

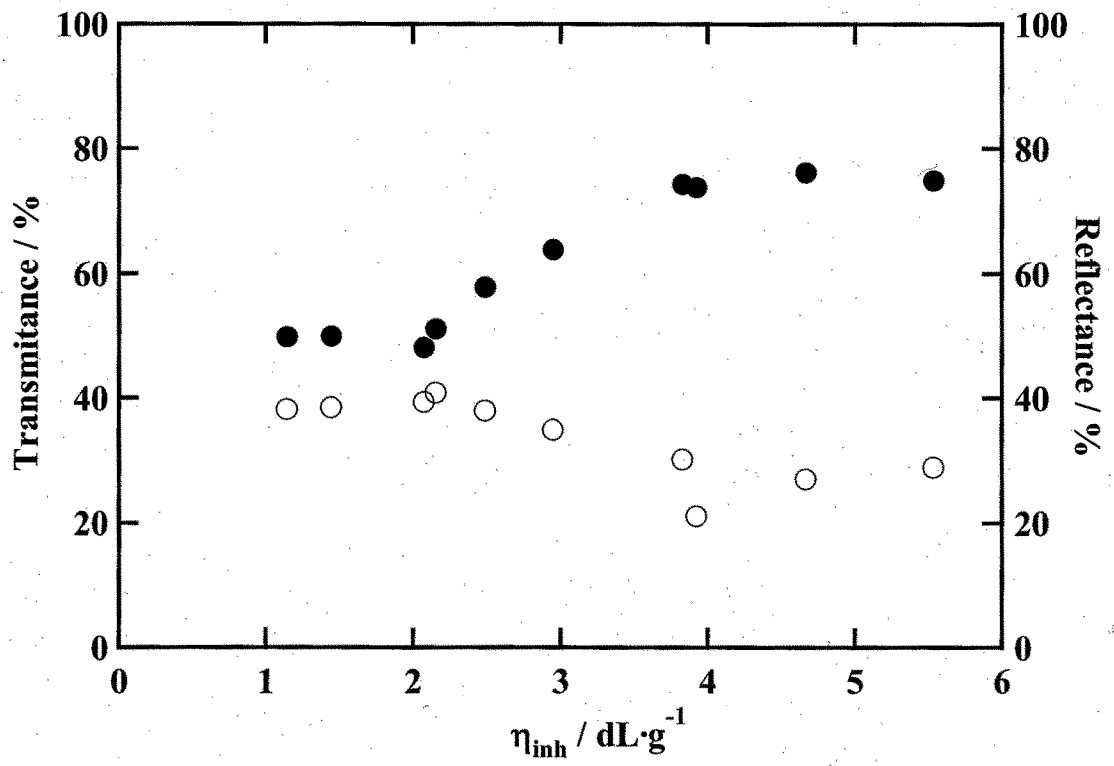

Figure 4-2. Variation of transmittance (○) and reflectance (●) with η_{int} in a series of **P-n** copolyesters.

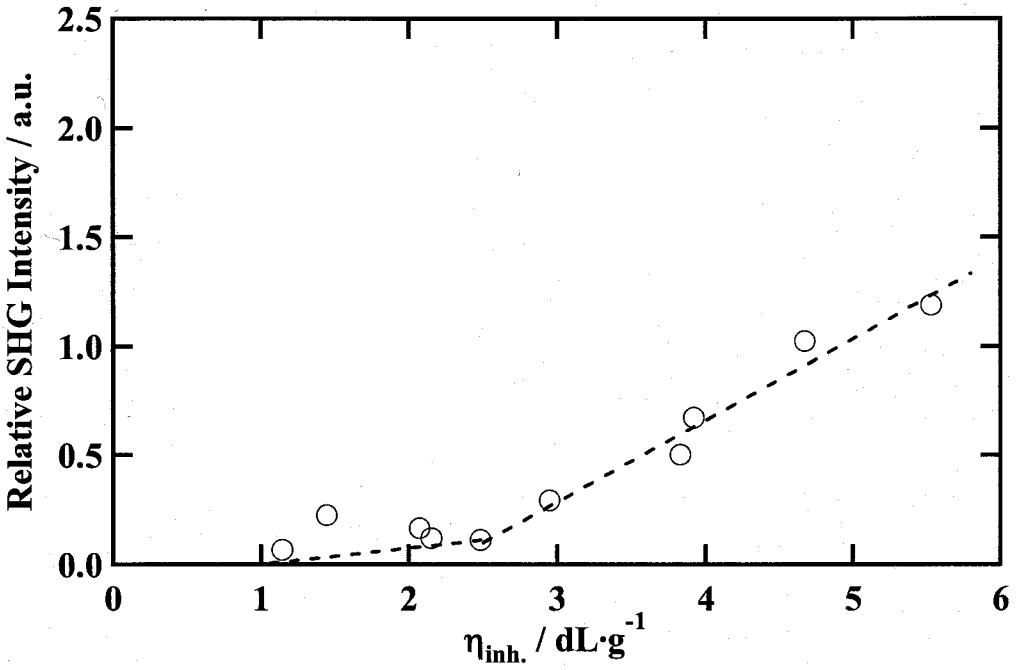

Figure 4-3. Variation of SHG intensity with η_{int} in a series of **P-n** copolyesters by reflection method.

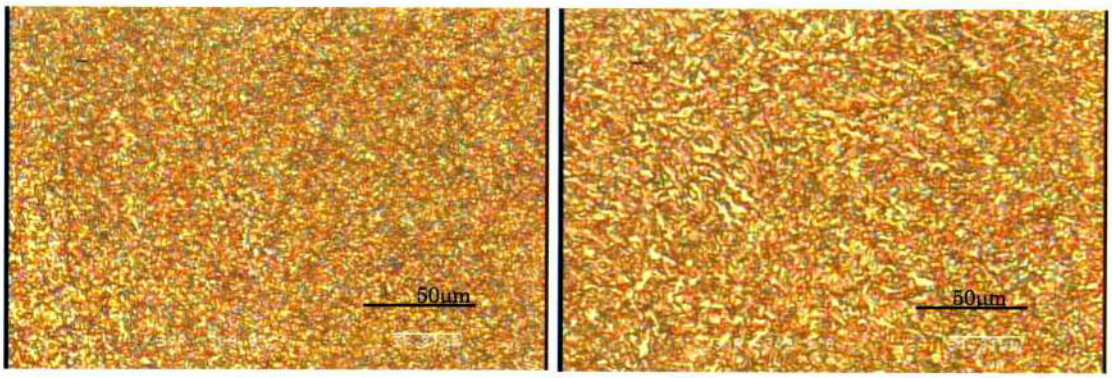

(a) (b)

Figure 4-4. Optical microscopic nematic textures of (a) **P-0.017** and (b) **P-0.029**. The sample thickness is around 10 μm.

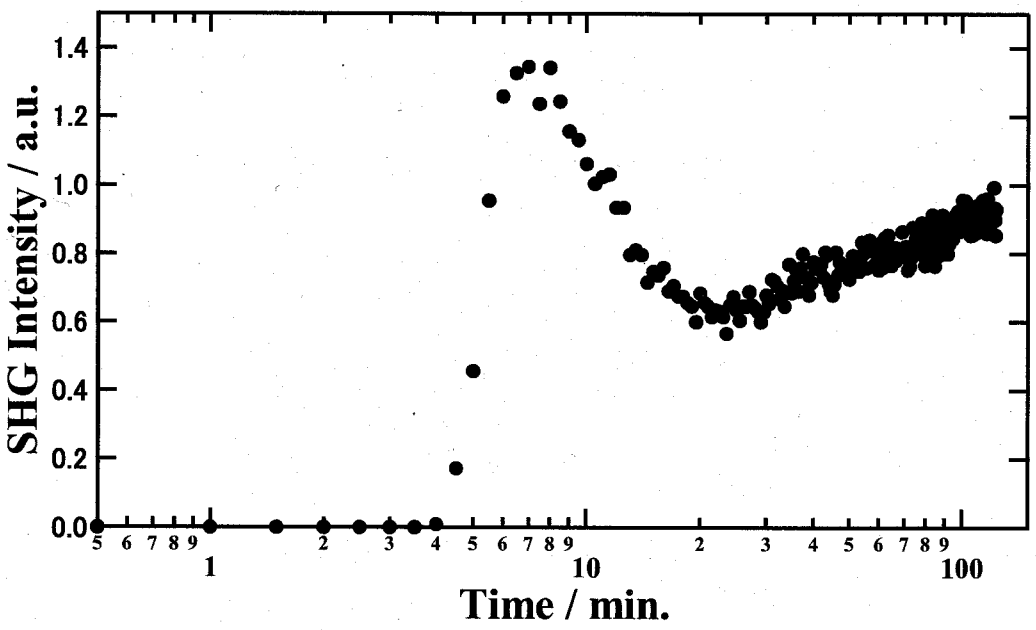

Figure 4-5. In site measurements of SH signal intensity during polymerization for **P-o** oligomer at 330 °C.

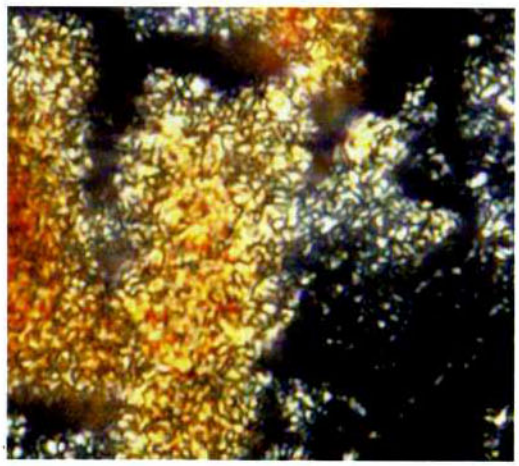

(a)

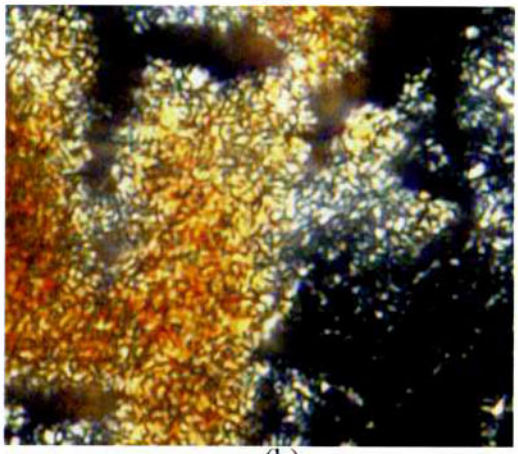

(b)

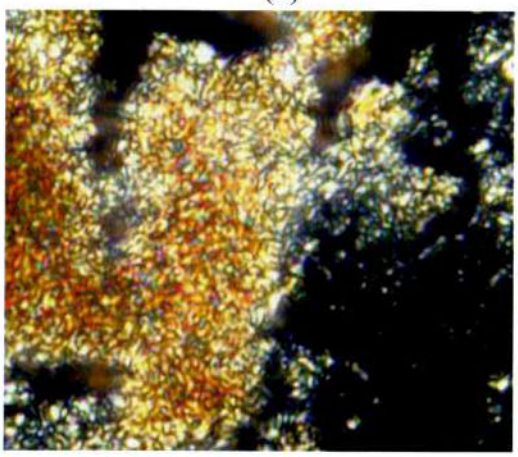

(c)

Figure 4-6. Optical microscopic nematic textures of (a) at 3.5 minutes, (b) 6 minutes and (c) 28.5 minutes from the beginning of polymerization. The thickness of cast film is around 10 μm.

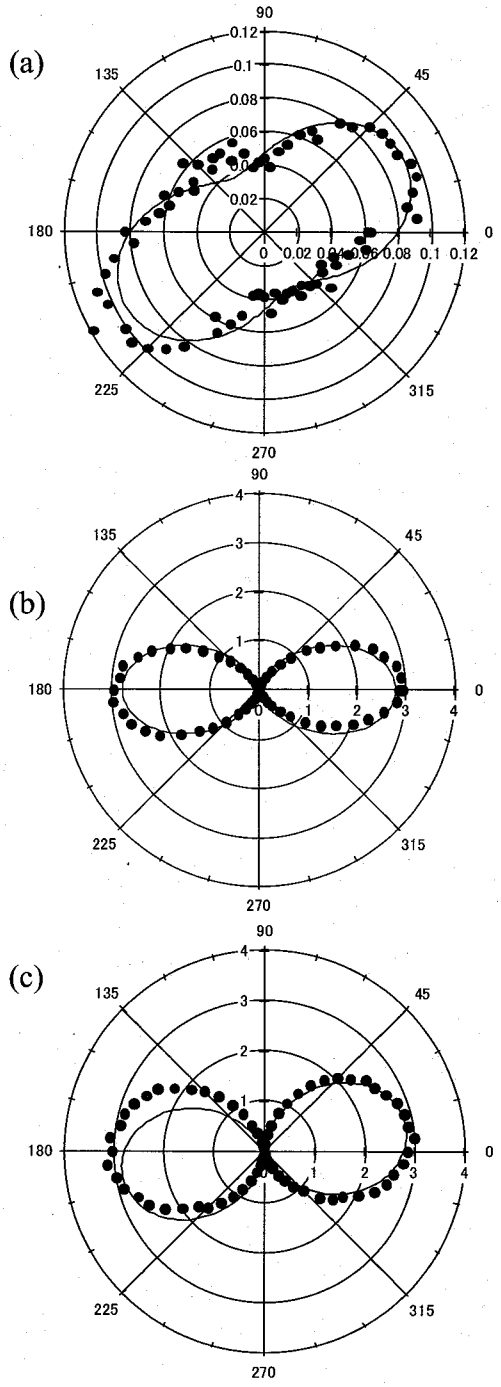

Figure 4-7. SHG profiles of **P-Std**, (a) I(ϕ p,0), (b) I(ϕ p,90), (c) I(0, ϕ a). The dots and lines indicate measured values and fitting results respectively. Fitting results are dealt with C_s symmetry, where the parameters are χ_{xxx}=0.12, χ_{xyy}=0.14, χ_{xzz}=0.29, χ_{zxx}=0.05, χ_{zyy}=0.53, χ_{zzz}=1.67.

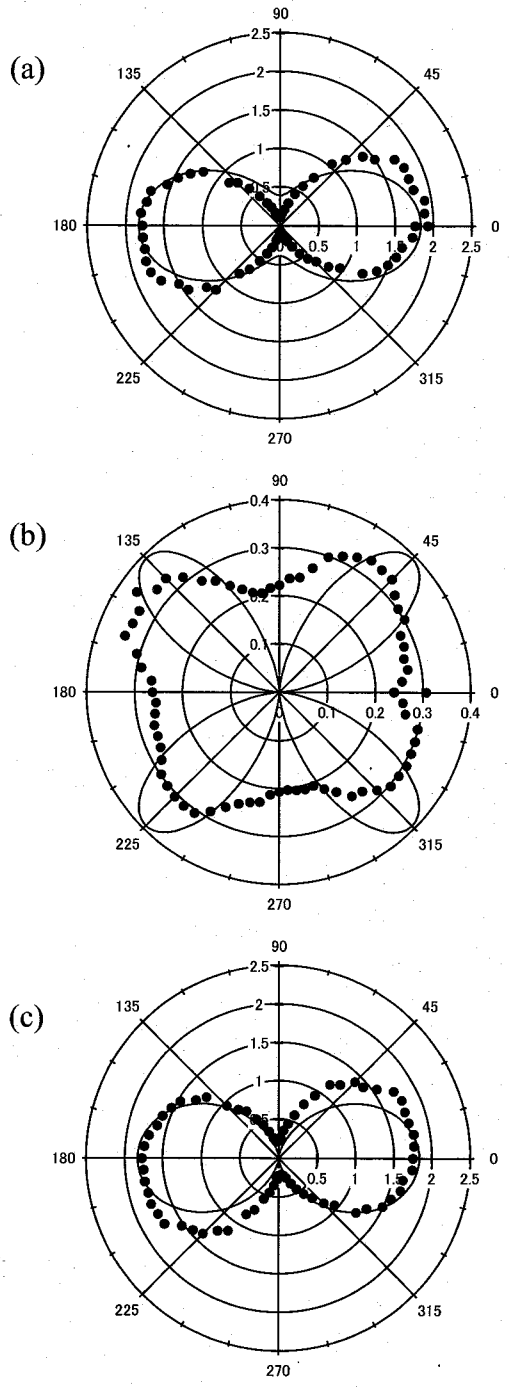

Figure 4-8. SHG profiles of **P-0.025**, (a) I(ϕ p,0), (b) I(ϕ p,90), (c) I(0, ϕ a). The dots and lines indicate measured values and fitting results respectively. Fitting results are dealt with $C_{\infty v}$ symmetry, where the parameters are χ_{zxx}=1.00, χ_{zzz}=0.91.

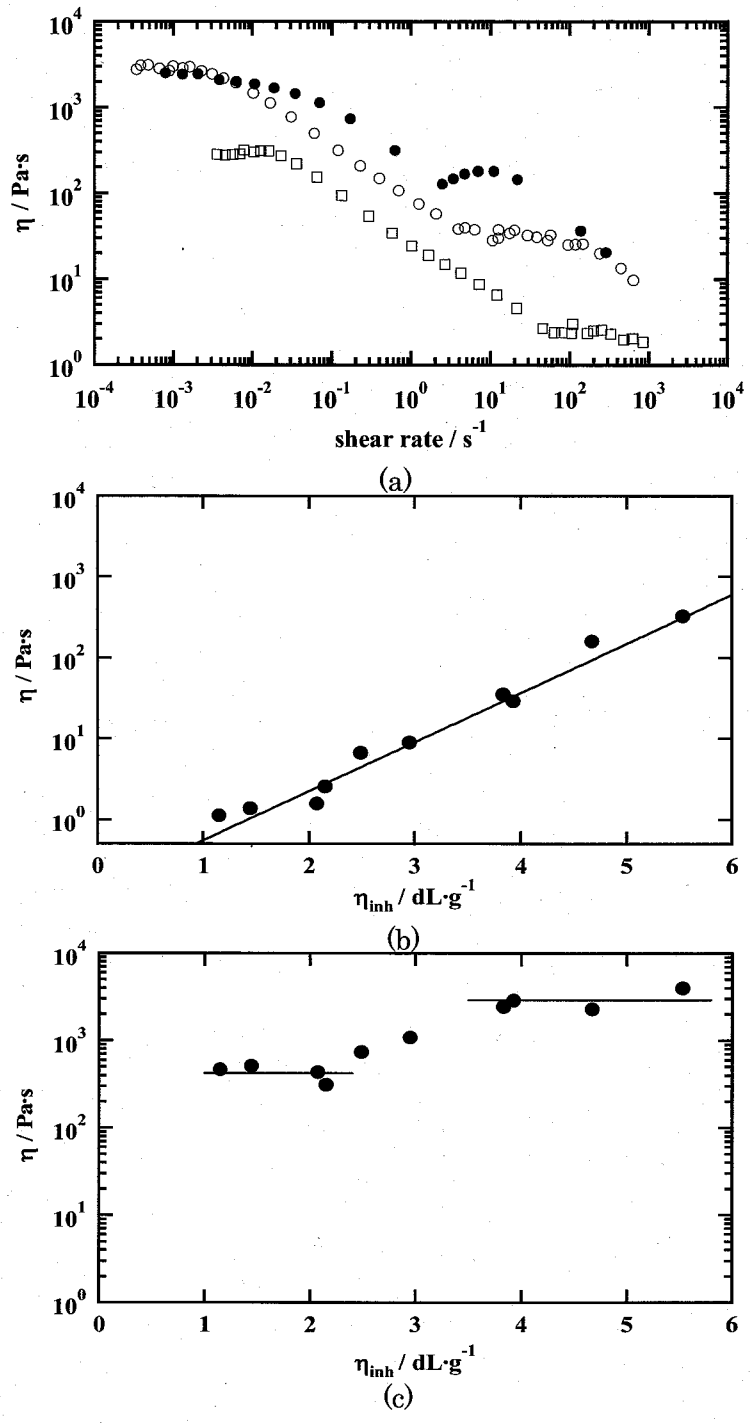

Figure 4-9. (a) Steady-state viscosity for the nematic LCPs of **P-Sdt** (●), **P-0.01** (○), and **P-0.025** (□). (b) Apparent viscosity in the high-shear-rate Newtonian plateau (region II) against η_{inh}, and (c) Apparent viscosity in the lowest –shear-rate Newtonian plateau (region 0) against η_{inh}.

Chapter 5

Unusual Transformation of Mechanically Induced Monodomain State to Polydomain one in Polar Nematic Liquid Crystals of Aromatic Polyesters

Abstract

I present an interesting phenomenon of the mechanically aligned monodomain state of polar nematic liquid crystals transforming into the polydomain one. This unusual transformation may result from mismatching of the dipolar vectors. By stretching or shear-flowing the polar nematic liquid crystal, the perfect orientation can be achieved with respect to the long molecular axis, but the misorientation exists with respect to the polar vector. After the prolonged annealing, then, the free energy of the molecules is minimized by producing new defects which satisfy the continuity of polar orientation, but lead to the loss of macroscopic molecular orientation.

5-1 Introduction

Aromatic polyesters are most important class of thermotropic liquid crystal polymers (LCPs) for commercial applications.[1] Thermotropic liquid crystallinity in aromatic polyesters can be achieved by random incorporation of aromatic monomer units which decreases the crystal melting point and makes the nematic LC phase thermally accessible.[2] Among aromatic LC polyesters, **VECTRA® A950** composed of 73 mol % of 4-hydroxy benzoic acid (HBA) and 27 mol % of 6-hydroxy-2-naphtoic acid (HNA), is an extraordinary class of LC polymers, since a head-to-tail connection of *p*-HBA and HNA[3-5] results in a huge dipole moment along the chain as a result of accumulation of the carbonyl dipole in ester linkage.[6] Because of such a polar rod-like conformation, **VECTRA® A950** can form the polar biaxial nematic LC, which has been experimentally confirmed by second harmonic generation (SHG) measurements[7,8] and predicted by computer simulation and theoretical calculation considering the dipole-dipole interaction.[9-13] It has been also reported that the polar nematic and cholesteric LCs are formed in the lyotropic solutions of polar α-helical polypeptide.[14-17]

As reported in the previous paper,[8] the head-to-tail character in **VECTRA® A950**, can be eliminated by an introduction of symmetrical units of terephthalic acid (TA) and biphenol (BP) which interrupts the dipole accumulation along the chain. I have thus prepared an interesting series of polyesters, the nematic LCs of which are SHG active and non-active depending on the content of TA and BP. Further, the biaxial nematic LC in **VECTRA® A950** has been altered to the uniaxial polar nematic LC by an introduction of 3-hydroxyl benzoic acid (*m*-HBA).[18] In this chapter, I treat three kinds of polymer, thus prepared, polar biaxial, polar uniaxial, and nonpolar nematic LC polymers, and show the interesting phenomenon that the mechanically

oriented polar nematic LCs lose their uniaxial orientation to transform into the polydomain state at nematic temperatures. Since such an extinction of macroscopic orientation dose not occur at all in the nonpolar nematic LC, it can be attributed to the polar structure.

5-2 Experiment

Three kinds of polymer as mentioned above were prepared by conventional melt condensation method. One is **VECTRA® A950** (Equation 5.1),

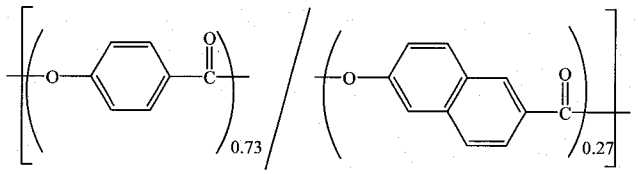

(5.1)

Poly-A

which is commercially available from Polyplastics Co., Ltd. The inherent viscosity is 4.7 dL/g as measured for solutions in an equivolume mixture of pentafluoro phenol and hexafluoro isopropanol at a concentration of 0.1 g dL^{-1} at 30 °C. The molecular weight (M_w) and the polydispersity of the molecular weight of **VECTRA® A950** have been estimated to be 30000,[19] and 2.45,[20] respectively. **VECTRA® A950** is named here **Poly-A**. Second polymer is the copolymer with *m*-HBA unit of 10% incorporated into **VECTRA® A950**,

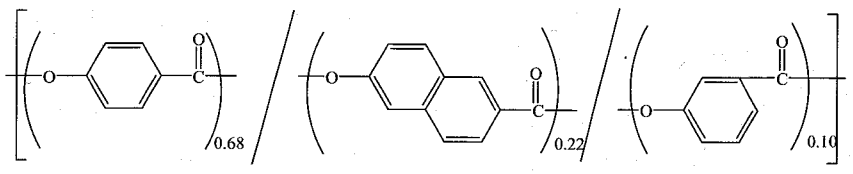

(5.2)

Poly-B

This polymer called here **Poly-B** (Equation 6.2) forms the uniaxial polar nematc.[18] In

the third polymer, **Poly-C**, TA and BP units were incorporated into **VECTRA® A950** as following Equation (6.3).

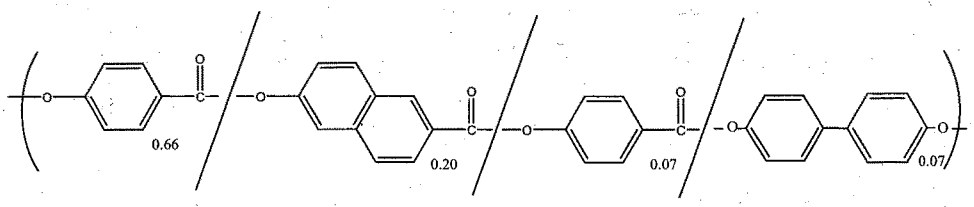

(5.3)

Poly-C

The content of TA and BP that should be equimolar to each other in order to properly perform the polymerization, is 0.07. **Poly-C** forms the typical nonpolar nematic LC.[8] The inherent viscosities of **Poly-B** and **Poly-C** are 4.5 and 4.6 dL/g, respectively, which is similar to that of **Poly-A (VECTRA® A950)**.

Crystal melting temperatures to the nematic phase, T_m, are 280, 240 and 290 °C for **Poly-A**, **Poly-B** and **Poly-C**, respectively. At temperatures higher than T_m, all of the polymers form the nematic phase as confirmed by polarized optical microscopy (Olympus BX 51 equipped with a Mettler FP82HT hotstage, and KEYENCE digital microscope VHX-1000) and wide-angle X-ray diffraction (Cu Kα radiation, Rigaku UltraX18 generator equipped with the hotstage). No nematic to isotropic phase transition was observed in the temperature region up to 350 °C.

5-3 Results and Discussion

5-3-1 Disorientation of Polar Nematic Liquid Crystal in Fiber

Figure 5-1a – 5-1c shows the X-ray patterns taken for the as-span fibers of three polymers which were spun at a nematic temperature of 330 °C and then quenched to the room temperature. At a glance, one knows that the high orientation is achieved for all of the fibers with the long axis of polymer aligned along the fiber axis. The cross-

polarized microscopy also shows the uniform texture in Figure 5-2a and 5-2c, which becomes dark and bright in a high contrast when the fiber is set in directions of 0 and 45° to the polarizer, respectively. This change in the brightness can be recognized from Figure 5-3 where the transmitted light intensity (given by closed circles) are presented with a function of angular displacement of the fiber axis to the polarizer.

Interesting phenomenon with respect to the orientation is observed when the fiber is again heated up to a nematic temperature of 330 °C and annealed for 10 min. Figure 5-1d –f shows the X-ray patterns of their annealed fibers. Obviously, the macroscopic orientation disappears completely in fibers of polar **Poly-A** and **Poly-B**, but not in nonpolar **Poly-C** fiber. Meanwhile, the shape of the fiber sample is retained so that the loss of orientation is caused by rearrangement of polymer molecules inside of the fiber. Optical microscopic texture offers a more definite illustration for this. Annealed fiber of **Poly-C** still shows highly bright and dark contrast of transmitted light by the rotation of the stage (see the data given by the open circles in Figure 5-3b), although uniform texture is altered to the banded texture (Figure 5-2d) which occasionally appears when some strain retained on stretching is relaxed.[21,22] On the other hand, the annealed fibers of **Poly-A** and **Poly-B** show a very distinct change in texture, as found in Figure 5-2c. The texture includes many fine schlierens. The inset of Figure 5-2c shows its enlarged view. One can clearly see that there are many defects composed of fine schlierens with $|s| = 1$. As a result, the brightness does not change at all by rotation of the sample stage (see the data given by open circles in Figure 5-3a), again indicating the disappearance of macroscopic orientation. Since the birefringence is still observed, the disorientation is not due to the transformation of the LC phase to the isotropic phase but to the simple change of monodomain to polydomain

structure.

5-3-2 Disorientation of Polar Nematic Liquid Crystal in Film

Similar phenomena are also observed for the oriented films which were prepared by the plate-plate rheometer (a Rheometric SR200 with parallel plate configuration with a 12.5 mm radius and a 1.5 mm gap) at a shear rate of 10^2 s^{-1} at 330 °C. At this shear rate in shear thinning zone "Region III" which promotes the molecular orientation, all of the samples show a similar viscosity of ~ 10 Pa·s characteristic to the nematic LC[23-26] (refer to Figure 5-4). After the shear flow for 10 min, the film-like sample was quenched and removed from the plate for X-ray measurement. The left-side photographs in Figures 5-5a and b show the X-ray patterns taken with an irradiation parallel to the velocity gradient ($\nabla \mathbf{v}$) direction. All of the samples show a good orientation of polymers with their long axes parallel to the velocity ($\mathbf{v}$) direction. Again, these oriented films were annealed at 330 °C and the X-ray patterns were taken after different annealing periods. Similarly as observed in the specimens, the macroscopic orientation of polymers completely disappeared in **Poly-A** and **Poly-B** after annealing for 15min, but not in **Poly-C** (see the right-side photographs in Figure 5-5a and b). Thus, I know that the disorientation behavior does not depend on the shape of sample, but on the polarity in nematic LC. In other words, it can be concluded that the mechanically oriented state is not stable in the polar nematic LCs irrespective of their uniaxiality and biaxiality. It should be noted that a similar disorientation behavior has been reported in **VECTRA® A950** (same as **Poly-A**) by Windle *et al.*[27].

On the transformation from the uniaxial orientation state to polydomain one, the

nematic LC phase has to pass over the high energy barrier and then increase its free energy because of new creation of the defects followed by the splay, bend and twist deformations.[28,29] Considering that the elastic distortion energies of splay and bend deformations are fairly large in a hard-rod polymer system such as the present system,[30] the polydomain structure should be much more energetically unfavorable. Thus, I have to consider the specific internal force that inevitably leads to the polydomain structure in polar nematic LCs of **Poly-A** and **Poly-B**. The example of the internal force is the internal stress produced by the stretching between the cross-linking points in the nematic LC elastomer. When the LC elastomer is stretched, its polydomain structure is altered to the perfect monodomain one.[31-34] On a release of strain (or stress), the elastomer tends to recover the initial polydomain structure by relaxing the residual stress working between cross-linking points. Such a relaxation mechanism, however, is unlikely in the present system because of no chance of chemical cross linkage (or some entanglement of polymers working as an apparent cross-linking through the melt-polymerization process. Furthermore, it is hardly considered that cross-linking preferably occurs in polar systems of **Poly-A** and **Poly-B**. As shown Figure 5-4, all of the polymers are commonly fluid exhibiting a similar flow behavior with a low viscosity of ~10 Pa·s in the high-shear-rate "Region III" which is characteristic of conventional polymeric nematic LCs[24-26].

All the polymers exhibit similar conventional flow behavior with low viscosity of ~10 Pa·s characteristic to the nematic liquid crystals. Thus, another kind of internal force should be considered. A more plausible explanation can be given on the basis of polar symmetry. When fibers or films are mechanically oriented in the polar nematic LC state, the perfect monodomain can be achieved with respect to the orientation of the

long molecular axis. However, the resulting structure is not homogeneous with respect to the polarity, as illustrated in Figure 5-6a. There are grain boundaries with respect to the dipolar vectors; the dipolar vectors abruptly change their direction on the boundary. This misorientation of dipolar vectors makes the free energy cost high so that the dipolar orientation tends to become continuous by producing new defects of strength |s| = 1 after the prolonged annealing. One of the possible mechanisms for the molecular rearrangement to eliminate the initial uniaxial orientation is illustrated in Figure 5-6. If this disorientation mechanism is proper, the distance between disclination lines (or points) may correspond to the size of the polar domain in the initially oriented sample. From Figure 5-2c, I know that this size is around 2-3μm.

There is another possibility for the disorientation according to the prediction by Pleiner and Brand.[35] In their prediction, some polar nematic phase with spontaneous splay defects would be energetically more favorable than the homogeneously oriented one, just similarly to the cholesteric helical phase in the chiral nematogens. It has been found to be the case for a temperature range close to the isotropic-polar nematic phase transition using Ginzburg-Landau type analysis.[36] Although the nematic temperature adopted in my study is fairly lower than the isotropization temperature and there are a lot of bend defects included in Figure 5-5, this possibility will also need to be considered.

5-4 Summary

As a summary, I report the first example of the spontaneous disorientation of the mechanically aligned nematic LC. This unusual transformation of the monodomain to polydomain state is characteristic of the polar nematic LC phases and is explained as

resulting from mismatching of the dipolar vectors. By stretching or shear-flowing the polar nematic LCs, the perfect orientation can be achieved with respect to the polar vector. After the prolonged annealing, then, the free energy of the molecules is minimized by producing the new defects which satisfy the continuity of the polar orientation, but lead to the elimination of macroscopic orientation of the molecular long axis.

5.5 Appendix: Growth Kinetics of LC Domain from Amorphous Films

The LC domain size which is enclosed disclination lines, was different between polar nematic LCPs and non-polar ones in the static state. To clarify this point, I observed the kinetics of growing the LC domains from the amorphous films for biaxial polar nematic, **Poly-A** and non-polar one, **Poly-C** under isotherm at 330°C by the laser light scattering method, as shown in Figure 5-7 and Figure 5-8 respectively. Each patterns show the four-leaves pattern, but its magnitude and its evolution of influence of annealing time were different. The patterns of **Poly-C** simply became larger with increasing annealing time. Those of **Poly-A** changed complicatedly. The scattering angle θ_m of the intensity maximum for the Hv scattering is related to the domain size, $D(t)$, as defined by Shiwaku[36],

$$D(t) = 2\pi/q_m(t) \tag{5.4}$$

Where

$$q_m(t) = (4\pi/\lambda)\sin[\theta_m(t)/2] \tag{5.5}$$

and λ is the wavelength of light in the medium. Thus the shift of θ_m towards smaller values corresponds to growth of $D(t)$ or a decrease in the number density of disclinations.

The influence of annealing time on the average distance between disclinations was determined from the scattering patterns, some of which are shown in Figure 5-7 and Figure 5-8.

Figure 5-9 shows the variation of $D(t)$ with annealing time. In case of non polar nematic LCP, **Poly-C**, within $15 < t < 120$, the time evolution of D approximately obeyed a power law with the exponent of c. 0.46, i.e.

$$D(t) \sim t^{0.46} \tag{5.6}$$

On the basis of the time-dependent Ginzburg-Landau model with non-conserved order parameter and assuming that defects are topologically point-like and that the attractive force between them is given by r^{-1}, where r is the separation between the two defects, Toyoki[37] obtained a scaling relation of $D(t) \sim t^{0.5}$ in two-dimensional space. This simulation result was almost consistent with my result.

On the other hand, in case of biaxial polar nematic LCP, **Poly-A**, within $15 < t < 45$, the time evolution of D approximately obeyed a power law with the exponent of c.a. 0.19. But, $t > 45$, that decreased with increasing t, and was constant at $t > 600$s.

Here, a question arises on why the time evolution of D of polar nematic LCPs breaks a power law. Figure 5-10 shows the possible mechanism for the transformation of an amorphous state to a polydomain one in the polar nematic liquid crystal. Firstly, when the amorphous films are heated up to nematic temperature, the nematic LC may form many kinds of disclinations with various strengths of $s = \pm 1/2, \pm 1$ and so on (see the above processes in Figure 5-10 are given in the case of $s = \pm 1/2$). The sum of the strengths of all disclinations in a sample should be zero. After a prolonged annealing time, however, disclinations of equal and opposite strengths attract one another and are annihilated, leading to the development of the large domain texture with low defect

density. Without surface anchoring nor external aligning fields, however, an appreciable number of disclinations is still remained in the pseudo-equilibrium state in which size and shape of domain no longer change with time.[38-40]

Such a simple development of the LC domains promoted by the director orientation would be unlikely in the case of the polar nematic phase. And the dipole moments was occurred the phase separation due to the molecular diffusion. Finally, the misorientation of dipolar vectors makes the free energy cost high so that the dipolar orientation tends to become continuous by producing new defects of strength $|s| = 1$ after the prolonged annealing, similar with the transformation of a mechanically aligned monodomain structure to a polydomain one in the polar nematic liquid crystal (see the below processes in Figure 5-10).

References

(1) Sawyer, L. C.; Linstid, H. C.; Romer, M., *Plast. Eng. (N.Y.)* **1998**, 54, 37.

(2) Blackwell, J.; Biswas, A., in *Developments in oriented polymers-2*; Ward I. M. Ed.; Elsevier: New York, 1987, p. 153

(3) Coulter, P.; Windle, A. H. *Macromolecules* **1989**, *22*, 1129.

(4) Jin, J. -I.; Antoun, S.; Ober, C.; Lenz, R. W. *Br. Polym. J.* **1980**, *12*, 132.

(5) Hummel, J. P.; Flory, P. J. *Macromolecules* **1980**, *13*, 479.

(6) Imase, T.; Kawauchi, S.;Watanabe, *J. Macromol. Theory Simul.* **2001**,*10*, 434.

(7) Watanabe, T.; Miyata, S.; Furukawa, T.; Takezoe, H.; Nishi, T.; Migita, A.; Sone, M.; Watanabe, J. *Jpn. J. Appl. Phys.* **1996**, 35, L505.

(8) Taguchi, Y.; Yen, C.-C.; Kang, S.; Tokita, M.; Watanabe, J. *Macromolecules* **2009**, 42, 8, 3179.

(9) Yu, C.-J.; Yu, M.; Lee, S.-D. *Jpn. J. Appl. Phys.* **2002**, *41*, L102.

(10) Groh, B.; Dietrich, S. *Phys. Rev. E* **1997**, 55, 2892-2901.

(10) Terentjev, E. M.; Osipov, M. A.; Sluckin, T. J. *J. Phys. A* **1994**, 27, 7047-7059.

(11) Biscarini, F.; Zannoni, C.; Chiccoli, C.; Pasini, P. *Mol. Phys.* **1991**, 73, 439-461

(12) Brand, H. R.; Cladis, P. E.; Pleiner, H. *Int. J. Eng. Sci.* **2000**, 38, 1099.

(13) Hirose, T.; Tokita, M.; Watanabe, T.; Miyata, S.; Watanabe, J. *Macromolecules* **1998** *31*, 5937

(14) Park, B.; Kinoshita, Y.; Takezoe, H.; Watanabe, J. *Jpn. J. Appl. Phys.* **1998**, *37*, L136.

(15) Yen, C.-C.; Tokita, M.; Park, B.; Takezoe, H.; Watanabe, J. *Macromolecules* **2006**, 39, 1313.

(16) Yen, C.-C.; Taguchi, Y.; Tokita, M.; Watanabe, J. *Macromolecules* **2008**, 41, 2755.

(17) Koike, M.; Yen C. C.; Yuqing, L.; Tsuchiya, H.; Tokita, M.; Kawauchi, S.; Takezoe, H.; Watanabe, J. *Macromolecules*, **2007**, 40, 2524

(18) Romo-Uribe, A.; Windle A. H. *Macromolecules* **1996**, *29*, 6246.

(19) Kromer, H.; Khun, R.; Pielartzik H.; Siebke, W.; Eckhardt, V.; Schmidt, M. *Macromolecules* **1991**, *24*, 1950

(20) Dobb, M. G.; Johnson, D. J.; Saville, B. P. *J. Polym. Sci. Polym. Phys. Ed.* **1977**, *15*, 569.

(21) Harrison, P.; Navard, P. *Rheol. Acta* **1999**, *38*, 569.

(22) Langellan, H. C.; Gotsis, A. D. *J. Rheol.*, **1996**, 40, 107.

(23) Sigillo, I.; Grizzuti, N. *J. Rhol.* **1994**, *38*, 589.

(24) Wissbrum, K. *J. Rheol.* **1981**, *25*, 619.

(25) Kim K. M.; Cho, H.; Chung I. J. *J. Rheol.* **1994**, *38*, 1271.

(26) Rome-Uribe, A.; Lemmon, T.; Windle, A. H. *J. Rheol.* **1994**, 38, 1271.

(27) Saupe, A. *Mol. Cryst. Liq. Cryst.* **1973**, *21*, 211.

(28) Kleman, M. "*Points, lines and Walls, in Liquid Crystals, Magentic Systems, and Various Ordered Media*", Wiley, Chichester **1983**.

(29) *Polymer Liquid Crystals*; Ciferri, A., Krigbaum, W. R., Meyer, R. B., Eds; Academic Presss; New York, **1982**; Chapters 5 and 6.

(30) Brand, H. R.; Finkelmann, H. In *Handbook of Liquid Crystals, Magnetic Systems, and Various Ordered Media*; Wiley: Chichester, U.K., **1983**.

(31) Ahir, S. V.; Tajbakhsh, A. R.; Terentjev, E. M. *Adv. Funct. Mater.* **2006**, *16*, 556.

(32) Tokita, M.; Tagawa, H.; Funaoka, S.; Niwano, H.; Osada, K.; Watanabe, J. *Jpn. J. Appl. Phys.* **2006**, *45*, 1729.

(33) Beyer, P.; Terentjev, E. M.; Zentel, R. *Macromol. Rapid Commun.* **2007**, *28*, 1485.

(34) Pleiner, H.; Brand, H. R. *Europhys. Lett.* **1989**, *9*, 243.

(35) Brand, H. R.; Pleiner, H.; Ziebert, F. *Phys. Rev.* E **2006**, *74*, 021713.

(36) Shiwaku, T.; Nakai, A.; Hasegawa, H.; Hashimoto, T.; *Polymer Commun.* **1987**, 28, 174.

(37) Toyoki, H.; *Phys. Rev. A.* **1990**, *42*, 911.

(38) Kleman, M.; "*Points, lines and Walls, in Liquid Crystals, Magentic Systems, and Various Ordered Media*", Wiley, Chichester 1983.

(39) Rey, A.D.; Tsuji, T.; *Macromol. Theory Simul.* **1998**, *7*, 623.

(40) Shiwaku, T.; Nakai, A.; Wang, W.; Hasegawa, H.; Hashimoto, T.; *Liq. Crystals* **1995**, 19, 679

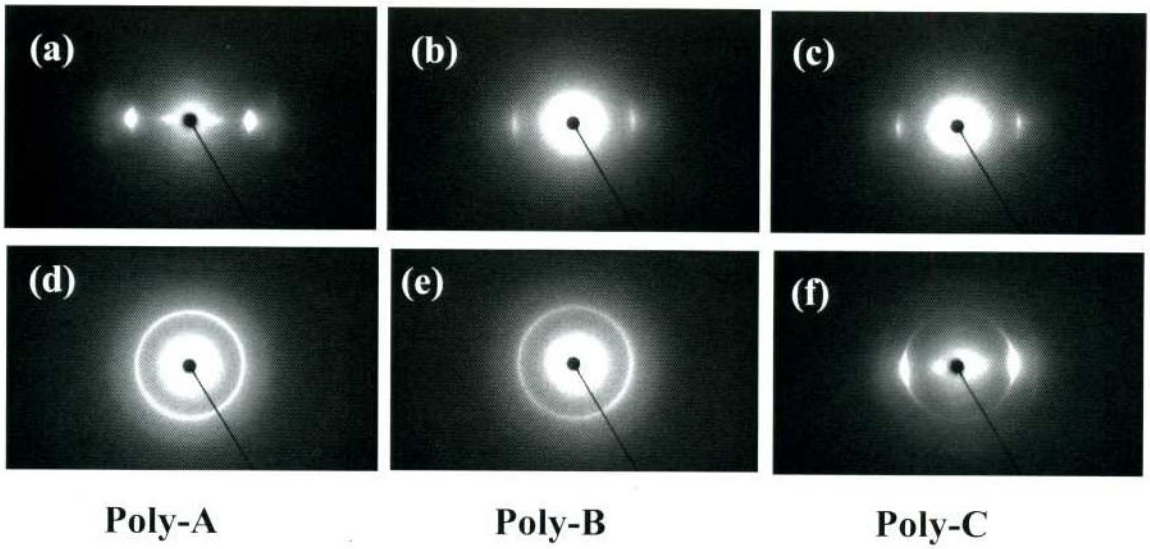

Figure 5-1. X-ray patterns taken for the fibers spun from the nematic LC at 330 °C; a) **Poly-A**, b) **Poly-B** and c) **Poly-C**. Corresponding X-ray patterns for the fibers annealed for 10 min at 330 °C are presented in (d)-(f). X-ray patterns were taken at room temperature with fiber axis set in the vertical direction. The strong reflection in the central part has a spacing of 4.8Å, which is attributed to the lateral packing of polymers.

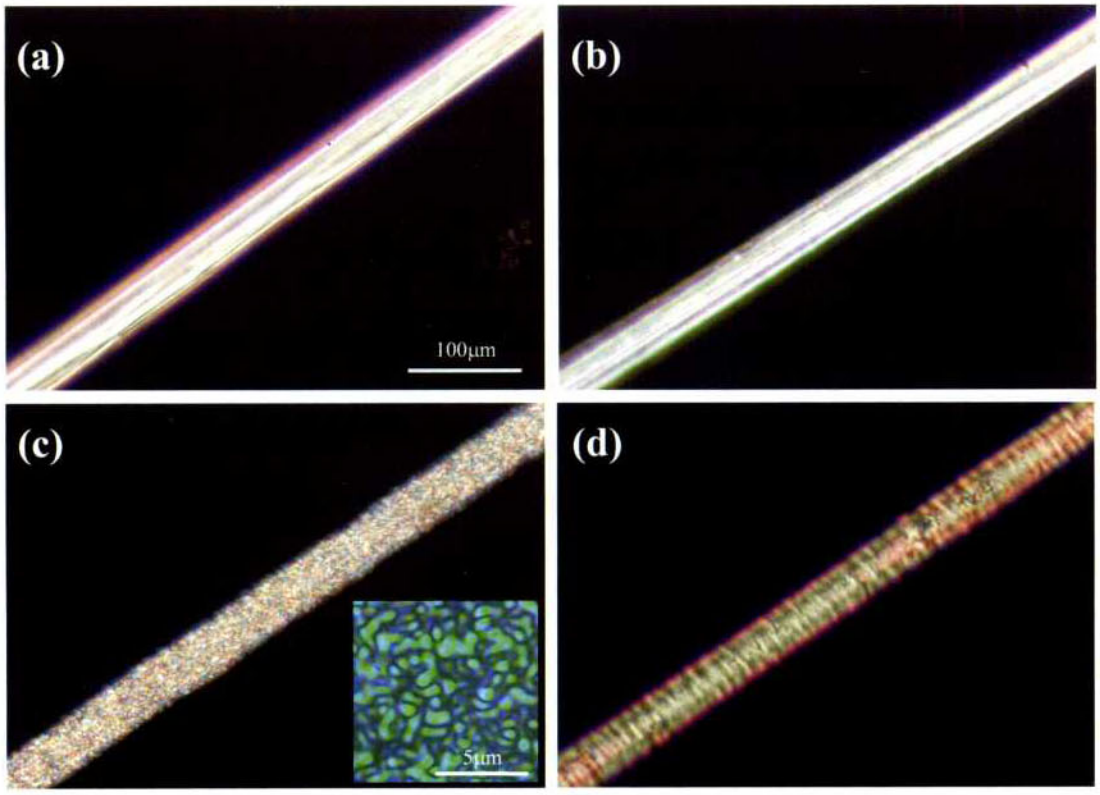

Figure 5-2. Optical microscopic textures for the fibers spun from the nematic LC at 330 °C; (a) **Poly-A** and b) **Poly-C**. The corresponding textures for the fibers annealed for 10 min at 330 °C are presented in parts (c) and (d). The inset of part (c) indicates the enlarged view of texture by digital microscope (KEYENCE digital microscope VHX-1000)). The data for **Poly-B** are the same as those of **Poly-A**.

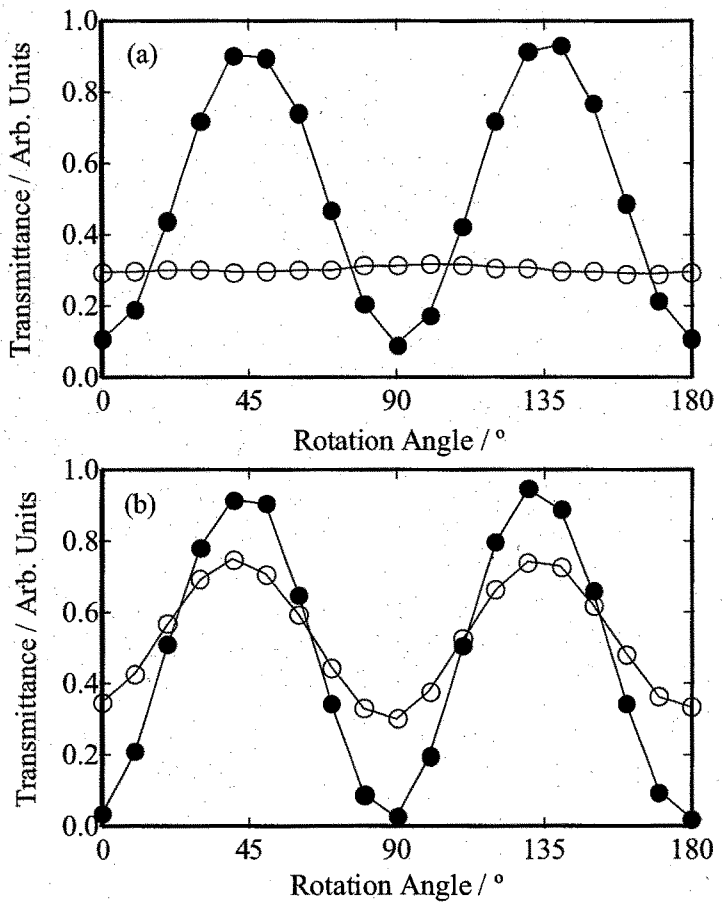

Figure 5-3. Transmitted light intensity measured under the cross polarization as a function of angular displacement of fiber axis to the polarizer; (a) **Poly-A** and (b) **Poly-C**. Closed and open circles are observed for as-spun fiber and annealed fiber for 10 min at 330 °C, respectively.

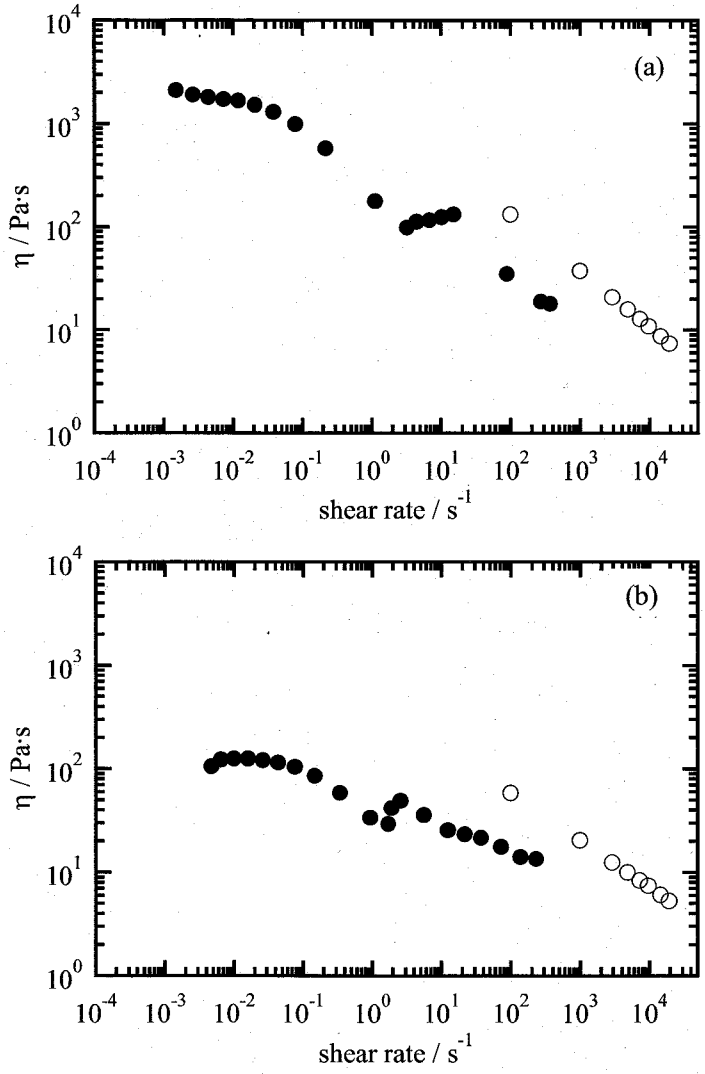

Figure 5-4. Steady-state viscosity for the nematic LCs of (a) **Poly-A**, (b) **Poly-C** at 330 °C. The data presented by closed and open circles are collected by the plate-and-plate rheometer and the capillary rheometer, respectively.

(a) **Poly-A**

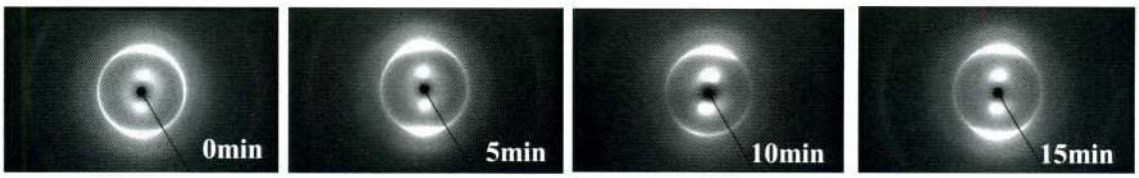

(b) **Poly-C**

Figure 5-5. X-ray patterns taken for the oriented films by the shear flow between plate-plate rheometer for the nematic LC at 330 °C; (a) **Poly-A**, (b) **Poly-C**. The time given on the photograph is the annealing period at 330 °C. The X-ray beam was irradiated along the velocity gradient ($\nabla \mathbf{v}$) direction and with the velocity ($\mathbf{v}$) direction set in a vertical one. The data for **Poly-B** are the same as those for **Poly-A**.

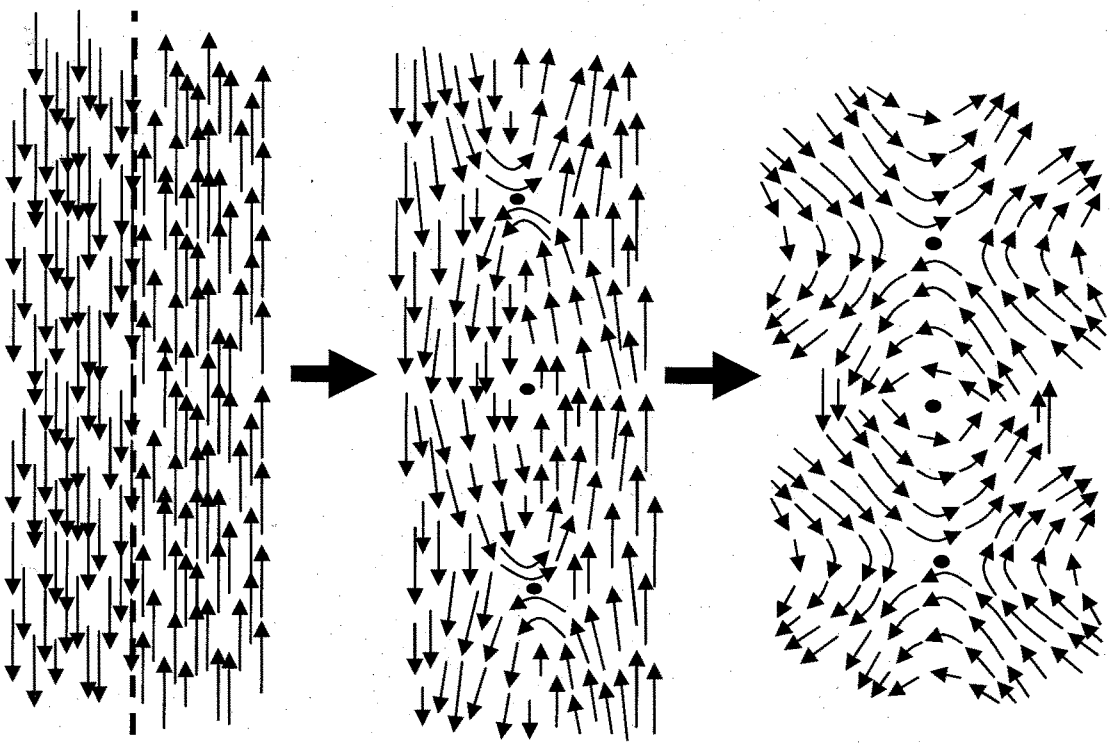

Figure 5-6. Possible mechanism for the transformation of a mechanically aligned monodomain structure to a polydomain one in the polar nematic liquid crystal. When the polar nematic liquid crystals are aligned mechanically, the perfect domain can be obtained with respect to the orientation order of the long molecular axis. In these samples, however, there are many grain boundaries with respect to the dipolar vector; the dipolar vectors abruptly change their direction on the boundary (dashed line), as illustrated in part (a). This misorientation of dipolar vectors is of high free energy so that the dipolar orientation becomes continuous by producing new defects of strength s = |1| after the prolonged annealing, as illustrated in parts (b) and (c). This leads to the elimination of the initial macroscopic orientation.

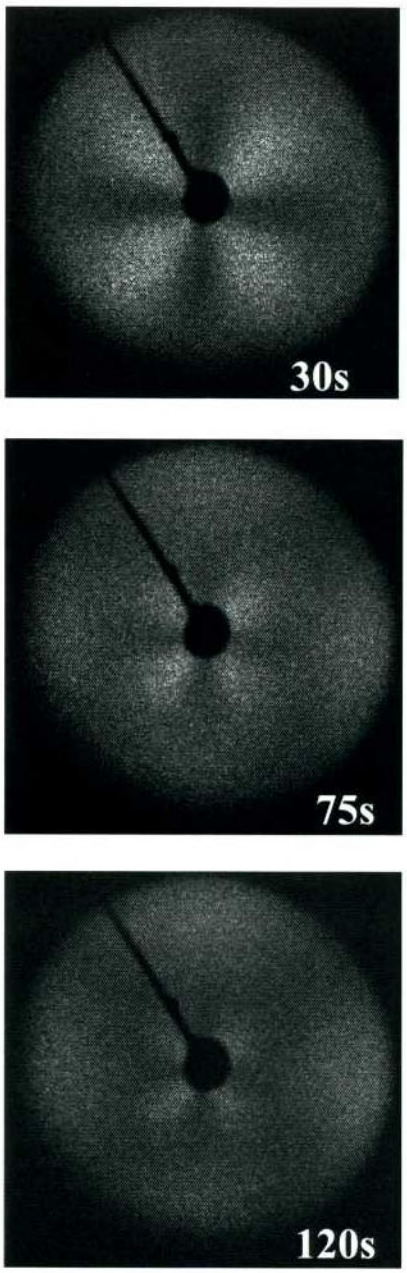

Figure 5-7. Variations of HV light scattering patterns of **Poly-C**. The time given on the photograph is the annealing period at 330 °C.

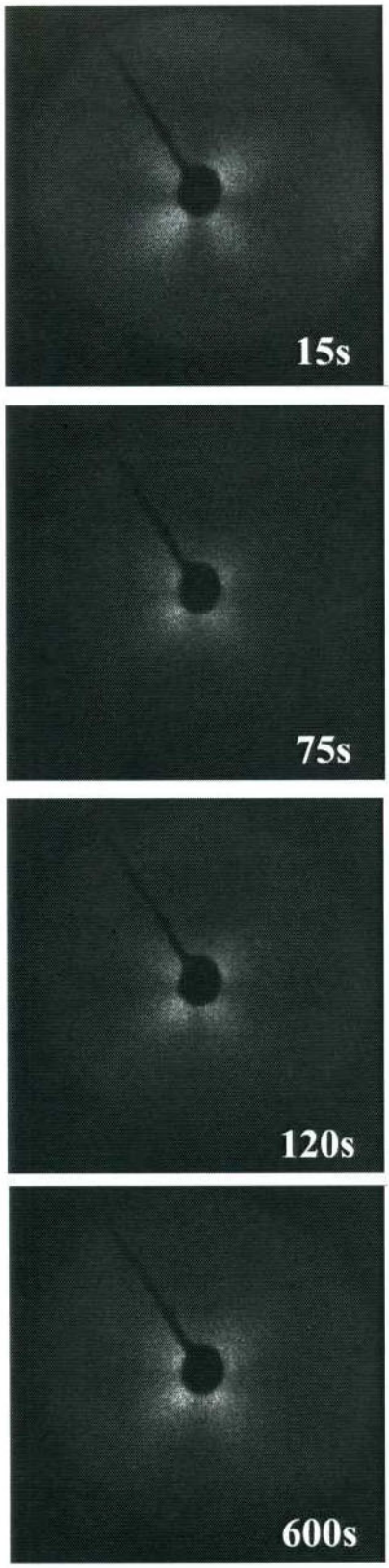

Figure 5-8. Variations of HV light scattering patterns of **Poly-A**(a). The time given on the photograph is the annealing period at 330 °C.

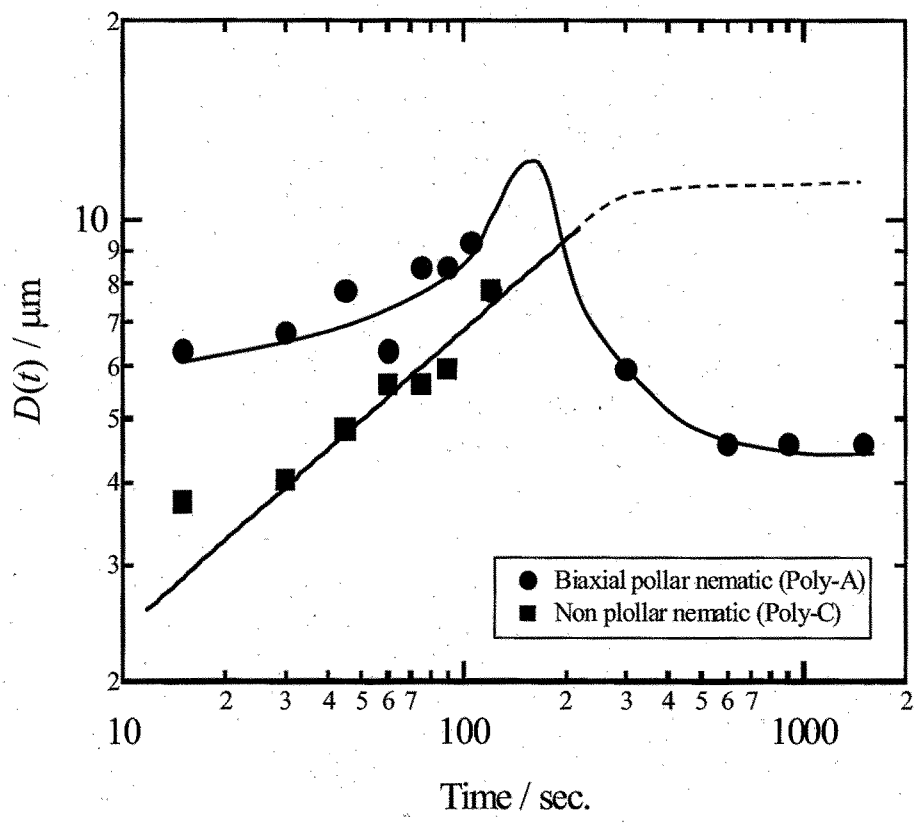

Figure 5-9. Diameter of LC domain determined by the light scattering method versus isothermal annealing time at 330°C.

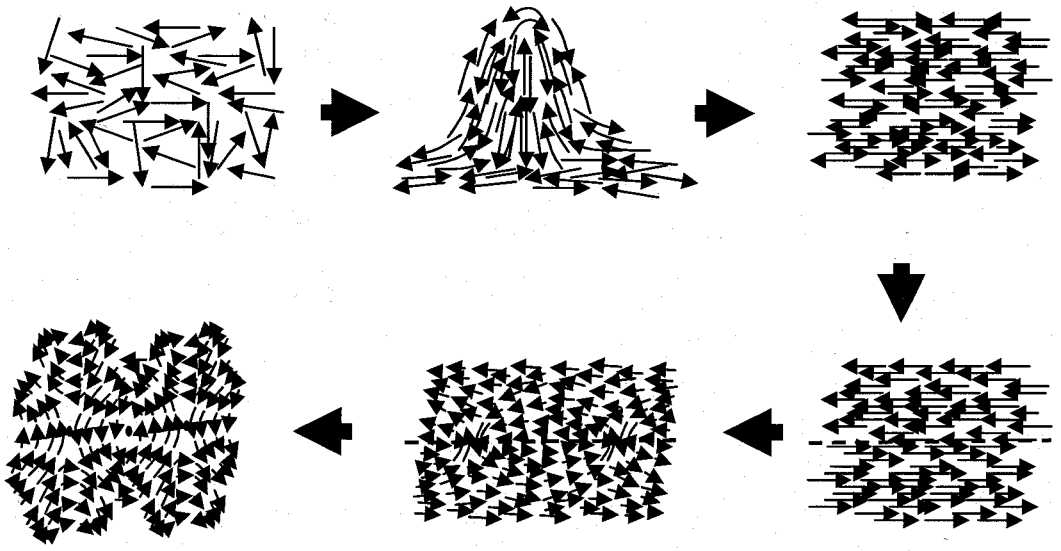

Figure 5-10. Possible mechanism for the transformation of an amorphous structure to a polydomain one in the polar nematic liquid crystal.

Chapter 6

Difference in Thermal Diffusivity between Polar and Non-Polar Nematic Liquid Crystals in Aromatic Polyesters Derived from VECTRA®

Abstract

Various head-to-tail nature LCPs or not was measured thermal diffusivity. The head-to-tail nature nematic LCPs are fundamentally higher thermal conductivity than the not head-to-tail nature ones. It is concluded that biaxial polar nematic LCPs, which have all the carbonyl groups directed to the similar direction as an average, is advantageous structure for obtaining a higher thermal diffusivity. Furthermore, as 6-hydroxy-2-naphtoic acid (HNA) is replaced to 4-hydroxybiphenoic acid (HBPA) in polymer element, the thermal diffusivity is increasing. While the thermal diffusivity of non-polar nematic LCPs doesn't depend on the molar content of kink monomer and is almost constant.

Similarly, the thermal diffusivity for poly($HBA_{73-x}/HNA_{27-x}/TA_x/BP_x$)s with various contents of TA (or BP) up to 0.10 was measured. With lack of the head-to-tail nature, thermal diffusivity of the polar nematic LC indicated is lower. On the other hand, as the polymer chain loses the head-tail character, the thermal diffusivity increased by about 0.2×10^{-7} m^2/s. At this time, because the number of disclination decreases, the disclination may cause the phonon scattering.

6-1 Introduction

Aromatic polyesters are most important class of thermotropic liquid crystal (LC) polymers for commercial applications.[1] Especially, aromatic LC polymers have been used in electric and electronic devices. Recently, these have been improved of heat from the internal conductor and have been designed to diffuse the heat efficiently. Because the conversion efficiencies of electric parts like the higher energy transduction element (for example, Light-Emitting Diode (LED), Photo Voltaic generation(PV), etc) decrease under the higher temperature. So, the materials are also required higher thermal conductivity.

Most polymers are thermally insulating. Typical thermal conductivity values in W / m K for some common materials are 0.2 – 0.3 for polymers. The thermal conductivity of polymer without the metallic bond is ruled by the phonon conduction. Therefore, the thermal conductivity of ordered LC polymers is 0.4 - 0.5 W / m K, which is higher thermal conductivity among polymers. For a further thermal conductivity improvement, one approach to improve the thermal conductivity of LC polymer is through the addition of a conductive filler material, such as carbon and metal.[2, 3] or polymer blends.[4] On the other hand, another approach to improve the thermal conductivity of polymer tried to control the high-order structure.[5]

VECTRA® A950 composed of 73 mol % of 4-hydroxy benzoic acid (HBA) and 27 mol % of 6-hydroxy-2-naphtoic acid (HNA), is an extraordinary class of LC polymers, since a head-to-tail connection of *p*-HBA and HNA [6-8] results in a huge dipole moment along the chain as a result of accumulation of the carbonyl dipole in ester linkage.[9] Because of such a polar rod-like conformation, **VECTRA® A950** can form the polar biaxial nematic LC, which has been experimentally confirmed by second

harmonic generation (SHG) measurements[10,11] and predicted by computer simulation and theoretical calculation considering the dipole-dipole interaction.[12-16] Moreover VECTRA® forms the biaxialty in the view of polarity, so that, it is necessary that the all carbonyl groups direct to the similar direction as an average[10,11].

In this chapter, I tried to examine that how the polar structure influence the thermal diffusivity. Various head-to-tail nature LCPs or not were prepared. The head-to-tail nature LCPs with biaxial polar structure are fundamentally higher thermal conductivity than the not head-to-tail nature ones. And the thermal diffusivity is also measured an interesting series of polyesters, the nematic LCs of which are SHG active and non-active depending on the content of TA and BP. And the difference in the domain size (or the number of defects) between polar and non-polar nematic LC polymer was effect on the thermal diffusivity.

6-2 Experiment

6-2-1 Materials

Various head-to-tail nature nematic LCs and not head-to-tail one were synthesized by the method according to the applied patent from Celanese.[17] The molar content of each comonomer is shown in Table 6-1. All head-to-tail nature nematic LCPs in Table 6-1(a) indicate SHG activity, as well as biaxialty. And the not head-to-tail nature ones indicate non SHG activity in Table 6-1(b). At temperatures higher than T_m, all of the polymers were confirmed to form the nematic phase by polarized optical microscopy (Olympus BX 51 equipped with a Mettler FP82HT hotstage). No nematic to isotropic phase transition was observed in a temperature region up to 350 °C.

Moreover, as used in Chapter 3, the copolymers in which terephthalic acid (TA) and biphenol (BP) units were incorporated into **VECTRA® A950** (abbreviated here as **P-Sdt**) were also used. The content of TA or BP that should be equimolar with each other in order to properly perform the polymerization was varied from 0 to 0.1. These copolymers with the following structure,

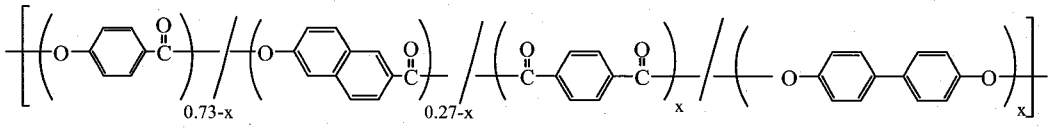

(7-1)

are designated as **P-x** where **x** is the molar content of TA or BP unit.

Mentioned in Chapter 3, **P-x** polymer chain loses the head-tail nature by an introduction of symmetric BP and TA units so that the resulting nematic LC loses the polarity as well.[11] This trend is clearly observed in Figure 2-1. SHG intensity sharply decreases with an increase in **x** and becomes zero for **P-x** with **x** more than 0.07, indicating that the perfect alteration from the polar nematic LC to the non-polar (or conventional) one is accomplished on increasing **x** up to 0.07.

The quantitative analysis for the domain size can be done by small-angle light scattering (SALS) method.[18] The domain sizes determined from the 2θ-intensity profile, are listed in six column of Table 6-3. The domain sizes in the SHG active copolymers are commonly estimated to be about 5μm, while those in non SHG-active ones are around 10μm or larger than it.

6-2-2 Methods

Thermal diffusivity measurement: Thermal diffusivity was measured by Thermal Wave Analysis (TWA) method using an Ai phase mobile-1u. The sensor element was

calibrated by using a zirconia plate as a standard with α being 1.15×10^{-6} $m^2 \cdot s^{-1}$. The films with thickness of ~100μm are measured. The 100μm-film sample was prepared for various polyesters used in Chapter 6-3-1 at 380C° and the **P-x** polymer used in Chapter 6-3-2 was prepared at 320C°. By wide-angle X-ray measurements, the molecular orientation of their films existed parallel to the film plane, but a very low level in the film plane shown in Figure 6-1.

6-3 Results and Discussion

6-3-1 Difference of Thermal Diffusivity between Polar Nematic LCs and Non-Polar Nematic LCs

The thermal diffusivity is measured for the thickness direction in 100μm-films, that is a perpendicular direction of molecular axis to see in Figure 6-1. Shown in Table 6-1 (a) and (b), the thermal diffusivity of the polar nematic LCs is higher than that of the non-polar ones as well. This trend is clearly observed in Figure 6-2 where the thermal diffusivity of the function of the molar content of kink monomer. Here, 6-hydroxy-2-naphtoic acid (HNA) and 2,6-naphthalic acid (NDA) is indicated as kink monomer. It was suggested in Chapter 3 that all the carbonyl groups in biaxial polar nematic LCPs are directed to the similar direction as an average, to produce the polarization along a perpendicular direction to the polymer chain as well as in the parallel direction. Therefore, the ordered carbonyl group might be a cause in the reason why the thermal diffusivity of biaxial polar structure is higher because it measures the thermal diffusivity for the perpendicular direction to the polymer chain in the actual experiment. Moreover, in the polar system, the thermal diffusivity of polar nematic LCPs increase remarkably with a decrease in the molar content of kink

monomer, namely, as the polymer conformation become linear. While the thermal diffusivity of non-polar nematic LCPs doesn't depend on the molar content of kink monomer and is almost constant. This result of the non-polar nematic LCs indicates that the thermal diffusivity of conventional wholly aromatic polyesters might be approximately a regular value at 1.4×10^{-7} m^2/s.

In Figure 6-2, only HNA was used as kink monomer. What influence does *m*-HBA unit, which is more kinkily, exert on the thermal diffusivity? The copolymer in which *m*-HBA unit were incorporated into poly(HBA/HBPA) were evaluated. This trend is clearly observed in Figure 6-3 where the thermal diffusivity of the nematic LCs in a series of poly(HBA/HBPA/*m*-HBA) is plotted against the content kink monomer. Introduction of *m*-HBA into poly(HBA/HBPA) is the lower thermal diffusivity than it of HNA into that.

6-3-2 Alternation of Thermal Diffusivity at Transition from Polar Nematic LCs to Non-Polar Nematic LCs

Then, the alternation of the thermal diffusivity in the process from which the polarity was lost was examined by using in a series of **P-x** polymer. **P-x** polymer chain loses the head-tail nature by an introduction of symmetric BP and TA units so that the resulting nematic LC loses the polarity as well.[11] Figure 6-4 shows an alternation of thermal diffusivity on the molar content of TA (or BP) in a series of **P-x** polymers. When **x** is between 0.015 and 0.05 and between 0.07 and 0.10 respectively, thermal diffusivity is almost constant. When the molar content of TA is low, which is below **x** = 0.015 the thermal diffusivity is increasing drastically with a decrease in **x**. The thermal diffusivity dominated by the phonon conduction is important for higher

ordering in the structure, so polar structures possess the higher thermal diffusivity, especially in the direction of perpendicular to the chain axis. In contrast, when the polarity is lost, the ordering in parallel to the chain axis can't be recognized, and that in perpendicular to the chain axis must be random distribution. As a result, the thermal diffusivity in non polar structure decreases. On the other hand, the non-polar nematic LCs is higher thermal diffusivity than the polar ones, which are close to the non-polar ones, and the difference of thermal diffusivity is about 0.2×10^{-7} m^2 s^{-1}. This discontinuous change of thermal diffusivity consists with the polar-nonpolar transition for **P-x** polymer, just the domain size change from about 5μm to over 10μm. By these results, I considered that the thermal diffusivity increased at the polar-nonpolar transition point because the number of disclination had decreased, that is the disclinations in LCPs cause the phonon scattering.

6-4 Summary

Various head-to-tail nature and not head-to-tail nature nematic LCs was measured thermal diffusivity. The head-to-tail nature nematic LCPs is fundamentally higher thermal conductivity than the not head-to-tail nature ones. The thermal diffusivity dominated by the phonon conduction is important for higher ordering in the structure, so biaxial polar nematic LCPs, which have all the carbonyl groups directed to the similar direction as an average, is advantageous structure for obtaining a higher thermal diffusivity. And the thermal diffusivity of polar nematic LCPs increase remarkably with a decrease in the molar content of kink monomer, namely, as the polymer conformation become linearity, thermal diffusivity increases. As the more kinkily conformation was introduced, the thermal diffusivity remarkably decrease.

While the thermal diffusivity of non-polar nematic LCPs doesn't depend on the molar content of kink monomer and is almost constant.

Similarly, the thermal diffusivity in a series of **P-x** polymer, which is poly(HBA/HNA/TA/BP)s with various contents of TA (or BP) up to 0.10, was measured. The polymer with the head-to-tail nature indicated the higher thermal diffusivity. On the other hand, as the polymer chain loses the head-tail character, the thermal diffusivity increased by about 0.2×10^{-7} m^2/s. At this time, because the number of disclination decreases, the disclination may cause the phonon scattering.

References

(1) Sawyer, L. C.; Linstid, H. C.; Romer, M. *Plast. Eng. (N.Y.)* **1998**, 54, 37.

(2) Rebecca A. H.; Jason M. K.; Julia A. King.;, Jennifer L. H. *J. Appl. Polym. Sci.* **2008**, 100, 2914

(3) Fabien, F.; Devaux, E.; Bourbigot, S; Rumeau, P.; Chapuis, P. -O.; Saha, S. K.; Volz, S. *Thermochim. Acta* **2008**, 477, 25.

(4) Jayasree, T.K.; Predeep, P.; Agarwall, R. Saxene, N. S. *Trends Applied Sci. Res.* **2006**, 3, 278.

(5) Akatsuka, M.; Takazawa, Y. *J. Appl. Polym. Sci.* **2003**, 89, 2464

(6) Coulter, P.; Windle, A. H. *Macromolecules* **1989**, *22*, 1129.

(7) Jin, J. -I.; Antoun, S.; Ober, C.; Lenz, R. W. *Br. Polym. J.* **1980**, *12*, 132.

(8) Hummel, J. P.; Flory, P. J. *Macromolecules* **1980**, *13*, 479.

(9) Imase, T.; Kawauchi, S.;Watanabe, J. *Macromol. Theory Simul.* **2001**,*10*, 434.

(10) Watanabe, T.; Miyata, S.; Furukawa, T.; Takezoe, H.; Nishi, T.; Migita, A.; Sone, M.; Watanabe, J. *Jpn. J. Appl. Phys.* **1996**, 35, L505.

(11) Taguchi, Y.; Yen, C.-C.; Sungmin, K.; Tokita, M.; Watanabe;J. *Macromolecules,* **2009**, 42, 8, 3179-3185

(12) Park, B.; Kinoshita, Y.; Takezoe, H.; Watanabe, J. *Jpn. J. Appl. Phys.* **1998**, *37*, L136.

(13) Yen, C.-C.; Tokita, M.; Park, B.; Takezoe, H.; Watanabe, J. *Macromolecules* **2006**, 39, 1313.

(14) Yen, C.-C.; Taguchi, Y.; Tokita, M.; Watanabe, J. *Macromolecules* **2008**, 41, 2755.

(15) Yu, C.-J.; Yu, M.; Lee, S.-D. *Jpn. J. Appl. Phys.* **2002**, *41*, L102.

(16) Groh, B.; Dietrich, S. *Phys. Rev. E* **1997**, 55, 2892-2901.

(17) Calundann, G. *U. S. Patent* 1979, 4 161 470.

(18) Hashimoto, T.; Nakai, A.; Shiwaku, T.; Hasegawa, H.; Rojstaczer, S.; Stein, R. S. *Macromolecules*, **1989**, *22*, 422.

Table 6-1. (a) Thermal diffusivity of various biaxial polar LC polymers

Composition*	Molar ratio/%	Molar content of kink monomer / %	Thermal diffusivity $\times 10^{-7}/m^2 \cdot s^{-1}$
HBA/HNA (**P-Sdt**)	73/27	27.0	1.99
HBA/HNA	79.8/20.2	20.2	1.93
HBA/HNA	24/76	76.0	1.68
HBA/HNA	23/77	77.0	1.81
HBA/HBPA/*m*-HBA	73/25/2	2.0	2.20
HBA/HBPA/*m*-HBA	73/20/7	7.0	2.19
HBA/HBPA	73/27	0	3.13
HBA/HNA/HBPA	73/2/25	2.0	2.76
HBA/HNA/HBPA	73/5/22	5.0	2.64
HBA/HNA/HBPA	73/10/17	10.0	2.44
HBA/HNA/HBPA	73/20/7	20.0	2.21
HBA/HNA/HBPA	60/15/25	15.0	2.17
HNA/HBPA	70/30	70.0	2.11

*Abbreviations

HBA: 4-hydroxy benzoic acid

m-HBA: 3- hydroxy benzoic acid

HNA: 6-hydroxy-2-naphtoic acid

HBPA: 4-hydroxybiphenoic acid

Table 6-1. (b) Thermal diffusivity of various non-polar LC polymers

Composition*	Molar ratio/%	Molar content of kink monomer / %	Thermal diffusivity $\times 10^{-7}/m^2 \cdot s^{-1}$
HNA/TA/HQ	60/20/20	60.0	1.49
HNA/TA/BP	60/20/20	60.0	1.32
HBA/HNA/TA/BP/APAP	50/2/24/14/5	2	1.39
HBA/HNA/TA/BP/APAP	60/5/17.5/12.5/5	5	1.36
HBA/HNA/TA/BP/APAP	66/20/7/7/0	20	1.38
HBA/HNA/TA/BP/APAP	65/19/8/8/0	19	1.16
HBA/HNA/TA/BP/APAP	64/18/9/9/0	18	1.14
HBA/HNA/TA/BP/APAP	63/17/10/10/0	17	1.28
HBA/NDA/TA/BP/APAP	60/12.5/7.5/15/5	12.5	1.53
HBA/NDA/TA/HQ/APAP	60/12.5/7.5/15/5	12.5	1.28

*Abbreviations

HBA: 4-hydroxy benzoic acid

HNA: 6-hydroxy-2-naphtoic acid

NDA: 2,6-naphthlic acid

TA: terephthalic acid

HQ: hydroquinone

BP: biphenol

APAP: N-acetyl-P-aminophenol

Table 6-3. Characterization in a series of **P-x** copolyesters

Sample	Molar content of TA unit	η_{inh} /dL g^{-1}	T_m /°C [a]	Relative SHG Intensity	D/μm
P-Std	0	4.67	283	1.00	5.3
P-0.003	0.003	3.46	283	0.78	4.6
P-0.006	0.006	3.91	280	0.63	6.8
P-0.015	0.015	4.26	278	0.42	6.3
P-0.03	0.03	4.38	277	0.05	5.6
P-0.05	0.05	4.23	273	0.03	5.3
P-0.07	0.07	4.14	251	0.00	>10
P-0.08	0.08	3.36	248	0.00	>10
P-0.09	0.09	4.17	248	0.00	>10
P-0.10	0.10	4.31	219	0.00	>10

[a] based on heating DSC data.

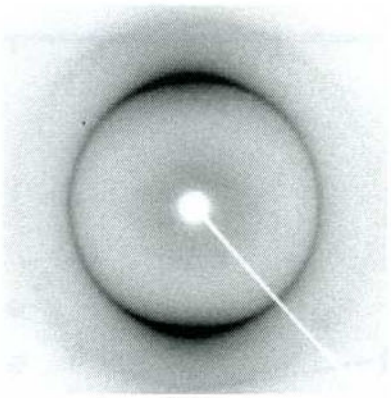

(a)

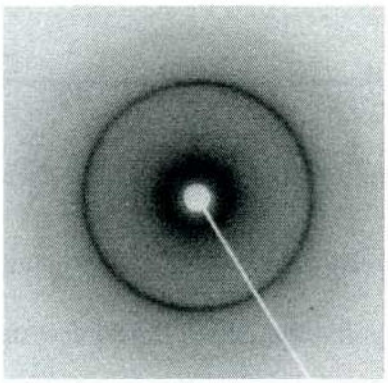

(b)

Figure 6-1. Wide-angle X-ray diffraction (Cu Kα radiation, Rigaku UltraX18 generator) pattern for film of **P-Sdt** (a) in the direction of edge view, (b) in the direction of through view. The molecular orientation of their films existed parallel to the film plane, but a very low level in the film plane.

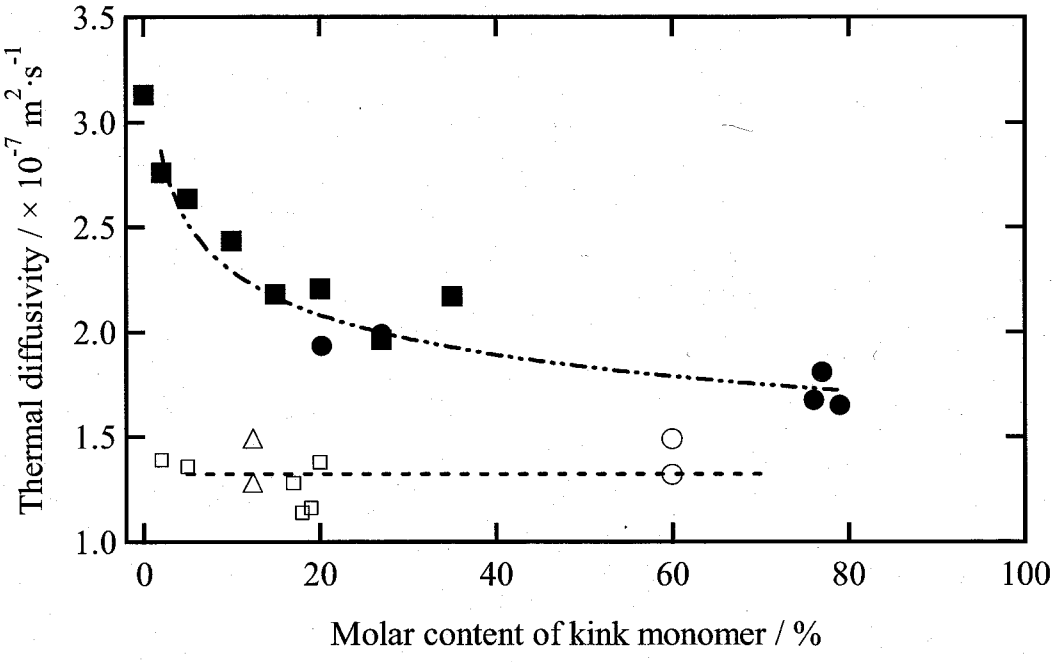

Figure 6-2. Correlation between thermal diffusivity and molar content of kink monomer. (●) represents polar nematic liquid crystals in a series of poly (HBA/HNA/HBPA), (■) in a series of poly(HBA/HNA), (○) non-polar nematic liquid crystals in series of poly(HNA/TA/BP or HQ), (□) in a series of poly(HBA/HNA/TA/BP/APAP), and (△) in a series of poly(HBA/NDA/ TA/BP or HQ/APAP).

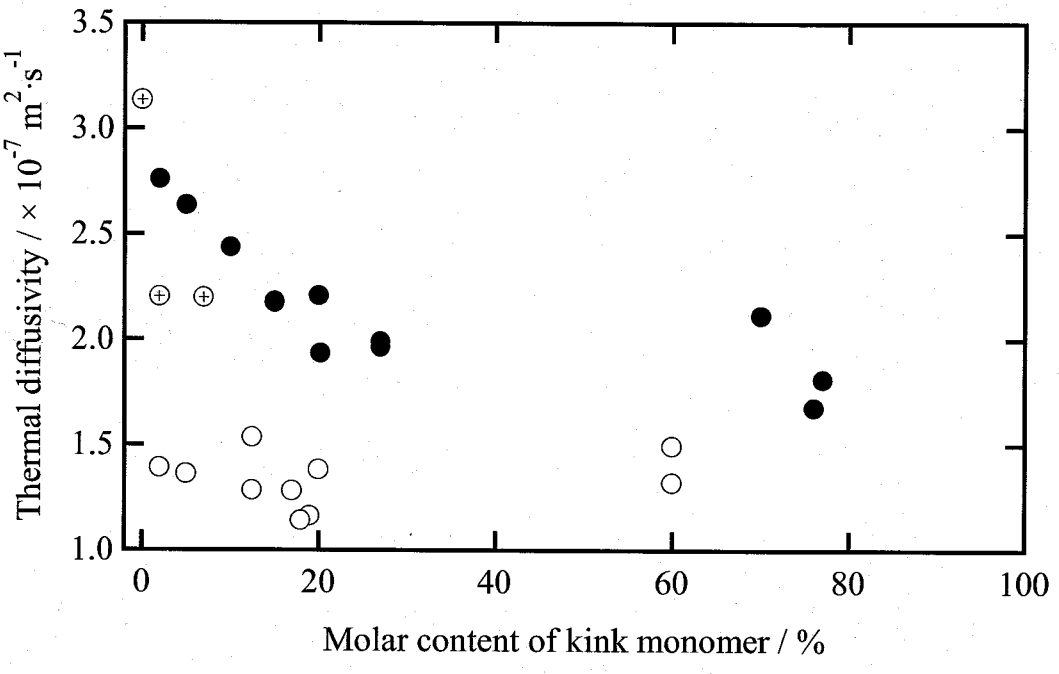

Figure 6-3. Correlation between thermal diffusivity and molar content of kink monomer. (●) represents biaxial polar nematic liquid crystals in a series of poly(HBA/HNA), or in a series of poly(HBA/HNA/HBPA), (⊕) in a series of poly(HBA/HBPA/*m*-HBA), (○) non-polar nematic liquid crystals in Table 6-1.(b).

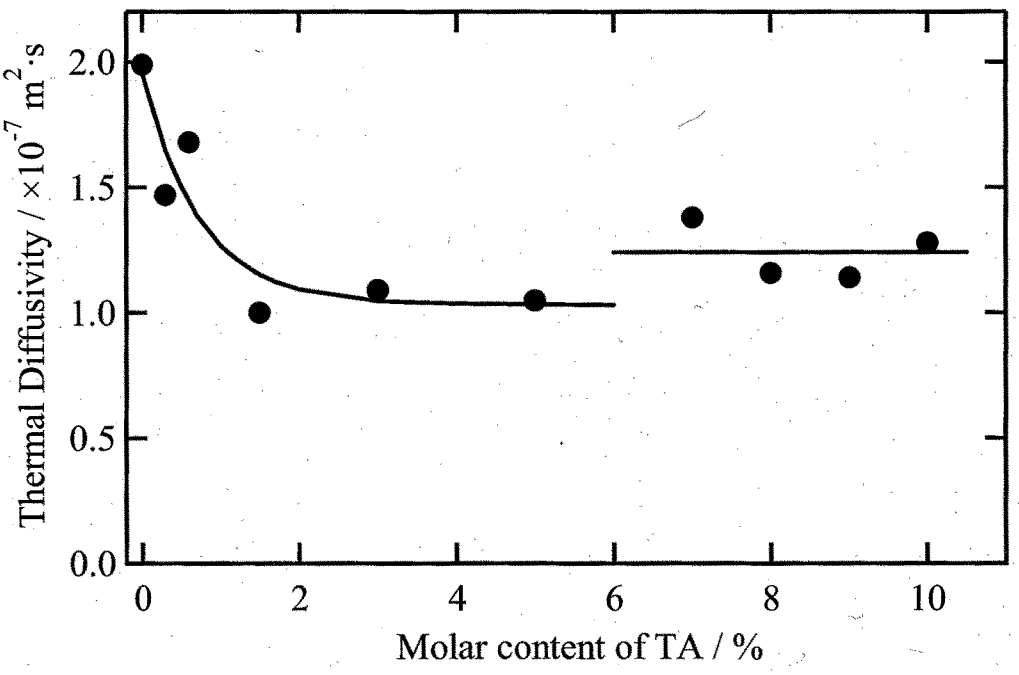

Figure 6-4. Variation of thermal diffusivity with the molar content of TA (or BP) unit in a series of **P-x** copolyesters.

Chapter 7

Conclusions

In this thesis, I investigate the nematic liquid crystal of **VECTRA® A950** and related polyesters through the SHG observation melt viscosity measurement, wide angle X-ray diffraction, polarized optical microscopy, small angle light scattering, and thermal diffusivity measurement. And these results lead to the following four conclusions.

1. **VECTRA® A950** forms a novel nematic liquid crystal with polar ordering along the nematic director. The SHG profiles as a function of incident or SHG polarizations are well simulated according to the model of C_s symmetry with its mirror plane rotationally disordered around the nematic director. The C_s symmetry is very significant since it requires the nematic liquid crystal of **VECTRA® A950** to possess the biaxiality. And the SHG activity is lost by an introduction of symmetrical TA (and BP) unit into poly(HBA/HNA) because the polymer chain loses the head-to-tail character. Furthermore, with increasing molecular weight on poly(HBA/HNA), the polar structure transfer from non polar, uniaxial polar to biaxial polar, because the stronger dipole moment is formed. As the kink conformation of *m*-HBA, which retains head to tail nature but loses the rod-like nature, is introduced, their liquid crystallinity is destabilized and polarity is lost. Furthermore, in the middle of the lost polarity, their biaxial polar structure transfers to the uniaxial one.

2. In the share-rate dependence of melt viscosity measurements for **VECTRA® A950** and related copolyesters, a Newtonian plateau at the lowest shear-rate region (R0) was appeared in addition to three regions which have been well elucidated in LC polymers. As far as I know, this is the first clear observation of region 0 in thermotropic LC system.

The Newtonian plateau region 0 reflected on the SHG activity or not. The viscosity of the biaxial polar nematic LCs in this region 0 was 10 times higher than that of the non-polar ones, and 5 times higher than that of uniaxial ones. The differences in these viscosities are connected to the differences in the LC domain size, which is lead to the polar structure. That is, the LC domains are smaller, and the viscosity in region 0 is higher.

3. In static state, the domain size in the biaxial polar nematic liquid crystals is smaller than that in the uniaxial ones and that in the non polar ones, and that in uniaxial polar nematic liquid crystals is smaller than that in the non polar ones. When the dipole moment vectors is overlapped with the two dimensional disclination models, $|s|=1/2$ cannot exist. By this reason, the disclinations in polar nematic LCPs can't be annihilated, and a large number of disclinations is kept. In addition, I found an interesting phenomenon of the mechanically aligned monodomain state of polar nematic liquid crystals transforming into the polydomain one. This unusual transformation may result from mismatching of the dipolar vectors. It can be concluded that each behavior is the same origin, which is that the free energy of the molecules is minimized by keeping many defects, or by producing new ones, based on the polar structure.

4. The head-to-tail nature nematic LCs possess fundamentally higher thermal conductivity than the not head-to-tail nature ones. And the thermal diffusivity of head -to-tail nature LCs decreases with an increase in the molar content of kink monomer, while that of not head-to-tail nature ones didn't depend on the molar content of kink monomer and were almost constant. As one suggestion for obtaining the higher thermal diffusivity, it is important that the carbonyl groups are ordered in the perpendicular direction of the axis of the molecule. Moreover, when the polymer chain loses the head-to-tail character, thermal the thermal diffusivity increased by about 0.2×10^{-7} m^2/s. At this time, because the domain size is bigger, the disclination may cause the phonon scattering.

List of Publications

(1) "Difference in Steady Shear Flow Viscosity between Polar and Nonpolar Nematic Liquid Crystals in Aromatic Polyesters Derived from VECTRA", Yoshiaki Taguchi, Chu-Chun Yen, Sungmin Kang, Masatoshi Tokita, Junji Watanabe, *Macromolecules,* **2009**, 42, 8, 3179-3185.

(2) "Unusual Transformation of the Mechanically Induced Monodomain State to the Polydomain one in Polar Nematic Liquid Crystals of Aromatic Polyesters", Yoshiaki Taguchi, Chu-Chun Yen, Sungmin Kang, Masatoshi Tokita, Junji Watanabe, *Journal of Physical Chemistry B*, **2009**, 113, 16, 5341-5344.

Publications not included in the thesis

(1) "Magnetic Properties of $Ba_2(Zn_{1-x}Mg_x)_2Fe_{12}O_{22}$ I. -Single Crystal Growth-", Nobuyuki Momozawa, Yoshiaki Taguchi, Hideki Sakai, Masahiko Abe, Katsuhiro Nishiyama, *Material Technology*, **1996**, 14, 16-20.

(2) "Magnetic Properties of $Ba_2(Zn_{1-x}Mg_x)_2Fe_{12}O_{22}$ II. -Characterization Single Crystals -", Nobuyuki Momozawa, Yoshiaki Tagushi, Hideki Sakai, Masahiko Abe, Katsuhiro Nishiyama, *Material Technology*, **1996**, 14, 42-46.

(3) "Neutron Diffraction study of Pb-Substituted Hexagonal Ferrite$(Ba_{0.2}Pb_{0.8})_2Fe_{12}O_{22}$", Nobuyuki Momozawa, Yoshiaki Taguchi, Yukinobu Nagao, Katsuhiro Nishiyama

Masahiko Abe, Hideki Sakai, Mutsuyoshi Matsumoto, Yasuo Yamaguchi, *Material Technology*, **1997**, 15, 20-24.

(4) "Magnetic Properties of $Ba_2(Zn_{1-x}Mg_x)_2Fe_{12}O_{22}$ III. -Magnetic Phase Diagram-", Nobuyuki Momozawa, Yoshiaki Taguchi, Yukinobu Nagao, Katsuhiro Nishiyama Masahiko Abe, Hideki Sakai, Mutsuyoshi Matsumoto, Yasuo Yamaguchi, *Material Technology*, **1997**, 15, 53-58.

(5) "Magnetic Properties of $Ba_2(Zn_{1-x}Mg_x)_2Fe_{12}O_{22}$ IV -Magnetic Structure-", Yoshiaki Taguchi, Yukinogbu Nagao, Hideki Sakai, Masahiko Abe, Katsuhiro Nishiyama, Nobuyuki Momozawa, *Material Technology*, **1997**, 15, 172-176.

(6) "Fabrication of Hybrid Layered Films of MoS_2 and an Amphiphilic Ammonium Cation Using the Langmuir-Blodgett Technique", Yoshiaki Taguchi, Ryota Kimura, Reiko Azumi, Hiroaki Tachibana, Naoto Koshizaki, Masaki Shimomura, Nobuyuki Momozawa, Hideki Sakai, Masahiko Abe, Mutsuyoshi Matsumoto, *Langmuir*, **1998**, 14, 6550-6555.

(7) "Polar nematic phase in lyotropic solutions of poly(γ-benzyl glutamate) and its temperature instability as detected by SHG measurement", Chu-Chun Yen, Yoshiaki Taguchi, Masatoshi Tokita, Junji Watanabe, *Macromolecules*, **2008**, 41, 8, 2755-2758.

Acknowledgment

It is a great pleasure to complete here this thesis based on the study carried out under the guidance of Professor Junji Watanabe, at Department of Organic and Polymeric Materials, Faculty of Engineering, Tokyo Institute of Technology from 2007 to 2010.

The author wishes to express his sincere gratitude to Professor Junji Watanabe for his continuous guidance and invaluable discussions as well as constant encouragement throughout this thesis.

The author also wishes to express his thanks to Associate Professor Masatoshi Tokita, Tokyo Institute of Technology, for his intensive guidance and invaluable discussion throughout this thesis.

The author also thanks to Assistant Professor Sungmin Kang, Ms. Mami Hida, secretary of Watanabe Laboratory, and members of Prof. Watanabe's laboratory for their useful advice, valuable suggestion, and kind help.

The author wishes to express his thanks to Dr. Toshio Shiwaku, manager of LCP Business Strategy Department, Polyplastics. Co. Ltd., for his kind supports and invaluable discussion throughout this thesis.

The author wishes to express his thanks to Mrs. Haruyasu Ito, Corporate officer, Toshihiko Endo and Kazufumi Watanabe, managers of Research and Development Center, Polyplastics Co. Ltd., and colleagues of Research and Development Center, for their kind supports and advices.

Finally, the author expresses his heartfelt thanks to his wife, his sons and his parents for their continuous supports and encouragements.

March, 2010

Yoshiaki Taguchi